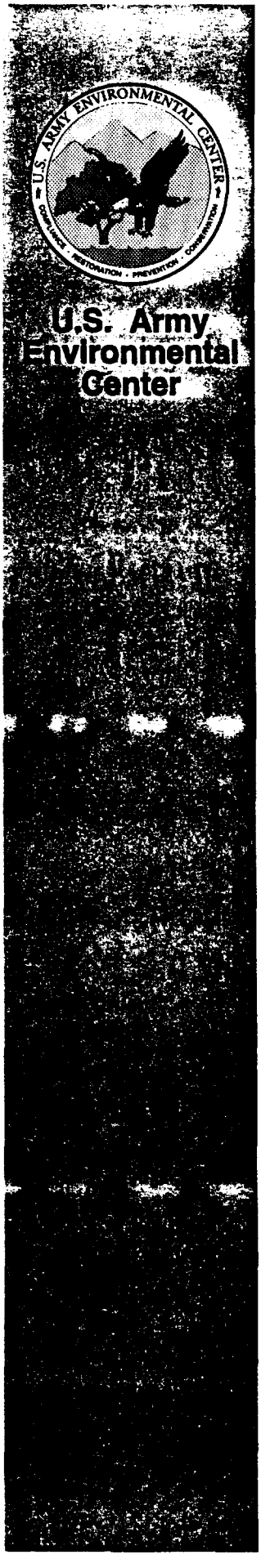

Report No. SFIM-AEC-ET-CR-97020

Development of Data Fusion Algorithms for Detecting and Identifying Ordnance with Magnetometers and Ground Penetrating Radar

September 1996

AD NUMBER

AD-B224 271

NEW LIMITATION CHANGE

TO

DISTRIBUTION STATEMENT A -
Approved for public release; Distribution unlimited.

Limitation Code: 1

FROM

DISTRIBUTION STATEMENT - E

Limitation Code: 4

AUTHORITY

C.R. Barry, Scty Mngr, SFIM-AEC-RMI, USA-EC, Aberdeen Proving Ground, MD

DISCLAIMER NOTICE

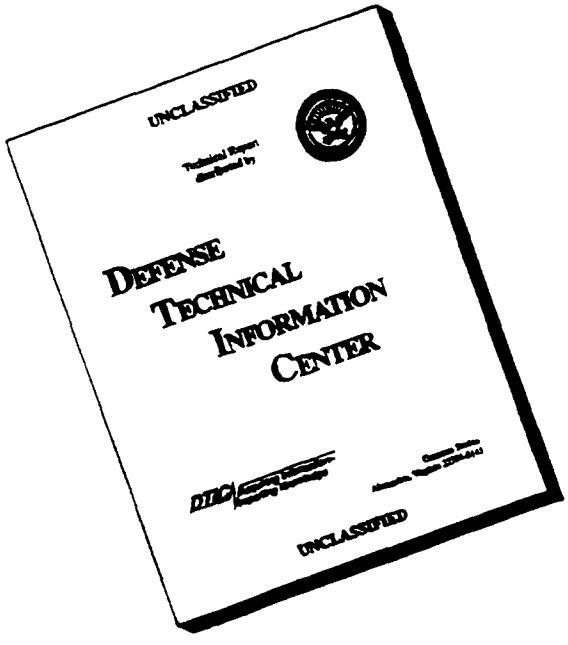

THIS DOCUMENT IS BEST QUALITY AVAILABLE. THE COPY FURNISHED TO DTIC CONTAINED A SIGNIFICANT NUMBER OF PAGES WHICH DO NOT REPRODUCE LEGIBLY.

Please expedite

PLEASE CHECK THE APPROPRIATE BLOCK BELOW: OCA 5/27/97 JM

-AQ # M97-08-5391

☐ 1 copies are being forwarded. Indicate whether Statement A, B, C, D, E, F, or X applies.

☒ DISTRIBUTION STATEMENT A:
APPROVED FOR PUBLIC RELEASE: DISTRIBUTION IS UNLIMITED

☒ DISTRIBUTION STATEMENT B:
DISTRIBUTION AUTHORIZED TO U.S. GOVERNMENT AGENCIES ONLY; (Indicate Reason and Date). OTHER REQUESTS FOR THIS DOCUMENT SHALL BE REFERRED TO (Indicate Controlling DoD Office).

☐ DISTRIBUTION STATEMENT C:
DISTRIBUTION AUTHORIZED TO U.S. GOVERNMENT AGENCIES AND THEIR CONTRACTORS; (Indicate Reason and Date). OTHER REQUESTS FOR THIS DOCUMENT SHALL BE REFERRED TO (Indicate Controlling DoD Office).

☐ DISTRIBUTION STATEMENT D:
DISTRIBUTION AUTHORIZED TO DoD AND U.S. DoD CONTRACTORS ONLY; (Indicate Reason and Date). OTHER REQUESTS SHALL BE REFERRED TO (Indicate Controlling DoD Office).

☐ DISTRIBUTION STATEMENT E:
DISTRIBUTION AUTHORIZED TO DoD COMPONENTS ONLY; (Indicate Reason and Date). OTHER REQUESTS SHALL BE REFERRED TO (Indicate Controlling DoD Office).

☐ DISTRIBUTION STATEMENT F:
FURTHER DISSEMINATION ONLY AS DIRECTED BY (Indicate Controlling DoD Office and Date) or HIGHER DoD AUTHORITY.

☐ DISTRIBUTION STATEMENT X:
DISTRIBUTION AUTHORIZED TO U.S. GOVERNMENT AGENCIES AND PRIVATE INDIVIDUALS OR ENTERPRISES ELIGIBLE TO OBTAIN EXPORT-CONTROLLED TECHNICAL DATA IN ACCORDANCE WITH DoD DIRECTIVE 5230.25, WITHHOLDING OF UNCLASSIFIED TECHNICAL DATA FROM PUBLIC DISCLOSURE, 6 Nov 1984 (Indicate date of determination). CONTROLLING DoD OFFICE IS (Indicate Controlling DoD Office).

☐ This document was previously forwarded to DTIC on _____ (date) and the AD number is _____.

☐ In accordance with provisions of DoD instructions, the document requested is not supplied because:

☐ It will be published at a later date. (Enter approximate date, if known).

☐ Other. (Give Reason)

DoD Directive 5230.24, "Distribution Statements on Technical Documents," 18 Mar 87, contains seven distribution statements, as described briefly above. Technical Documents must be assigned distribution statements.

_____
Print or Type Name

_____
Authorized Signature/Date

_____
Telephone Number

REPORT DOCUMENTATION PAGE

Form Approved
QMB No. 0704-0188

1. AGENCY USE ONLY (*Leave Blank*)	2. REPORT DATE	3. REPORT TYPE AND DATES COVERED
	September 1996	

4. TITLE AND SUBTITLE

Development of Data Fusion Algorithms for Detecting and Identifying Ordnance with Magnetometers and Ground Penetrating Radar

5. FUNDING NUMBERS

6. AUTHOR(S)

Eugene R. Leach and Associates

7. PERFORMING ORGANIZATIONS NAME(S) AND ADDRESS(ES)

Naval Explosive Ordnance Disposal Technology Division
Project Manager: Gerard Snyder 301-743-6855 ext 260
Engineer: Arnold P. Burr 301-743-6850 ext 270
2008 Stump Neck Road
Indian Head, Md. 20640-5070

8. PERFORMING ORGANIZATION REPORT NUMBER

NAVEODTECHDIV

9. SPONSORING/MONITORING AGENCY NAME(S) AND ADDRESS(ES)

U.S Army Environmental Center
Project Officer: Kelly Rigano 410-612-6868
Aberdeen Proving Ground, MD 21010-5401

10 SPONSORING/MONITORING AGENCY REPORT NUMBER

SFIM-AEC-ET-CR-97020

11 SUPPLEMENTARY NOTES

12a DISTRIBUTION/AVAILABILITY STATEMENT

~~Unlimited Distribution~~

12b. DISTRIBUTION CODE

A B

13. ABSTRACT (*Maximum 200 words*)

This report records work performed to develop data fusion algorithms to detect buried unexploded ordnance with magnetometers and ground penetrating radar. Task I characterized the performance of a cesium magnetometer, a gradiometer, and a 3-axis fiber optic magnetometer. Data which was measured and/or generated by validated models were used to develop a set of appropriate target features that could be used to identify and characterize buried ordnance. The applicability of applying techniques such as the use of neural nets, fuzzy logic and wavelets to the ordnance detection and identification problem were also evaluated.

14. SUBJECT TERMS

Unexploded Ordnance, Magnetometers, Gradiometers, Ground Penetrating Radar, Data Fusion

15. NUMBER OF PAGES

16. PRICE CODE

17. SECURITY CLASSIFICATION OF REPORT	18. SECURITY CLASSIFICATION OF THIS PAGE	19. SECURITY CLASSIFICATION OF ABSTRACT	20. LIMITATION OF ABSTRACT
UNCLASSIFIED	UNCLASSIFIED		

Development of Data Fusion Algorithms for Detecting and Identifying Unexploded Ordnance with Magnetometers and Ground Penetrating Radar

FINAL REPORT

Contract No. N00174-95-C-0027
TASK I
CDRL Report 003

September 20, 1996

Submitted to

Commanding Officer
Naval Explosive Ordnance Disposal Technology Division
Code NEODTD 50B22
Indian Head, MD 20640-5070

Submitted by

Eugene R. Leach
Eugene R. Leach and Associates
1356 W. Second Avenue
Columbus, OH 43212

Milton R. Seiler
Consultant

Table of Contents

List of Figures

List of Tables

Disclaimer

This report is a work prepared for the United States Government by Eugene R. Leach & Associates. In no event shall either the United States Government or Eugene R. Leach & Associates have any responsibility or liability for any consequences or any use, misuse, inability to use, or reliance upon the information contained herein, nor does either warrant or otherwise represent in any way the accuracy, adequacy, efficacy, or applicability of the contents hereof.

Acknowledgments

The authors wish to acknowledge the support of Ms. Kelly Rigano, U.S. Army Environmental Center, and the Contracting Officer's Technical Representative for this task, Mr. Gerard Snyder, Naval Explosive Ordnance Disposal Technology Division (NAVEODTECHDIV). We appreciate the technical comments and suggestions provided by Mr. Arnold Burr, NAVEODTECHDIV. We thank Mr. Bobby Walters, Advanced Engineering Concepts, Inc., for his hardware and software support.

1.0 INTRODUCTION

1.1 BACKGROUND

Hazardous waste and ordnance contamination is a primary environmental and safety concern at a number of military installations scheduled for closure. The environmental cleanup of military installations is congressionally directed under the Defense Environmental Restoration Program (DERP).[1] DERP efforts were intended to cover both active installations and formerly used DoD properties and include the following:

- o Hazardous and Toxic Waste Disposal
- o Ordnance and Explosive Waste Removal
- o Building Demolition and Debris Removal

The estimates of such clean-up costs, however, far exceed the appropriations. For example the 1989 estimate to cleanup the ordnance (explosive munitions and depleted uranium penetrators) for the Jefferson Proving Ground in Madison, Indiana was more than $500 million.[2] Consequently, in order to make ordnance contaminated site restoration practical, the cost of the restoration must be significantly reduced. Technological advances have a major role to play in lowering the cost of detection, identification, excavation, and disposal of ordnance and other environmental contaminants.

The Indian Head Division of the Naval Surface Weapons Center issued in 1993 a broad agency announcement(BAA) for Fundamental and Applied Technologies in the unexploded ordnance area.[3] This effort was to be technically monitored by the Naval Explosive Ordnance Disposal Technology Division(NAVEODTECHDIV) under tasking from the U.S. Army Environmental Center. The goals of this effort were to develop capabilities to achieve the following:[4]

- o rapid surveys of large areas regardless of terrain
  - determine density of unexploded ordnance(UXO)
  - establish boundary of the contamination
- o ability to discriminate and identify detected UXO
  - maximize detection and reduce false alarms
- o accurately determine UXO location, size, depth and orientation
- o demonstrate technology integration from complementary systems

- o reliable systems that can provide an economical means of characterizing and remediating UXO-contaminated sites.

The development of a Subsurface Ordnance Characterization System(SOCS) as part of the NAVEODTECHDIV effort was to provide an autonomous ground towed system. This system would be capable of utilizing multiple sensors operating simultaneously and incorporating sensor specific discrimination techniques and also provide a very precise target locating capability. The system would also serve as a test bed for demonstrating new technologies.

Previous ordnance detection, identification and navigation technologies have summarized in a report prepared for the US Army.[5][6] Historically, traditional surveillance systems have relied upon a single sensor (such as radar or some form of a magnetometer) for target detection. In many of these types of systems, optimal signal processing was based on statistical estimation and hypothesis testing methods.[7] Recently, as reflected by the cited BAA, there has been a great deal of interest, driven by diverse military requirements including range clearance, in the synergistic use of multiple sensors to significantly increase the capabilities of mobile surveillance systems.

For a mobile platform such as SOCS which utilizes a variety of sensors for locating and identifying buried ordnance, the classical signal processing techniques may be inadequate because of the dissimilar nature of the sensors. Consequently, the classical framework of detection theory must be extended to provide an optimal combination of sensors for ordnance detection.

1.2 SCOPE OF THIS PROGRAM

Eugene R. Leach and Associates in response to this BAA proposed a two-task effort to develop data fusion algorithms to detect buried unexploded ordnance with magnetometers and ground penetrating radar. In Task 1 of the effort the performance of total field and multiaxis magnetometers such as the cesium magnetometer, a gradiometer and a 3-axis fiber optic magnetometer were to be characterized and cataloged. Data which has been measured and/or generated by validated models were to be used to develop a set of appropriate target features that can be used to identify and characterize buried ordnance. The applicability of applying techniques such as the use of neural nets, fuzzy logic and wavelets to the ordnance detection and identification problem were to be evaluated. This report is directed towards the presentation of the results of the Task 1 efforts.

2.0 MAGNETOMETERS

2.1 THE EFFECT OF BURIED ORDNANCE ON THE EARTH'S MAGNETIC FIELD

Buried ordnance possess an induced magnetic dipole that has a measurable effect on the earth's magnetic field. The perturbing field intensity **H** of an arbitrarily oriented dipole with magnetic moment **M** may be expressed in terms of its components H_x, H_y, and H_z (z axis is vertical) in a Cartesian coordinate system whose origin coincides with the dipole and the dipole is chosen to lie in the x-z plane:[8]

$$H_z = (1/4\pi)|\mathbf{M}|\{(2z^2-x^2-y^2)\cos\beta-3xz\sin\beta\}[x^2+y^2+z^2]^{-5/2}$$

$$H_y = (y/z)H_z+(y/z)|\mathbf{M}|(x^2+y^2+z^2)^{-2}$$
$$*\{(y^2z^2+[xz\cos\beta+z^2\sin\beta]^2)+(xz\sin\beta+(x^2+y^2)\cos\beta)^2\}^{1/2}([x+z\tan\beta]^2+y^2)^{-1/2}(1/4\pi)$$

$$H_x = (x/z)H_z+|\mathbf{M}|(x+z\tan\beta)$$
$$*(x^2+y^2+z^2)^{-2}(1/z)$$
$$*\{y^2z^2+(xz\cos\beta+z^2\sin\beta)^2+[xz\sin\beta+(x^2+y^2)\cos\beta]^2\}^{1/2}([x+z\tan\beta]^2+y^2)^{-1/2}(1/4\pi)$$

where $|\mathbf{M}|$ is the magnitude of the magnetic moment **M** and β is the angle between the dipole and the z axis.[9]

The total local field in the vicinity of the dipole is

$$\mathbf{H_T} = \mathbf{H} + \mathbf{H_o}$$

where $\mathbf{H_o}$ is the ambient field of the earth. Magnetometers detect this change in the earth's local field which may indicate the presence of buried ordnance.

Rigorous calculations using a buried general ellipsoid and ellipsoidal shell to model the perturbing field **H** of buried ordnance have been developed for the Naval Explosive Ordnance Disposal Technology Division, Indian Head MD for use with the MK 22 ferrous ordnance locator OPEVAL.[10] The model is written in Fortran and has not to-date been successfully rewritten in "C". It could not therefore be used as a source of "data" for this effort. A similar model was presented at the recent UXO Forum 1996 conference.[11]

2.2 GENERAL MAGNETOMETER DISCUSSION

Passive magnetic locators (typically referred to as magnetometers) detect anomalies in the earth's magnetic produced by ferromagnetic targets. There are generally two types of magnetometers: those which respond to the magnitude of the local magnetic field strength, and those which respond to the gradient or rate of change of the local magnetic field. This latter type is sometimes called a gradiometer. A given type of magnetic sensor can be used to construct either type of magnetometer.

Historically there have been several different types of magnetometers which have been used for buried ordnance detection: flux-gate magnetometers used in the Navy MK 10 and EC-37[12], optically pumped magnetometers used in the Navy MK 22[13] and Surface Towed Ordnance Locator System (STOLS)[14], and nuclear precession magnetometers (sometimes called proton precession magnetometers) used in the MK 14 and EX 11[15].

Magnetometers should be capable of detecting magnetic fields as low as 0.01 to 10 gamma (10^{-7} to 10^{-4} gauss) range if they are to be useful for buried ordnance detection. Thus, state-of-the-art Hall effect sensors, sensors which use magnetodiodes or magnetotransistors, and magneto-optical sensors lack sufficient sensitivity for ordnance detection applications.

Other types of magnetometers which have been considered are the Superconducting Quantum Interference Device (SQUID) magnetometers used in S.H.E. Corporation's GMS-45 for geophysical applications[16], magnetoresistive magnetometers used in fuzes[17], and fiber optic magnetometers[18].

Although these magnetometers possess great sensitivity they can only indicate that there is a local anomaly in the earth's magnetic field; they cannot identify the magnetic anomaly. Neural network-magnetometer systems may contribute to the capability of distinguishing the magnetic signature of buried ordnance from buried shrapnel and other man-made and naturally occurring magnetic anomalies.

2.3 TEST SENSORS

Magnetometers selected for evaluation in this study were the commercial Geometrics G-822L Cesium Magnetometer, a commercial Vallon EL 1302 ferrous locator and a laboratory prototype of a 3-axis fiber optic magnetometer. All testing for these magnetometers was conducted in a rural region south of Columbus OH.

2.3.1 Geometrics G-822L Cesium Magnetometer

The G-822L cesium magnetometer is an improved versions of the military Mk22 odnance locator. The cesium vapor magnetometer is an optically-pumped sensor

which uses a radio frequency(rf) driven cesium atomic vapor. Geometrics has commercially available two optically pumped magnetometers: one employing cesium and the other helium.[19] The helium version is the model 833. The cesium magnetometer is essentially a digital version of the Mk22 military ferrous ordnance locator. The 822 has recently been superceeded by a 858 version which incorporates a data logger and a Global Positioning System(GPS). Both the 822 and the 858 are packaged as a two cylinder pair with a cable between them. Both sensors require an external counter to convert the Larmor frequencies into an RS-232 signal that represents the oscillation measurements as a gamma reading. The cesium magnetometer comes with a counter that has a resolution of 0.1 gamma with a sampling rate of 10 Hz. The sensor provides a magnetic field measurement range of 20,000 to 95,000 gamma.

Geometrics previously had available for the 822L, in addition to the counter display console, an optional miniature computer data acquisition system with G822LOG software installed.[20] This data acquisition system is no longer available as an off-the-shelf accessory. Thus, in order to acquire the quantity of data needed for this study we developed the software and hardware to allow us to acquire data from the G- 822 at the 10 Hz sampling rate using a laptop computer. The software is controlled by the keyboard of the laptop(a Compaq Contura) or by a remote control and provides for single or continuous sampling with the magnetometer. Data stored in the laptop can be imported into commercially available contouring programs such as MAGLOC and Golden's SURFER. This software is presented in Appendix A. Geometrics specifications for the G- 822L are shown in Table 2-1.[21]

2.3.2 Vallon El 1302A1 Gradiometer

The Vallon EL 1302A1 gradiometer is used for detecting buried ferrous objects in the ground by measuring the magnetic field gradients with the second harmonic method.[22] It is a very sensitive instrument which allows field strength measurements in the range of 0.5 to 2000 gammas. The measured result is indicated by a meter with regard to polarity and strength. In addition, the iron detector is provided with an analog output for connection to a thermal recorder and/or a micro computer (designated as the MC1). The micro computer was not available for our measurements and all data were manually recorded from the indicating meter. Detector amplification can be varied to seven settings which allow field measurements to be made in seven scales. These were 100, 30, 10, 3, 1, 0.3 and 0.1 gamma/scale degree.

The ferrous detector consists basically of the following parts:

o Separately connected detectors arranged in a sensor protecting tube which can be screwed- off for adjustment of the sensor, a fix mounted indication meter and a

Table 2-1. Specifications for the Geometrics G-822L

Operating Principle	Self-oscillating split-beam cesium vapor magnetometer
Range:	20,000 to 95,000 gammas
Resolution:	1 part in 50,000
Heading error:	+/- 1 gamma
Output:	5-digit display, audio tone through non-magnetic speaker or headphones and RS-232 at 1200 or 9600 baud
Environmental:	Operates from -35 to +50 deg C, waterproof, operates with sensor immersed in water to a depth of 1 meter
Power:	Waist-carried rechargeable battery pack(supplied with 110/220 volt charger
Physical:	Sensor wand: 1.22 m X 74 mm, 1.8 kg
	Display electronics: 25 X 18 X 10 cm, 2.3 kg
	Total system weight: with battery, 8.8 kg

slewable carrying bar with control panel and connection socket for an earphone.

o Electronic housing with a battery compartment for 6 D-cells as well as voltage stabilization circuits, signal amplifier with outputs for the indication meter, thermal-recorder as well as Micro-CAMAD. A function selector for "lin", "log" as well as "battery check".

Technical data for the 1302A are presented in Table 2-2.

2.3.3 Three-Axis Fiber Optic Magnetometer Prototype

Two types of fiber optic transducers have been suggested for use in magnetic field measurement.[23] In one type the fiber is coated with a magnetostrictive material such as metglas either over the bare fiber or over a fiber already coated with a nonmagnetic material yielding a continuous length of magnetically sensitive fiber. In another approach the fiber is wrapped around a magnetostrictive material whose dimensions are dependent on the direction and extent of the magnetic field. The use Mach-Zehnder interferometers using transducers such as these have been technically evaluated over the past decade and several approaches have been proposed and evaluated.

Optical Technologies has fabricated under NAVEODTECHDIV support a Prototype Tri-Axial Magnetometer System(PTFOM).[24] The PTFOM (shown in Figure 2.3) detects a magnetic field utilizing a fiber-optic interferometer to measure magnetostriction in three mutually perpendicular transducers. Magnetostriction is the effect which causes a ferromagnetic material to undergo a dimensional change when exposed to a magnetizing field. The particular magnetostrictive material used is metglass. The metglass is formed into a cylinder and wound with single-mode optical fiber. This fiber constitutes the sensing path in a fiber optic interferometer. When the METGLASS undergoes a dimensional change due to the presence of a magnetizing field the fiber optic is strained. A second path serves as a reference arm. When the light in the two paths is combined, interference occurs. The interference is in the form of phase modulation proportional to the strain in the sensing fiber. The phase modulation at the output of each interferometer is detected and converted to a voltage proportional to the magnetic field. The three voltages are digitized and processed in software to give an indication of total field, relative field, and relative field azimuth and elevation. The data is presented to the user via a Liquid Crystal Display(LCD)

The PTFOM is composed of two major assemblies: a boom assembly and a backpack. These units are connected via a multi-wire cable. The boom assembly weighs approximately 20 pounds. The backpack assemble weighs approximately 15 pounds. No operating specifications for this device were provided. The boom assembly

Table 2-2. Specifications for the Vallon EL 1302A1

Power supply:	6 X 1.5 volt round cells(IEC R 14) or 6 Ni-Cad RSH 1.8
Operating weight of set:	~4.5 kg(without earphone)
Distance of sensors:	510 mm
Diameter of sensor tube:	42 mm
Sensitivity steps:	7 with 20 scale divisions- full scale deflection of 20000, 6000, 2000, 600, 200, 60 and 20 gammas
Function mode:	lin x 1, lin x10, log, battery check
Indication:	Visual and acoustical
Signal output:	Analog measuring voltage 0 to +/- 5 volts for analog recorder 0 to +/-6.2 volts or micro-computer MC1
Operational time:	~20 h with alkaline batteries
Transportation case:	785 x 285 x 140 mm
Shipping weight of set:	~ 11 kg
Dimensions of exterior battery power supply	60 x 30 x 170 mm

includes the following components:[25]

1. Detector head - The detector head contains the METGLAS sensors and Michelson interferometers.

2. Down-stem - The downstem mechanically couples the detector head to the electro-optic module and provides a conduit for fiber and wire connections between the two.

3. Electro-optic module - The electro-optic module contains the optical source,associated drive circuitry, optical isolator and polarizer, optical couplers and connectors, and optical receivers.

4. Liquid crystal display - The Liquid Crstal Display(LCD) provides a digital display to the operator and is mounted in a unit along with the system power switch and five push-buttons for display selection.

5. Battery box - The battery box is a container which houses a 12V 8 A-hr gel-cel battery, a battery charging jack and charging indicator, a 32V 2.5A fuse, a pair of DC/DC convertors and three multipin connecting jacks and three BNC connectors which can be used forf degrausing the sensing elements as required.

Numerous operating problems were encountered in the use of this prototype. In many instances the battery did not appear to be taking an appropriate charge. A charger was acquired from the battery manufacturer and the limited quantity of magetic field measurement data taken were consistently significantly higher in magnitude than those taken with the Geometrics cesium vapor magnetometer. The measured field values were not consistant with the earth's field levels for the Ohio region. This fiber optic magnetometer then ceased to function and no data could be collected.

3.0 ORDNANCE

The land clearance problem includes all munitions which could range from 20 mm to 8-inch projectiles, mortars, air dispersed mines and bombs. For this study six pieces of inert ordnance were provided by NAVEODTECHDIV. These inert-certified items were as follows:

o 60 mm HE mortar M49 with M525 fuze	ID No.2549
o 60 mm HE mortar M49 with M525 fuze	ID No.2550
o 105 mm HE projectile, M1	ID No.2551
o 105 mm HE projectile, M1	ID No.2552
o 155 mm HE projectile, with M557 fuze	ID No.2553
o 155 mm HE projectile, with M557 fuze	ID No.2554

Pictures of these ordnance types are presented in Figures 3-1 through 3-4. Drawings of these ordnance items are presented in Figure 3-5. The physical characteristics of these ordnance items are shown in Table 3-1.[26]

Table 3-1. Test Ordnance Characteristics

ordnance type	inert weight,kg	length,m	Average impact velocity[1], m/s	estimated maximum penetration, m sandy	estimated maximum penetration, m clay
60 mortar	1.47	0.29	7.9	0.26	0.79
105	14.3	0.42	211.2	1.45	3.04
155	43.2	0.61	211.2	2.24	4.36

The ability to detect these ordnance items depend upon their depth of burial and their orientation relative to the earth's field. The depth of penetration of a projectile into the soil is a function of projectile weight, shape, impact velocity, angle of entry and soil characteristics. The depth of penetration of a projectile is typically very unpredictable. Behavior variations could include end-over-end movements and resurfacing after in ground ricochet. "J" shaped underground penetration paths are typical for many projectiles. Penetration of bombs and projectile into soil can be estimated from a

[1] The depth of penetration of a projectile into soil is function of the projectiles nose tip shape and the impact velocity

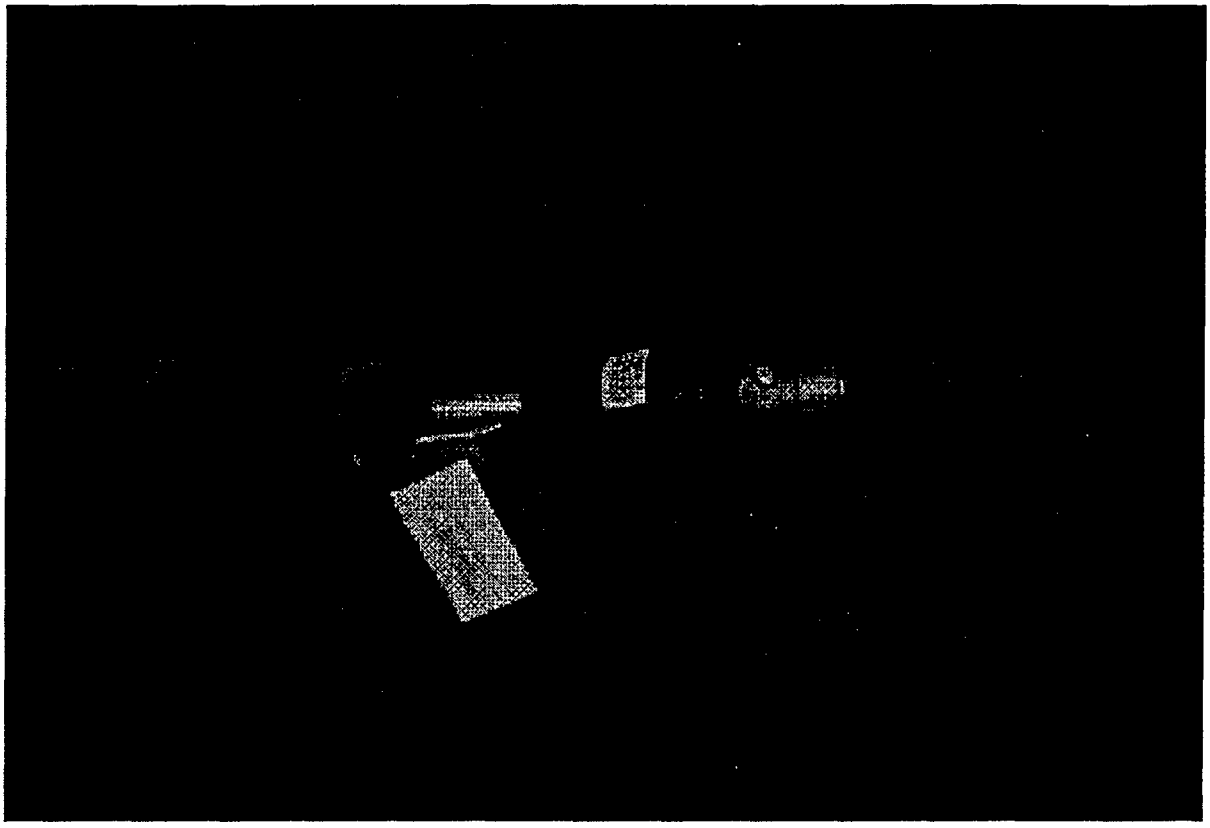

Figure 3-1. 60 mm HE mortar M49

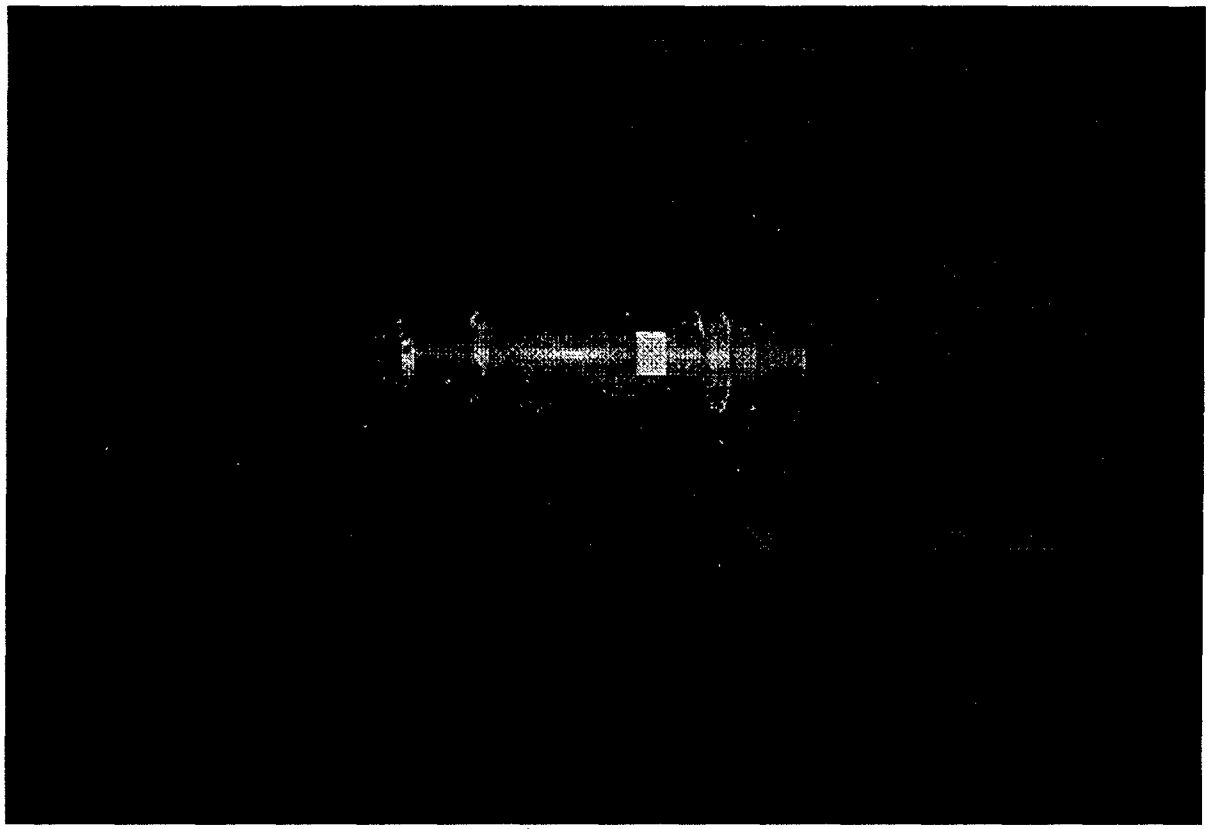

Figure 3-2. 105 mm HE Projectile

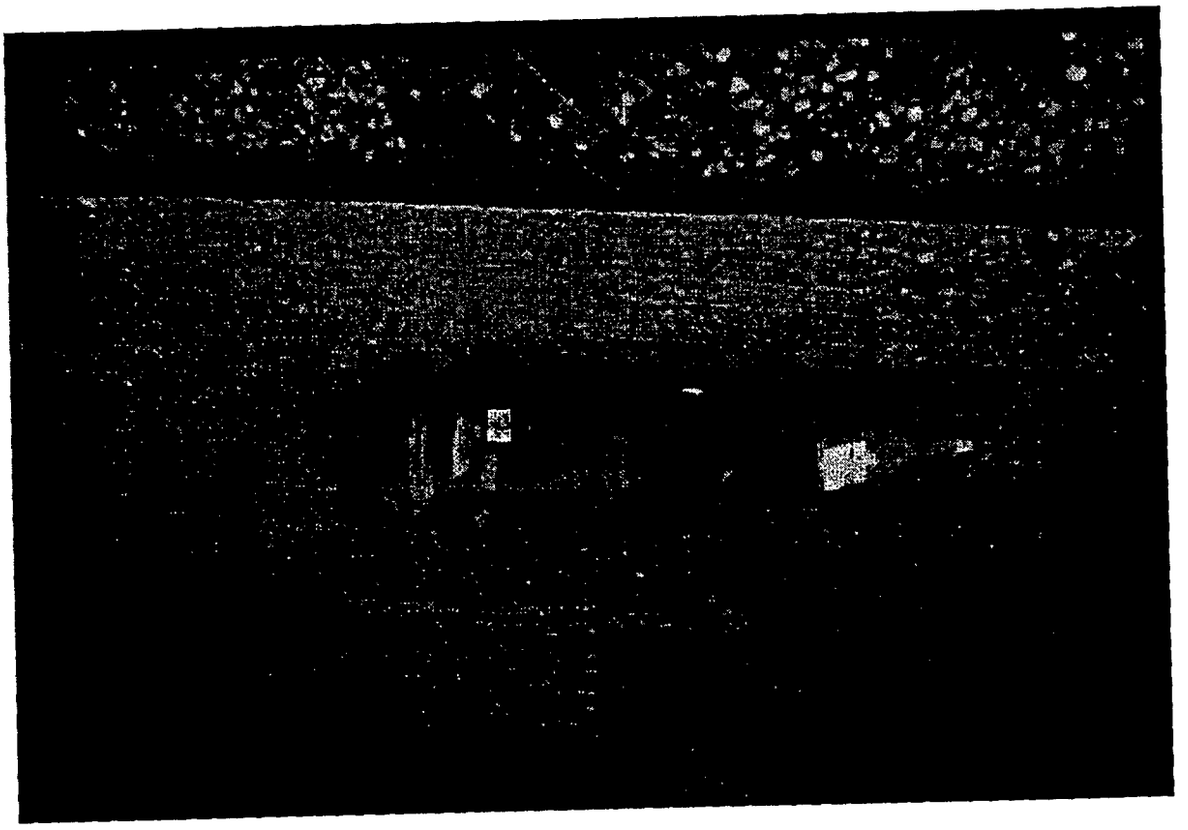

Figure 3-3. 155 mm HE Projectile

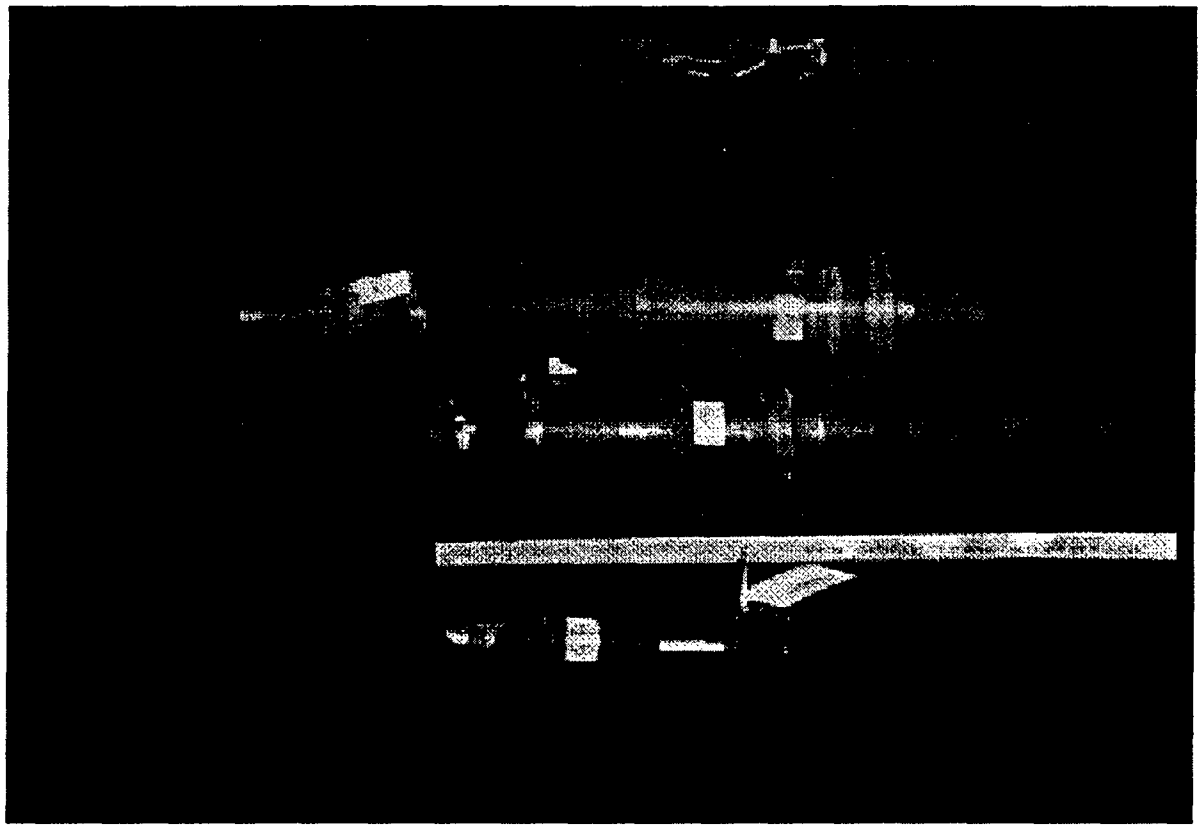

Figure 3-4. 60 mm Mortar, 105 mm and 155 mm Projectiles

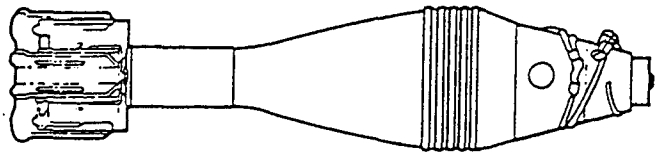

60 mm Mortar

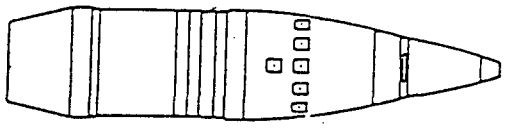

U.S. 105-mm Projectile,

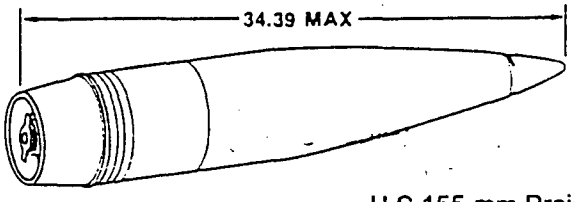

U.S.155-mm Projectile

(not to scale)

Figure 3.5. Geometric Depiction of the 60 mm Mortar, 105 and 155 Projectiles

nomogram presented in Reference 28.

4.0 SENSOR FUSION

4.1 MULTIPLE SENSOR SYSTEM

In a generic advanced multiple sensor system each sensor or detection system has the capability to make a decision on whether or not an anomaly has been detected. Each sensor then communicates this decision to a data fusion center which evaluates the information and makes a determination as to whether an ordnance item has been detected. This decision making process can be modeled in the following manner.

Consider the system shown in the figure on the following page. Let each detector D_i, make a decision u_i, based on its observation y_i, I = 1, 2,...,N of an anomaly H (y_i could be the radar return for a GPR, field change for a magnetometer, temperature change for an IR system, etc.). Each decision u_i may take the value of 0 or 1 depending on whether the detector D_i(GPR, IR, magnetometer, etc.) decides between two hypotheses H_o or H_1. H_o may be the hypothesis that some target of interest is not present. H_1 that the target of interest is present. The data fusion center makes a global decision **U** (ordnance item is or is not present) based on the an evaluation of the individual decisions u_i of each detector. The detection characteristics of each local detector are usually specified by a probability of detection P_{di} and a probability of false alarm P_{fi}.

In a multi sensor system that would include a ground penetrating radar (GPR) and a magnetic anomaly detector for example, both the GPR and the magnetic field sensor are designed to be sensitive to a particular parameter(an electromagnetic wave in the case of the GPR and a change in the local magnetic field for a magnetic sensor). Because these sensors do not distinguish ordnance items from clutter having similar conductive or magnetic properties, it is often difficult to make an accurate global decision on whether an ordnance item has been detected, based on a set of decisions from each sensor, u_1, u_2,...,u_N, that may contain errors. In the remainder of this section we briefly describe a variety of statistical and pattern recognition techniques that may be employed to alleviate this problem.

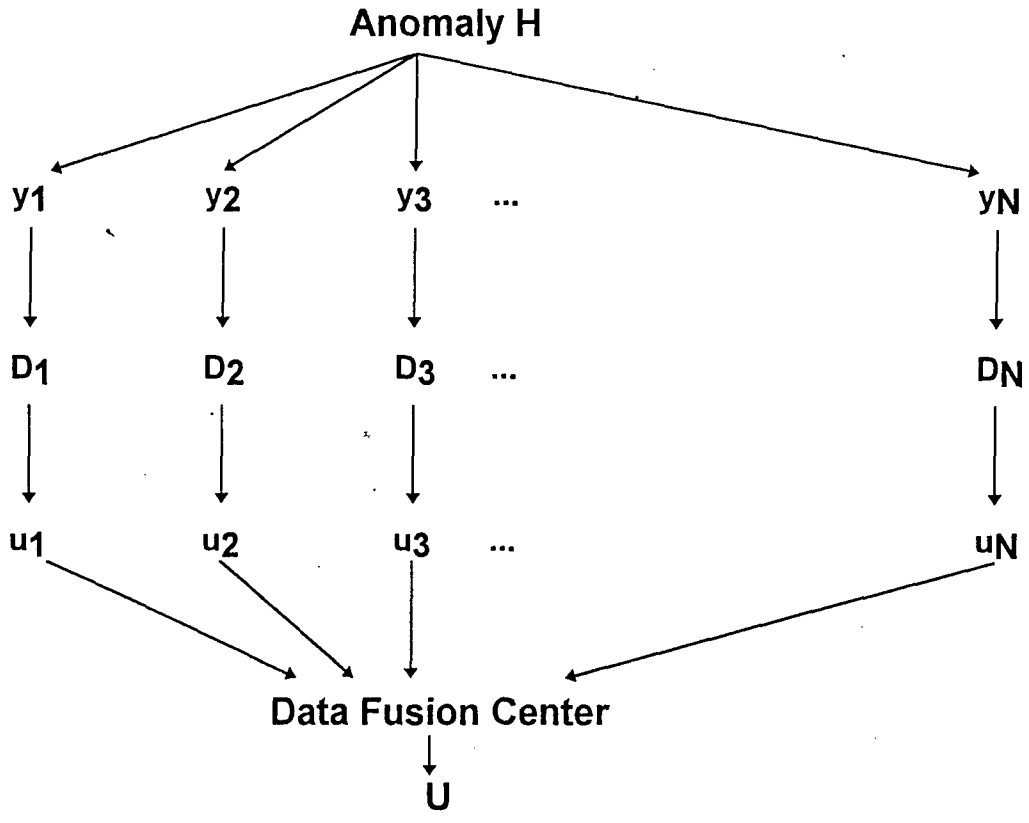

A portion of the technical efforts for this task concentrated on the acquisition and review of relative technical documentation related to the evolution of such a data fusion system by technology developed for expert systems. Topics covered included pattern recognition, neural nets, fuzzy logic and technical information associated with the magnetometers being evaluated under this program. Neural nets and fuzzy logic are briefly discussed in the following text.

4.1.1 Neural Networks

Neural networks are modeled after biological neural nets which are composed of many simple processor cells (neurons) each cell having many connections to other cells. Neurons send and receive signals between themselves depending on whether the sum of the input signals exceeds a prescribed threshold. The connections between the processing elements are weighted. These weights serve as memory for the network. The processing speed of the network as well as its memory capacity is determined by the number of connections between the processing elements. Training the net to perform some task involves adjusting the weights of these connections.

Neural nets can "learn" a target signature by adjusting the net's interconnection weights. This action stores the target signature in the net memory. Using the stored library of target signatures in the net memory, neural nets have correctly identified targets from target signature data that has been incomplete or corrupted by noise.[27]

For ordnance detection applications, using the target signature data generated by the platform sensors, the neural net must be trained to be able to distinguish an ordnance signature from the following: radar returns from rocks and other soil inhomogeneities in the case of the GPR, magnetic anomalies in the case of magnetic field sensors, and other anomalies and clutter that would affect the platform sensors. To accomplish this, some representative features of the ordnance item must be presented to the neural net for it to "learn". Radar techniques which use the target's complex resonances would be an appropriate starting point for extracting ordnance features that the neural net could learn. Ordnance magnetic measurement data and/or a validated magnetometer model could also be used as input to the neural net.

4.1.2 Fuzzy Sets

Fuzzy sets, unlike conventional sets, do not have a sharply defined membership as for instance the set of all even numbers. The transition between membership and non-membership is gradual rather than sharp in a fuzzy set. The degree of membership in a fuzzy set is specified by a number between 1.0 signifying full membership and 0.0 signifying non-membership. For example, in the set of expensive cars, a Rolls Royce might have a membership grade of 1.0 (full member), a Cadillac may have a membership grade of 0.5 (partial member), and a Toyota Tercel a grade of 0.0 (not a member).

Because fuzzy sets allow more freedom in the classification of data, they have proved to be effective in pattern recognition and decision making where often the data or the choices presented are not amenable to a simple YES-NO type of decision.[28]

Fuzzy sets can also be used in conjunction with neural net techniques to create a more flexible ordnance detection system which can determine "how close" a particular sensor signature pattern matches a stored ordnance item signature in the Data Fusion Center memory and to reduce the time needed to train the neural net on new ordnance signature data.[29]

4.3 MAGNETIC SENSOR FUSION WITH FUZZY LOGIC AND NEURAL NETWORKS

The task of buried ordnance detection, location, and classification will require the ultimate use of a variety of sensors. When these sensors are located on moving surveillance vehicles, whose locations are monitored by precise navigation systems such as GPS, there will be a need to collect, store, and process the data in such a manner as to allow decisions about the size, type, and location of the objects that are producing the signals to be made in acceptable time periods. Some sensors may only be used for initial detection of object presence, while others may yield additional information as to the object classification.

Sensor fusion, as previously mentioned, is a concept widely used in the past decade to integrate information in such a manner that will allow more valid conclusions about the object location and classification than would any single sensor, or, for that matter, even from the sum of the information from the sensors.

There have been numerous studies and fusion strategies for the various types of sensors with application to radar target detection and optical image processing.[30] Dasarathy has made a study of four fusion approaches that have potential for being more innovative than conventional approaches.[31][32] By this is meant that the process must be highly flexible in the nature and number of inputs. The approach must also allow for other inputs such as ground speed of the traversing vehicle, data interval, vehicle navigation coordinates and other information that may become available. Dasarathy found four innovative concepts or approaches after studying related fields such as artificial intelligence and pattern recognition. In his study these four, and only these four, were found to be suited for real-world field data. They were: (1) Neural Network (NN) Approach, (2) Adaptive Learning (AL) Approach, (3) Evidential Reasoning (ER) Approach, and (4) Concurrence Seeking (CS) Approach. The first two permit both decision and feature extraction inputs to the fusion process. The last two primarily handle only decision level inputs. Dasarathy further concluded that the first two were the most promising and he examined them in greater detail through simulation experiments. His preliminary conclusion was that the AL approach was preferred if there was a problem in the convergence of training data in the NN approach.

In our current study of the signals from various types of ordnance rounds, and in the application of those signals to the training of neural networks, we do not have conclusive evidence that convergence of the training data will be a problem. Furthermore, since the NN approach was the primary method to be explored on the contract, and since the sensor fusion by neural network can allow for feature inputs arising from fuzzy logic algorithms, the NN approach appeared to be the most simple and direct route to successful sensor fusion. It is important to point out that the AL approach differs from traditional fusion systems in that a feedback learning loop is

added to update the fused decision. This allows for progressive improvement of the output decision, even with target classes that are currently unknown, by examination and review by the operator. Both the NN and AL approaches require a training phase, need ground truth (in our case navigation data), require data normalization, are adaptable to new data, require prior experience with the method, can handle decision as well as feature inputs, have good expansion capability to more inputs, and can provide outputs that give detection and classification labels. The operational phase computation load of the NN approach appears to be lower.

Figure 4.1 shows the NN approach to magnetic sensor fusion. There are three primary sensors, a total field magnetometer, a 3-axis magnetometer that resolves the three orthogonal components of the field, and a gradiometer, which is responsive to the magnetic field gradient in one or more directions. A GPS receiver provides navigation coordinates with sufficient accuracy, on the order of 0.1 meter, to allow computational algorithms to make decisions about target features. Feature extraction will never be precise. Fuzzy-logic feature extraction appears suited to this application by the very nature of the many unknowns associated with the ordnance object. These unknowns are the ordnance type (155, 105, mortar, etc), it's pointing direction, horizontal distance and direction from the sensor, it's depth below the surface, and even it's rotation angle about it's longitudinal axis (the rounds are all asymmetric from a magnetic standpoint).

Fuzzy-logic feature extraction will depend upon knowledge of the signal received versus location on the navigational grid. From the trends observed over a series of grid coordinates, the first features to be extracted are the presence and approximate size or mass of the object from the total field magnetometer. This instrument is likely to be a

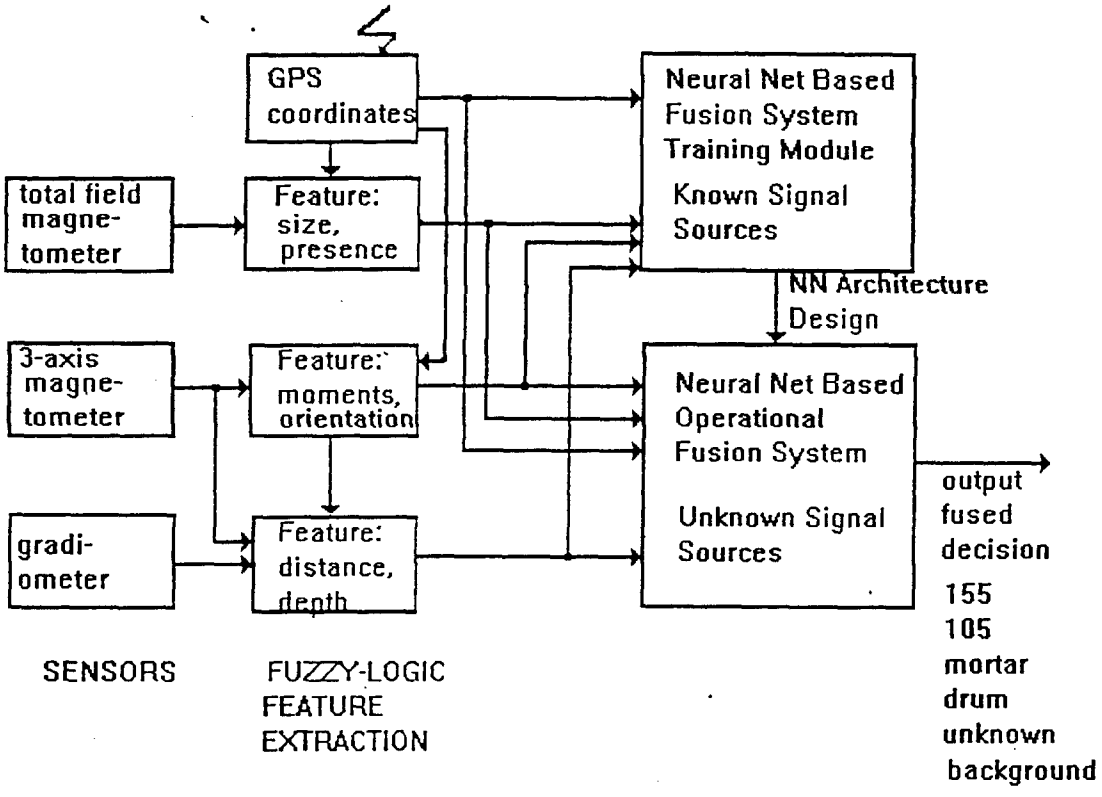

Figure 4-1. Neural Network/Fuzzy Logic Approach to Sensor Fusion

valuable screening element that alerts the other feature extraction networks. The second feature extraction is associated with the 3-axis magnetometer. By isolating the three orthogonal components of the measured field, rather than just the total field of the first sensor, the 3-axis system can estimate the three orthogonal magnetic moments of the object after trends are observed for varying grid coordinates and distances from the object. This in turn allows an estimate of the geometrical orientation of the object; i.e., the pointing direction. The third feature extraction uses the 3-axis and gradiometer signals to form an estimate of distance and depth of the object, depending upon which spatial gradients are measured. This distance evaluation is based upon simplified assumptions that lead to using the ratio of the magnetometer signal to the gradiometer signal-- the result being a measure of range. The basic equations assume that only one dominant moment is present in the object-- a condition that may rarely exist. Hence, we expect "noisy" feature extraction from this operation.

The output of the fuzzy-logic feature extraction becomes input to the neural network training or operational systems. The inputs to the neural networks are the extracted features and the initial signal data. Feature information may be in the form of normalized classification labels; i.e., relative numbers indicating size of the object or pointing direction, as well as derived numbers indicating distance and depth. With the passed-through sensor data, the neural network training can be accomplished. A variety of neural networks are available, including back-error-propagation (BEP), self-partitioning[33] and probabilistic[34]. Our experience on the current project has been limited to the BEP approach, which appears suitable based upon the limited quantity of data analyzed.

We have trained neural networks with data obtained from field measurements and found that there are advantages to having more than one network in the system. Greater convergence or correlation of predicted and measured data occurs when one neural network is assigned to predict only one output, regardless of the number of inputs. Hence, we envision a number of parallel neural networks in the training and operational system. Although not shown in Figure 4.1, this choice of system could lead to the necessity of a supervisory neural network that looks at the outputs of the previous parallel networks and subsequently makes a more educated overall output by looking for self-consistency and synergism.

Concepts learned in the training phase would be applied to the architecture of the operational neural network system. The system remains flexible since, even in the operational phase, new data always can be handled . The overall system can continually learn and improve as data or sensors are added.

The primary overall output of the system will be an indicator of the object classification, it's location on the grid coordinate system, and it's depth. Additional information, perhaps less critical, would be the pointing direction.

5.0 SELECTION OF A NEURAL NET MODEL

As part of this program numerous neural net and fuzzy logic models were evaluated relative to their applicability to the ordnance detection/identification problem. Literature searches showed that one previous study had been conducted which a neural net model was written in the C++ language. The software was developed to assist EOD technicians with the identification of ordnance items and appropriate render safe procedures.

A table with the title "Applications of Neural Networks" is presented in Appendix B. This is a compilation of the result of a survey which was conducted to reveal various neural net applications, the sensors or devices to input the neural network, the result or output of the network, and a reference. This list is only a small fraction of the hundreds of references occurring in the last five years, but it does indicate the very broad application of neural networks. The last two items in this table were found in Science Abstracts, Computers. They appeared to be particularly relevant, and the authors were contacted to obtain a copy of their papers.

Searches were conducted on the Internet for various available neural net and/or fuzzy logic models. An "under construction" compilation of Commercial Neural Network Software" was found. This compilation is presented in Appendix C.

Neural software demos were obtained from NeuroDimension of Gainesville. FL and ARD Corp of Columbia, MD. Information on software from Ward Systems Group of Frederick, MD was evaluated. The NeuroSolutions software from NeuroDimensions was by far the better package. It provided a wide range of control over the network design and training. The advanced version of the product could produce C language code for use in applications software. This would allow inclusion of the neural net in the data acquisition system instead of in a separate package. Problems were found in the Propagator demo from ARD Corp which prevented a thorough evaluation of its capabilities but they appear to be much less than the NeuroSolutions and NeuDesk(Neural Computer Services) software packages. The NeuroWindows and NeuroShell software from Ward Systems Group appear to be targeted mainly at financial predictions(stock market, horse racing, etc.)

A variety of neural net software tools were investigated. Seven tools were examined and rejected for use in this project due to lack of graphical ability, lack of control over the network, difficulty in use, etc. Neural net tools which showed promise for use with this project include:

- Nnmodel from Neural Fusion in Middletown, NY. This simulator has been used for several months on this project. It has good graphing tools and data manipulation but provides only limited control over the network itself.

- NeuDesk from Neural Computer Services in the United Kingdom. Provides extensive control over the network and its training including seven training algorithms. Many other tools are available from NCS for using the simulator data in real world applications.

The software program NNMODEL was obtained from the internet. The trial version is provided on the internet by Neural Fusion, 15 Standish Avenue, Middletown, NY, 10940. This is a backward- error- propagating (BEP) model with a considerable number of adjustable parameters. It can use either designed or unstructured data matrices. There are 15 examples of TEST SETS within the model, with descriptions, so that one may use them to gain some familiarity with the NNMODEL capability. An important feature of the model is that data matrices, as long as they are in the specified ASCII format, may be imported into a training or test matrix that fits the needs of the magnetometer program. The internet version of NNMODEL has been used for most of the program neural net analyses. A commercial licensed version of this software has not been obtained to-date. The NNMODEL software is discussed in Appendix D.

A Neural software demonstration package was obtained from NeuralWare. The NeuralWare Predict software is an automated neural product that provides solutions to prediction and classification network technology without requiring an in- depth knowledge of neural network technology. We found the technical assistance from NeuralWare to be very good. The demo program, however, did not readily allow us to input measurement data into the program. We would strongly suggest that the NeuralWare software be evaluated for future ordnance related data fusion applications.

6.0 TEST AND MODELING DISCUSSIONS

6.1 TESTS TO DERIVE MAGNETIC MOMENTS

A series of surveys were conducted for the purpose of obtaining magnetic field perturbation data caused by the three types of rounds under very controlled geometries. From this data, collected by the Geometric 822L total field magnetometer, approximate magnetic moments of the rounds could be obtained after analysis on a Mathcad 6.0 program. This program, using a dipole moment approach, was used to generate predicted magnetic field data, which in turn could be iterated to produce a best fit to the experimental data. The following subsections provide a description of the measurement grid, provide data on the surveys for the mortar, 105, and 155 rounds, provide a summary of the magnetic moments that were estimated for the rounds, and show typical diurnal variation data for the local magnetic field.

6.1.1 The Test Site

Surveys were conducted around a square, 90 cm on a side, at intervals of 15 cm. Figure 6-1 shows the orientation of the square and defines the direction of the surveys.

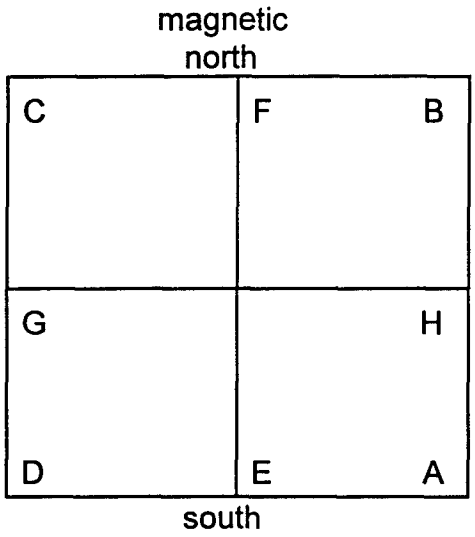

Figure 6-1. Survey Grid, 90 cm on a side

For each survey the round was placed in the center of the square and the survey was conducted in one of six different ways:

AB. Along a line from A to B, the east side of the square.
BC. Along a line from B to C , the north side of the square.
CD. Along a line from C to D, the west side of the square.
DA. Along a line from D to A, the south side of the square.

EF. Along a line from E to F, over the top of the round, from south to north.
GH. Along a line from G to H, over the top of the round, from west to east.

We will continually refer to these surveys as type AB, etc. For each survey the magnetometer was located at some elevation above the square, usually 45 cm above the round unless otherwise specified. All directions are relative to magnetic north. Typically the dip angle in this locality is about 67.1 degrees, which means that the vertical component and the horizontal component are in the ratio of tan(67.3)=2.37. Nominal values are 50400 gamma downward and 21262 northward for a total field of 54700 gamma, subject to diurnal variation.

6.1.2 Surveys on Horizontal Mortar Rounds

A mortar round was pointed in three different directions, south, east, and north for surveys around a 90 cm square. These files are reported separately below.

6.1.2.1 The Mortar South Survey

This survey was taken 9-28-95. A mortar round (#2549) was oriented toward magnetic south while resting at ground level. The survey was taken around a square 90 cm on a side and at a height of 50 cm above the ground (47.5 cm above the round centerline). The sides of the square are parallel and transverse to magnetic north. The survey results in gamma are first tabulated below and then displayed graphically. The graphs are plotted relative to the ambient field, 54710 gamma.

Table 6-1. Mortar Round Pointed South-Data

	gamma						
A-B	54700	54707	54710	54702	54690	54683	54682
B-C	54682	54678	54677	54678	54682	54687	54690
C-D	54685	54687	54695	54705	54712	54712	54705
D-A	54705	54713	54718	54715	54703	54692	54684
E-F	54712	54728	54738	54718	54684	54672	54675
G-H	54706	54720	54735	54725	54693	54675	54675
	0	15	30	45	60	75	90
	centimeters						

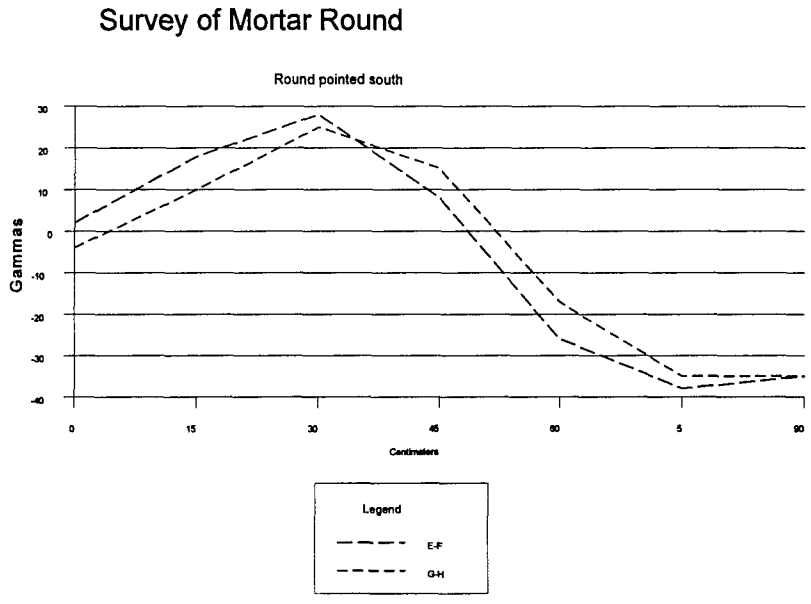

Figure 6-2. Survey of Mortar Round Pointed South

The following graph(Fig. 6-3) compares theory and experiment for the mortar round. The theoretical moments are x-axis (west)=0; y-axis (vertical) =-55 gamma-meter^3; z-axis (north)=30 gamma-meter^3 (this is a permanent moment only, directed toward the base of the round). The comparison is for the AB survey; that is, x=45 cm., y=-45 cm. The Mathcad 6.0 model is provided in Appendix A, along with an example of a calculation.

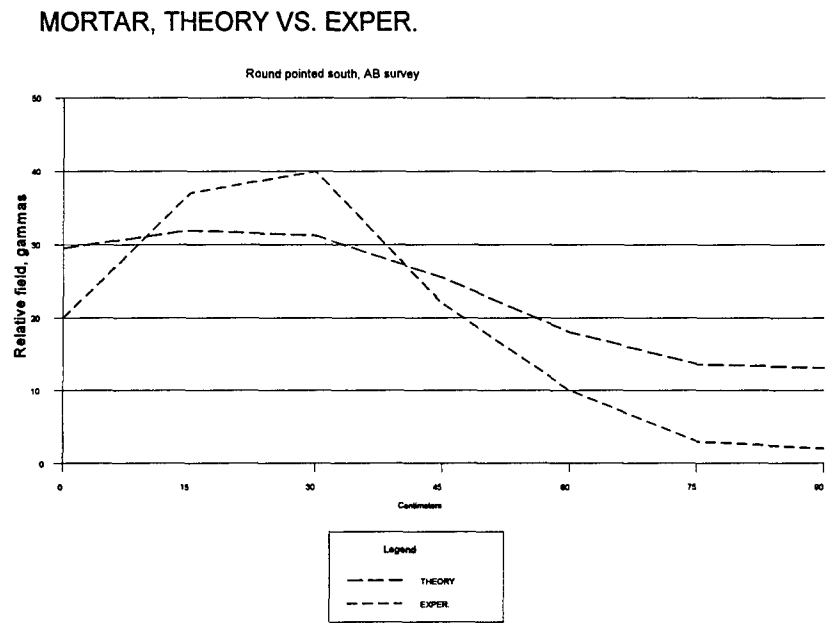

Figure 6-3. Mortar South, Theory vs Experiment, AB Survey

The next graph(Fig. 6-4) compares theory and experiment for the EF survey. Moments are as before, but the distances are now x=0 cm., y=-45 cm. Note that the theory in both of these graphs departs somewhat from experiment, although the shape of the curves has the right trend. This was subsequently found to be caused by rotation of the round about it's longitudinal axis between the data collected for the north pointing round and the data for the south pointing round. The mortar has a pin in the fuze that causes considerable asymmetry about it's long axis. This phenomena has been investigated and is documented later in this report.

MORTAR, THEORY VS. EXPER.

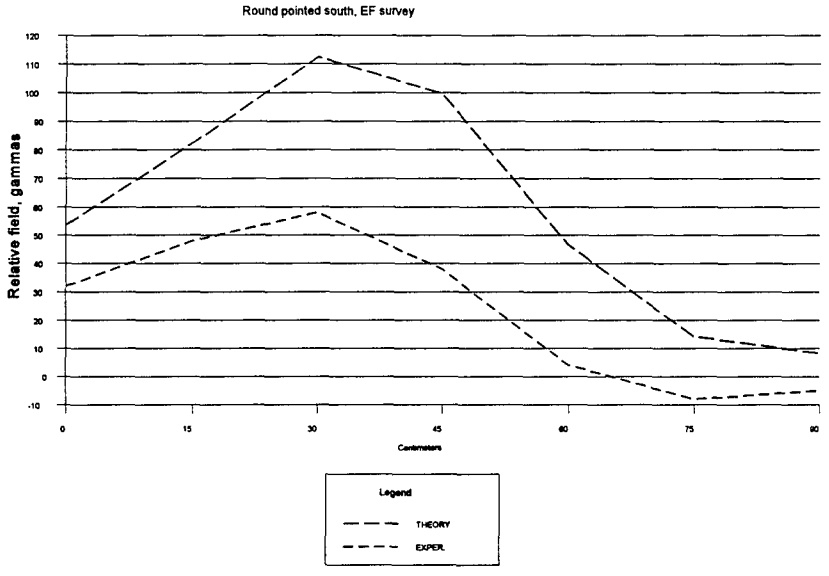

Figure 6-4. Mortar South, Theory vs Experiment, EF Survey

6.1.2.2 The Mortar East Survey

This survey was taken 9-28-95. A mortar round (#2549) was oriented toward magnetic east while resting at ground level. The survey was taken around a square 90 cm on a side and at a height of 50 cm above the ground (47.5 cm above the round centerline). The sides of the square are parallel and transverse to magnetic north. The survey results in gamma are first tabulated below and then displayed graphically. The graphs(Fig. 6-5) are plotted relative to the ambient field, 54710 gamma.

Table 6-2. Mortar Round Pointed East-Data

Total field, gamma

A-B	54698	54706	54712	54710	54700	54692	54688
B-C	54686	54682	54679	54676	54675	54680	54685
C-D	54682	54678	54676	54680	54686	54690	54691
D-A	54692	54702	54714	54725	54721	54709	54700
E-F	54700	54727	54778	54798	54762	54712	54696
G-H	54681	54685	54700	54720	54718	54703	54695
	0	15	30	45	60	75	90

centimeters

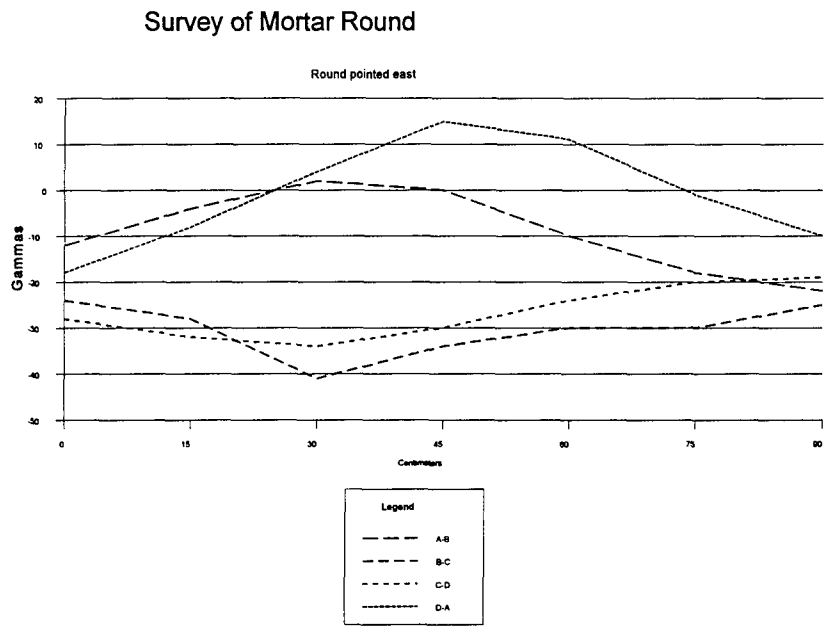

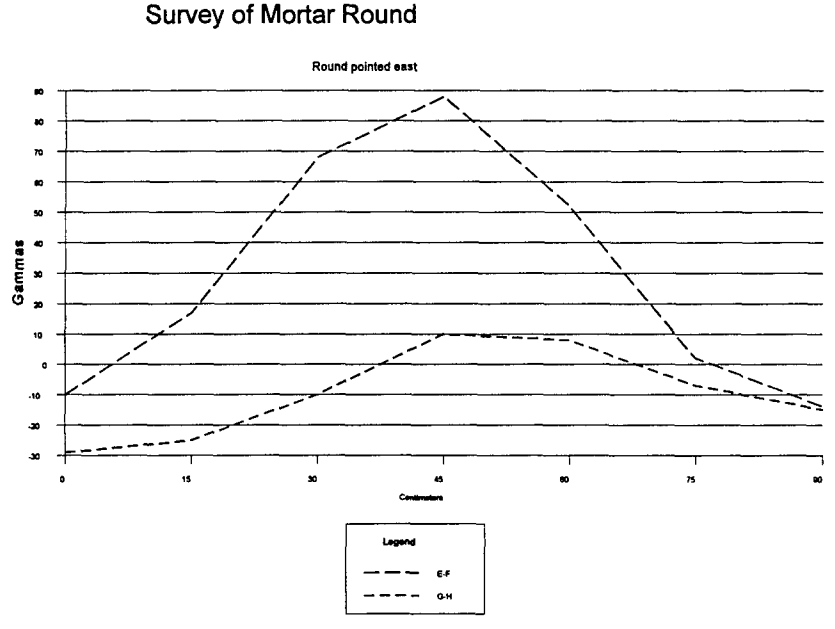

Figure 6-5. Mortar East Surveys

6.1.2.3 The Mortar North Surveys

This survey was taken 9-28-95. A mortar round (#2549) was oriented toward magnetic north while resting at ground level. The survey was taken around a square 90 cm on a side and at a height of 50 cm above the ground (47.5 cm above the round centerline). The sides of the square are parallel and transverse to magnetic north. The survey results in gamma are first tabulated below and then displayed graphically. The graphs(Fig. 6-6) are plotted relative to the ambient field, 54710 gamma.

Table 6-3. Mortar Round Pointed North-Data

gamma

A-B	54691	54697	54704	54705	54698	54692	54688
B-C	54688	54690	54687	54682	54680	54681	54684
C-D	54682	54678	54676	54674	54678	54682	54684
D-A	54685	54688	54698	54709	54712	54706	54699
E-F	54712	54745	54788	54800	54753	54702	54682
G-H	54676	54676	54694	54730	54743	54778	54712
	0	15	30	45	60	75	90

centimeters

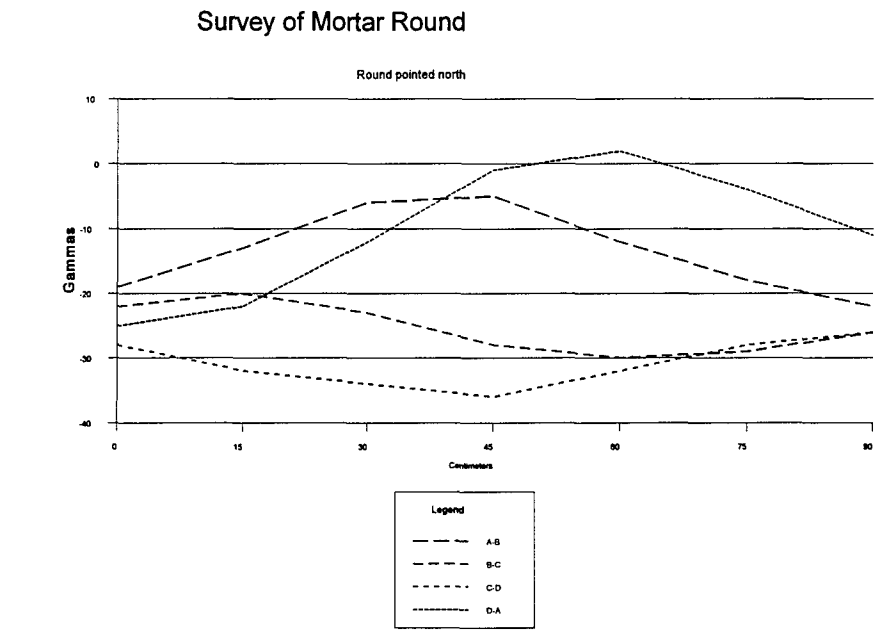

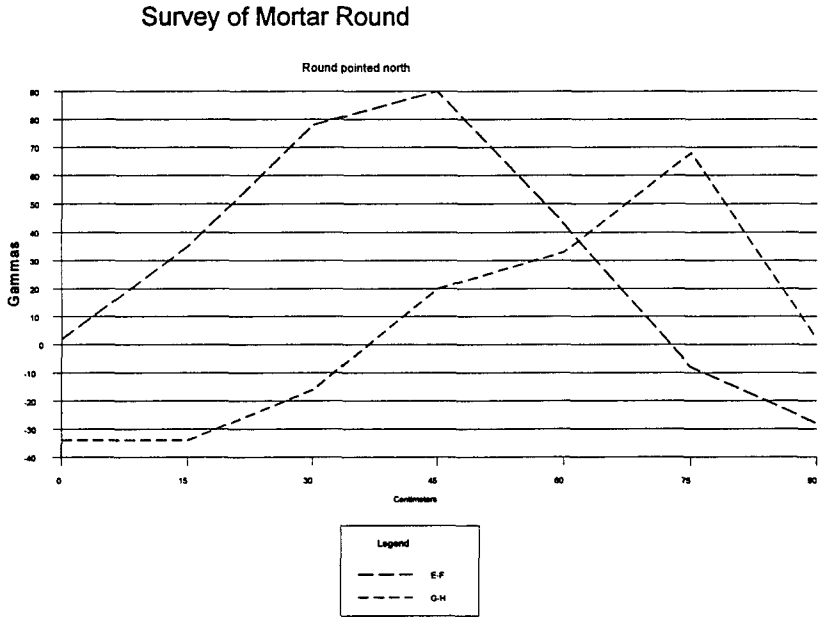

Figure 6-6. Mortar North Surveys

Figure 6-7 compares theory and experiment for the mortar using survey AB. The theoretical moments are x-axis (west) =0; y-axis (vertical) =-55 gamma-meter^3; z-axis (north)=-30 gamma-meter^3 (caused by a permanent moment toward the base). The distances are x=45 cm., y=-45 cm.

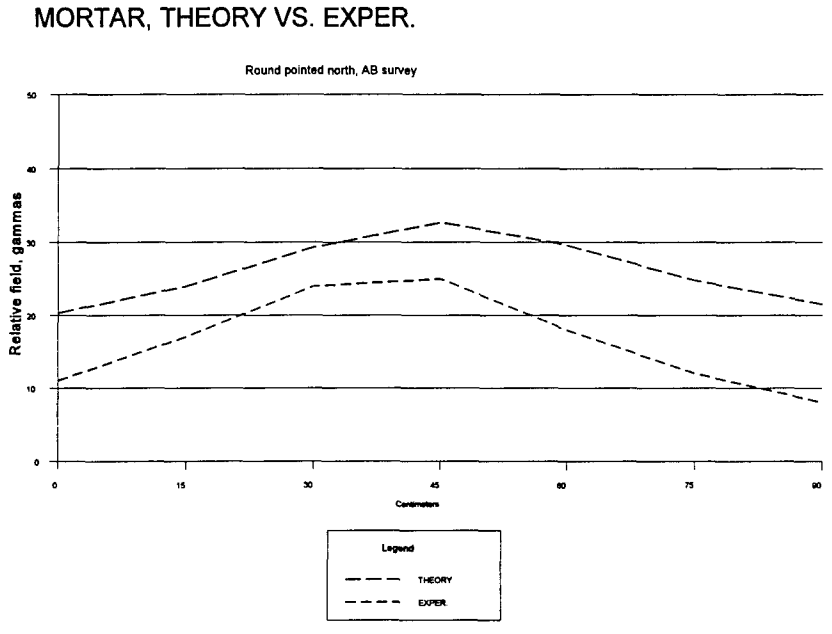

Figure 6-7. Mortar North, Theory vs. Experiment, AB Survey

Figure 6-8 compares theory and experiment for the EF survey. The moments are the same as above, but the distances are now x=0; y=-45 cm.

MORTAR, THEORY VS. EXPER.

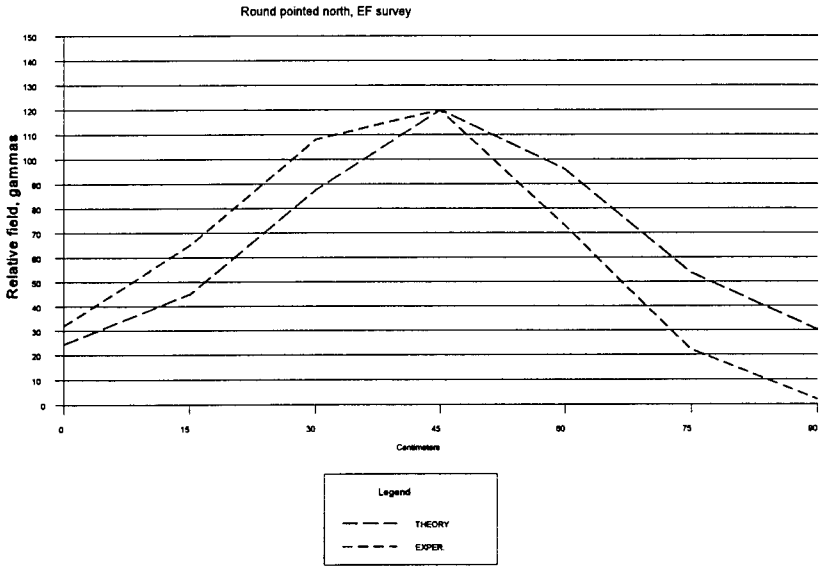

Figure 6-8. Mortar North, Theory vs. Experiment, EF Survey

6.1.3 Surveys on Horizontal 105 Rounds

105 rounds were pointed south, east, and north for surveys on the 90 cm grid. Results are reported separately below.

6.1.3.1 105 Round South Surveys

This survey was taken on 11-6-95 of a 105 Round pointed south. The survey was taken around a square 90 cm on a side as well as over the top of the square with the round horizontal and centered in the square. The height above the round was 45 cm above the centerline. The data is tabulated below in Table 6-4.

Table 6-4. 105 Round pointed South-Data
Total field, gammas

A-B	54918	54895	54767	54564	54405	54366	54420
B-C	54424	54272	54090	53982	54058	54251	54419
C-D	54435	54380	54420	54575	54748	54844	54858
D-A	54848	55024	55278	55427	55375	55162	54978
E-F	55496	55720	55460	54565	53824	53820	54125
G-H	54475	54412	54460	54630	54720	54705	54675
	0	15	30	45	60	75	90

centimeters

Figure 6-9 is a plot of the above results, shown relative to the ambient field of 54710 gamma.

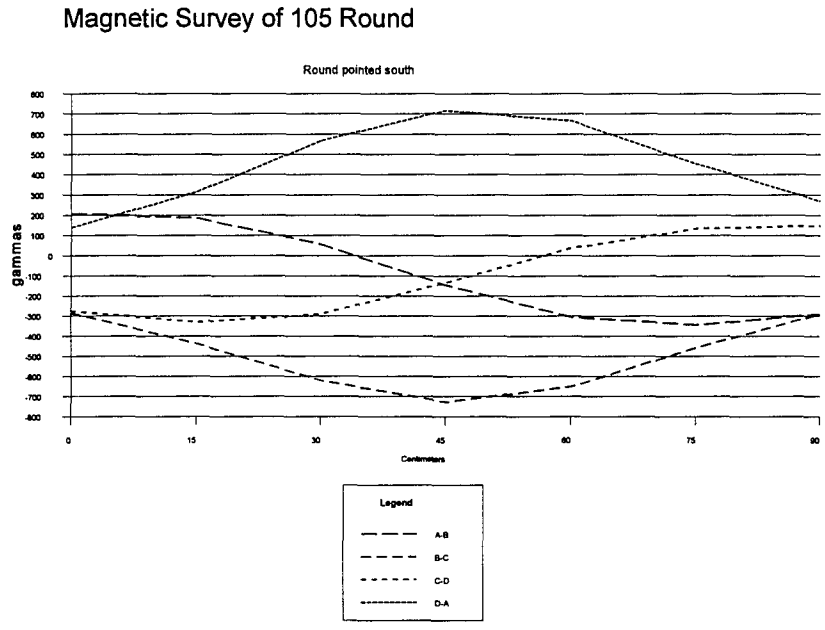

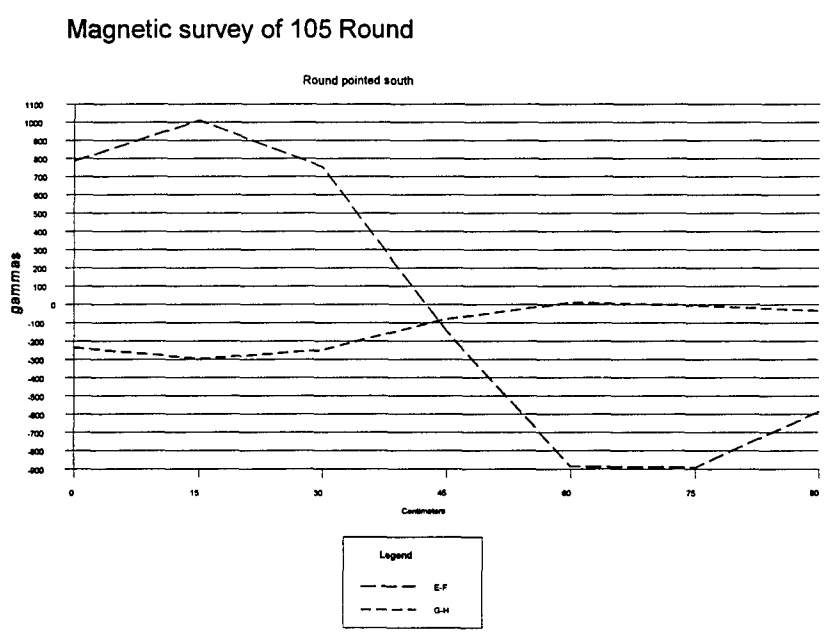

Figure 6-9. 105 South, Survey Results

Figure 6-10 compares theory and experiment for the 105 Round pointed South using the E-F survey results. The theoretical results are from the Mathcad program using the following moments: x-axis moment, 0; y-axis moment, -325 gamma-meter^3; z-axis moment, 1250 gamma-meter^3 (825 permanent, 425 induced). The permanent moment is toward the base.

105 ROUND, THEORY VS. EXPER.

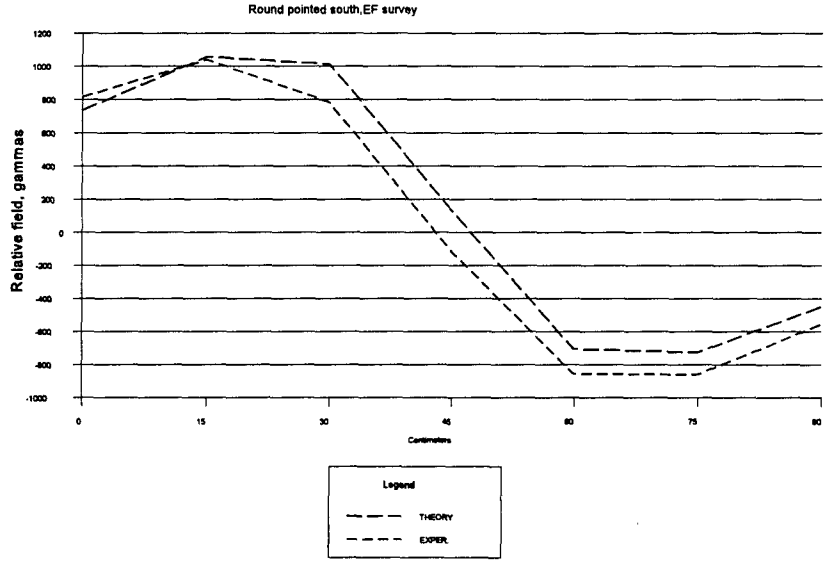

Figure 6-10. 105 South, Theory vs. Experiment, EF Survey

Figure 6-11 compares theory and experiment for the AB survey. The trends of these predictions are encouraging, considering the relatively long length of the round and the presence of a large permanent moment.

105 ROUND, THEORY VS. EXPER.

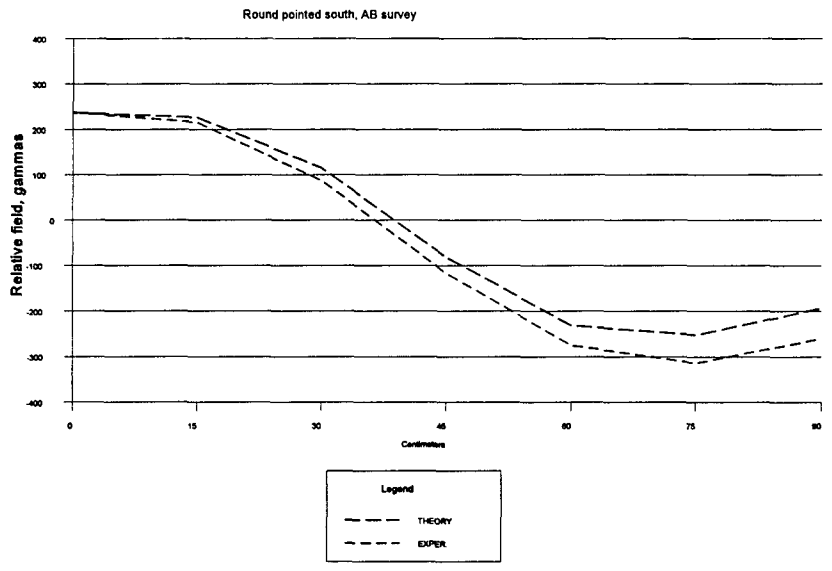

Figure 6-11. 105 Round South, Theory vs. Experiment, AB Survey

6.1.3.2 105 East Surveys

For these surveys the 105 round was pointed to magnetic east. The graphs of Figure 6-12 are plotted relative to the ambient field, 54710 gamma.

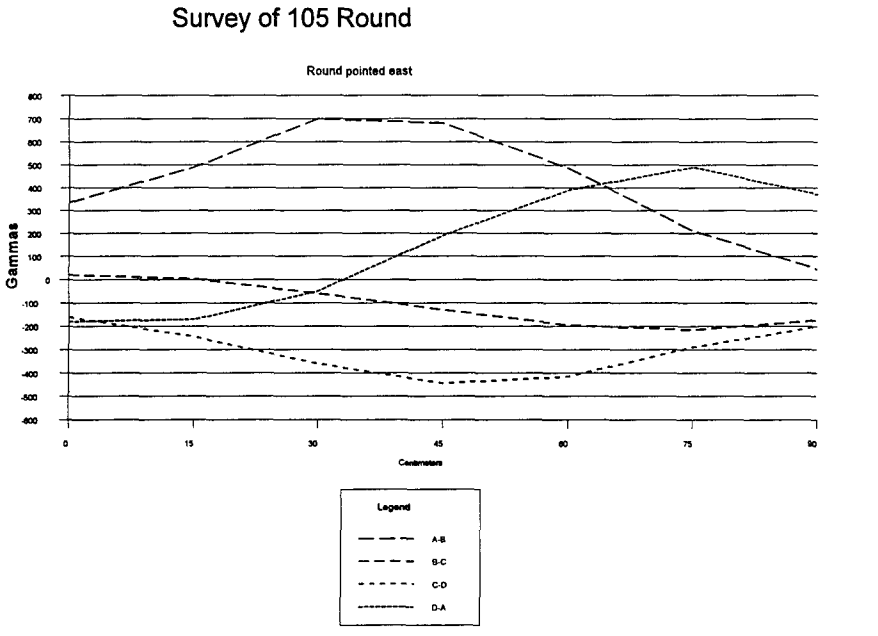

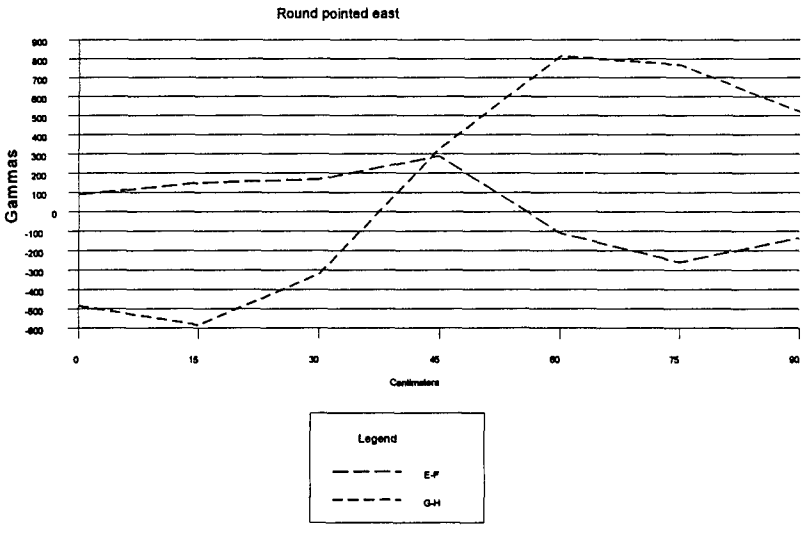

Figure 6-12. 105 Round East, Survey Results

The total field values are tabulated in Table 6-5.

Table 6-5. 105 Round Pointed East-Data
Total field, gamma

A-B	55045	55200	55410	55390	55195	54920	54755
B-C	54730	54712	54650	54580	54514	54498	54535
C-D	54550	54465	54350	54265	54295	54420	54508
D-A	54530	54540	54660	54900	55100	55200	55080
E-F	54800	54860	54880	55000	54600	54450	54575
G-H	54225	54125	54390	55040	55525	55478	55230
	0	15	30	45	60	75	90

centimeters

Figure 6-13 compares theory and experiment for the 105 Round pointed east using the E-F survey (south to north survey over the top of the round). The theoretical moments used in the analysis were as follows: x-axis (west direction), 825 gamma-meter^3 permanent moment; y-axis (vertical), -425 gamma-m^3; z-axis (north direction), 170 gamma- meter^3. The effect of the permanent moment, now directed along the x-axis, is not significant in the theoretical results. The y and z moments are in the ratio of the relative earth field in those directions.

105 ROUND, THEORY VS. E

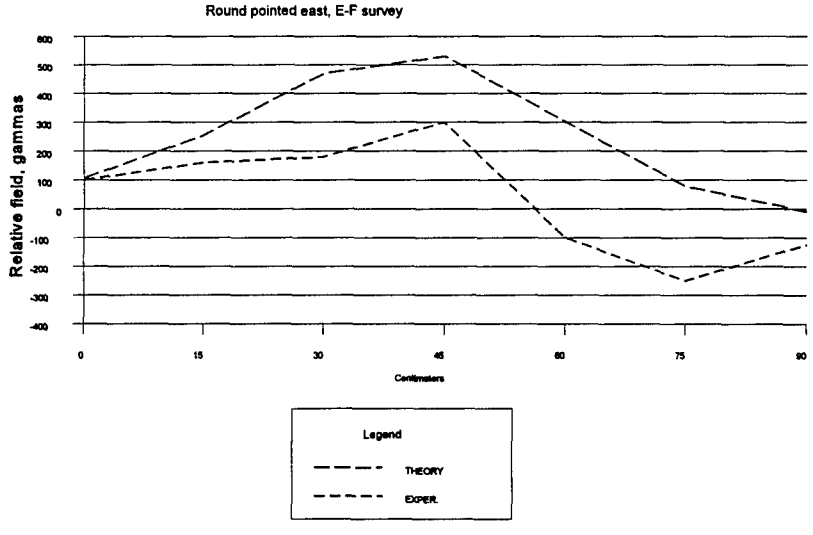

Figure 6-13. 105 East, Theory vs. Experiment, EF Survey

6.1.3.2 105 North Survey

Figure 6-14 shows the survey results for 105 round #2552 pointed toward magnetic north. The graphs are plotted relative to the local ambient field of 54710 gamma.

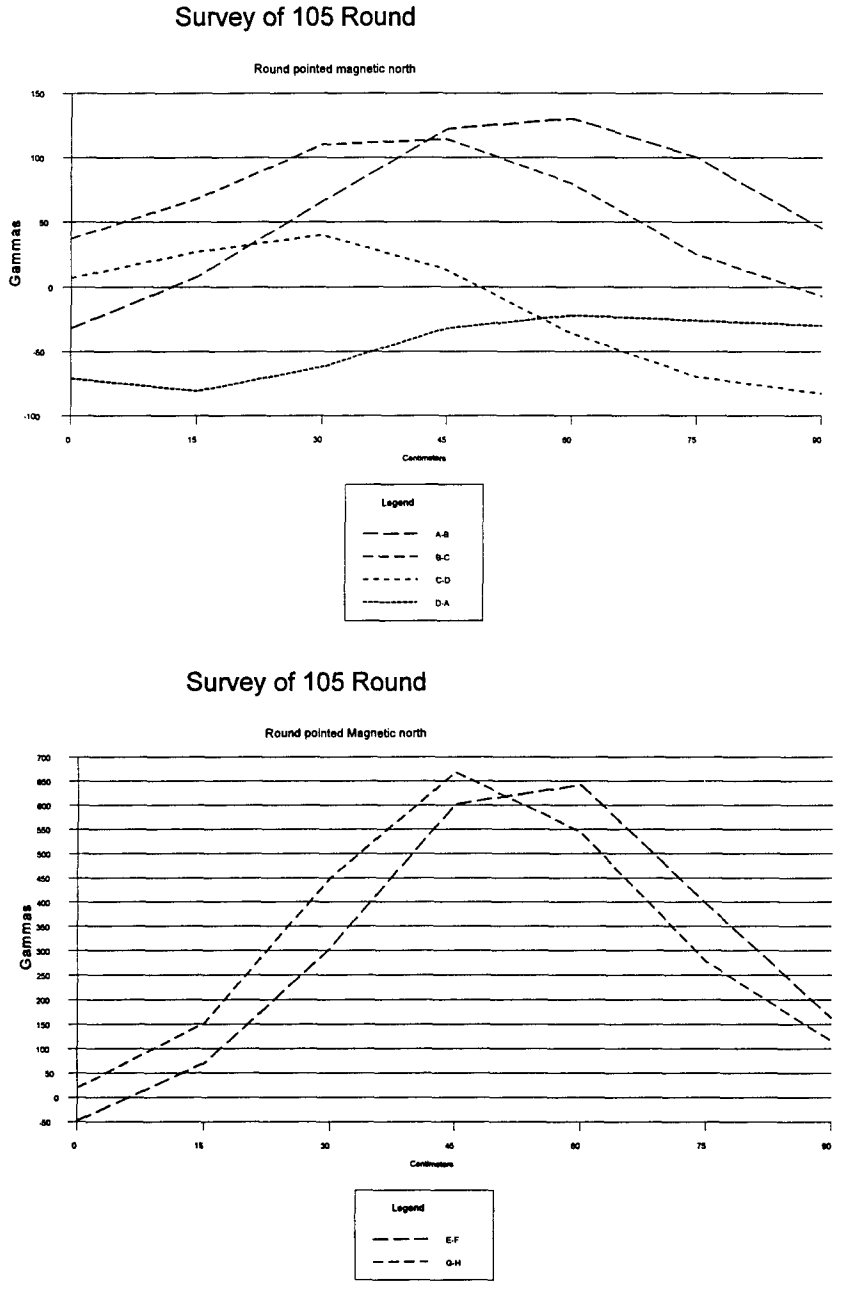

Figure 6-14. Magnetic Surveys of 105 Round Pointed North

Table 6-6 tabulates the total field data for these surveys.

Table 6-6. 105 Round Pointed North-Data

gammas							
A-B	54678	54718	54776	54832	54840	54810	54755
B-C	54747	54778	54820	54824	54790	54735	54703
C-D	54717	54737	54750	54723	54674	54640	54627
D-A	54639	54629	54648	54678	54688	54684	54680
E-F	54662	54780	55015	55312	55352	55107	54873
G-H	54730	54862	55160	55378	55254	54988	54826
	0	15	30	45	60	75	90
	centimeters						

Figure 6-15 compares theory and experiment for the E-F survey results. The theoretical results are from Mathcad using the following moments:
x-axis moment,0 gamma-m^3 ; y-axis moment, -325 gamma-m^3; z-axis moment, -400 gamma-m^3(-825 permanent, 425 induced)
The permanent moment is pointed toward the base of the round.

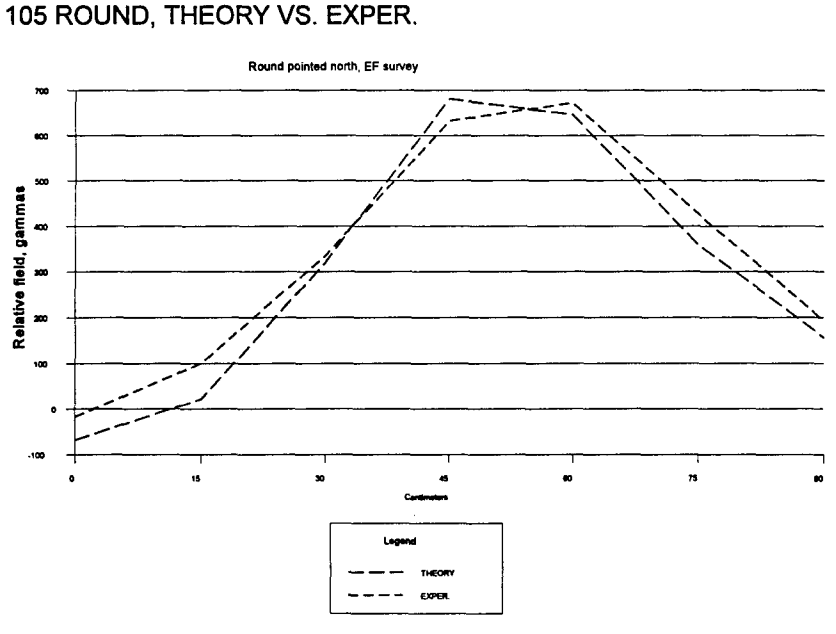

Figure 6-15. 105 Round North, Theory vs. Experiment, EF Survey

Figure 6-16 compares theory and experiment for the AB survey. All moments are as before, but the distances are x=45 cm, y=-45 cm.

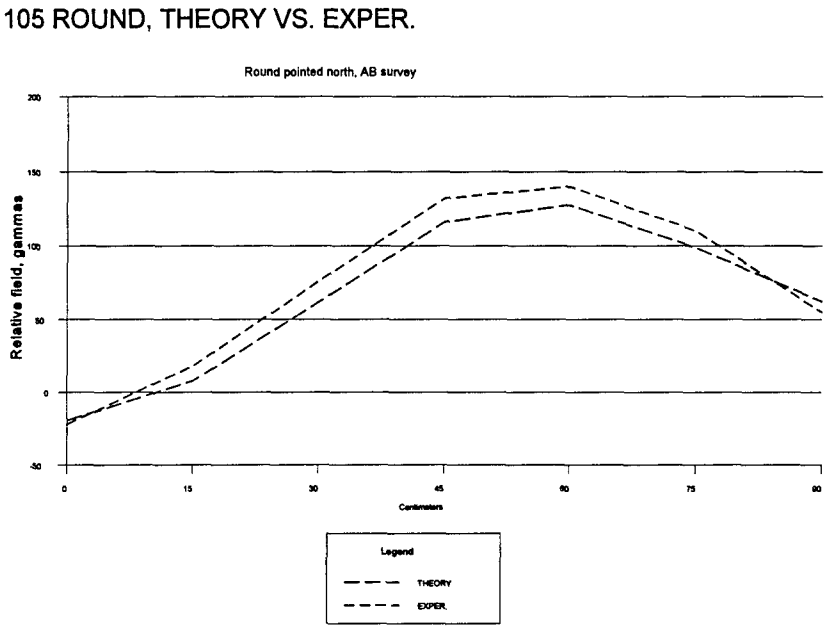

Figure 6-16. 105 Round North, Theory vs. Experiment, AB Survey

In general the derived moments appear to be consistent for different orientations, but the anticipated error is on the order of 10% considering factors that will be discussed later in the report--such as the effect of rotation of the round about it's longitudinal axis.

6.1.4 Surveys on Horizontal 155 Rounds

A 155 round was oriented south, east, and north for surveys around the 90 cm. square. Results for each direction are given below.

6.1.4.1 The 155 South Survey

Table 6-7 shows the survey results, tabulated as total field. A 155 round (#2554) was oriented toward magnetic south while resting at ground level. The survey was taken around a square 90 cm on a side and at a height of 50 cm above the ground (42.5 cm above the round centerline). The sides of the square are parallel and transverse to magnetic north.

Table 6-7. 155 Round Pointed South-Data
Total field, gammas

A-B	54907	54907	54850	54740	54625	54541	54508
B-C	54477	54419	54390	54386	54349	54358	54426
C-D	54390	54346	54386	54509	54665	54781	54820
D-A	54854	55085	55417	55591	55430	55137	54917
E-F	55553	55855	55875	55536	55045	54570	54332
G-H	54530	54692	55170	55630	55348	54938	54721
	0	15	30	45	60	75	90

centimeters

Figure 6-17 Provides a graph of the results, plotted relative to the ambient field.

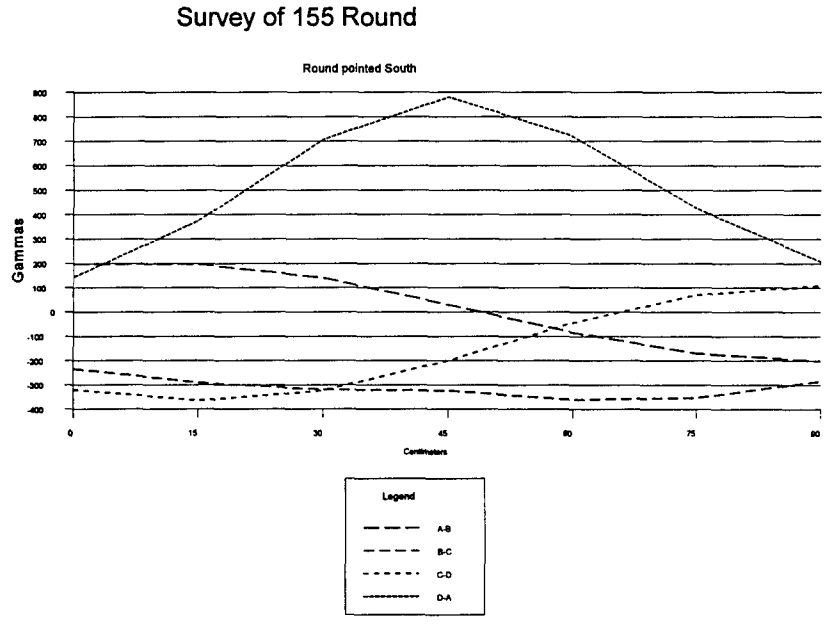

Figure 6-17(a). Survey Results for 155 Round, Pointed South

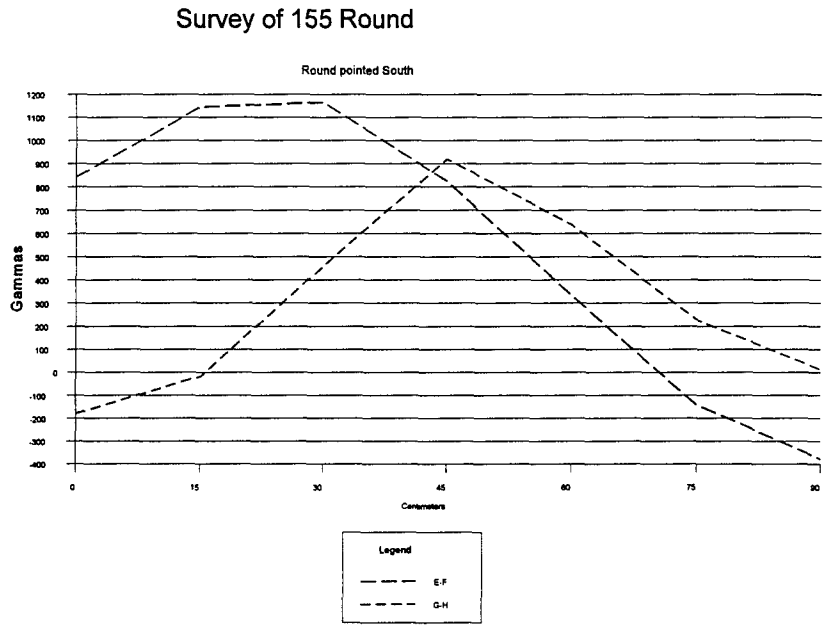

Figure 6-17(b). Survey Results for 155 Round, Pointed South

Figure 6-18 is a comparison of theory and experiment for the 155 round oriented toward magnetic south using the EF survey. The total field recorded by the Geometrics magnetometer is noted on the graph along with a Mathcad 6.0 prediction. The moments used in the prediction are as follows:

x-axis (horizontal, transverse to axis) ;0
y-axis (vertical, transverse to axis) ;-650 gamma-m^3
z-axis (along the axis) 500 gamma-m^3 (1750 induced-1250 permanent)

This shows the effect of the permanent moment toward the nose in opposition to the induced moment, which will lead to an overall reduction in signature when compared with the subsequent data for the north- pointed round.

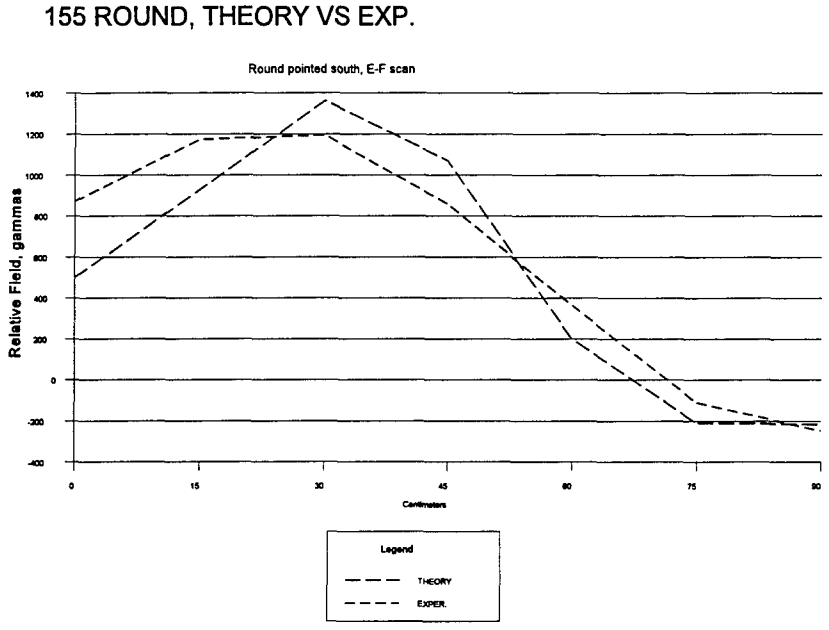

Figure 6-18. 155 South, Theory vs. Experiment, EF Survey

Figure 6-19 compares theory and experiment for the AB survey, where x=45 cm., y=-42.5 cm. All moments are as before. Again, the comparison is reasonable and the theory shows the proper trends in the signature.

155 ROUND, THEORY VS. E

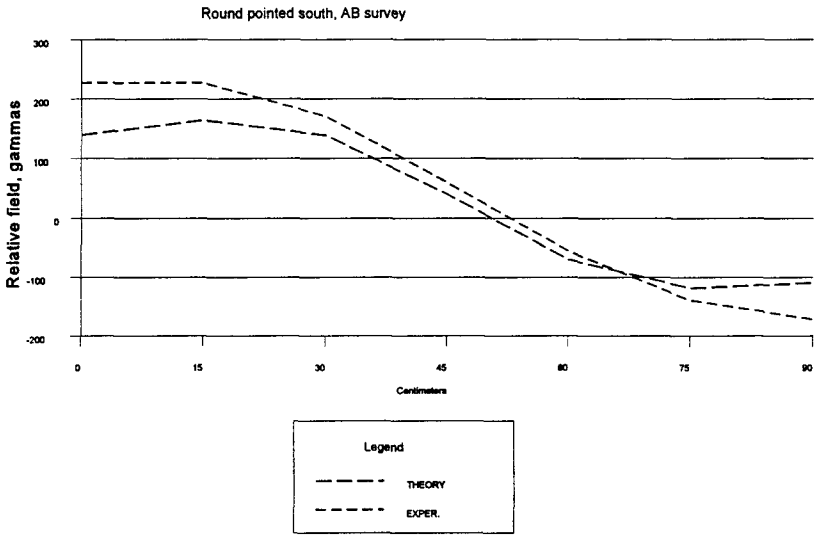

Figure 5

Figure 6-19. 155 Round South,Theory vs. Experiment, AB Survey

6.1.4.2 The 155 East Survey

This survey was taken 9-28-95. A 155 round (#2554) was oriented toward magnetic east while resting at ground level. The survey was taken around a square 90 cm on a side and at a height of 50 cm above the ground (42.5 cm above the round centerline). The sides of the square are parallel and transverse to magnetic north. The survey results in gammas are first tabulated below in Table 6-8 and then displayed graphically.

Table 6-8. 155 Round Pointed East-Data

Total field, gammas

A-B	54805	54876	54928	54880	54737	54636	54600
B-C	54618	54581	54535	54502	54498	54512	54536
C-D	54518	54572	54833	55171	55184	54992	54830
D-A	54785	54868	54932	54942	54914	54860	54800
E-F	55025	55360	55860	55772	55000	54507	54447
G-H	55290	55765	55910	55727	55428	55145	54890
	0	15	30	45	60	75	90

centimeters

Figure 6-20 shows plots of the above data relative to the ambient field.

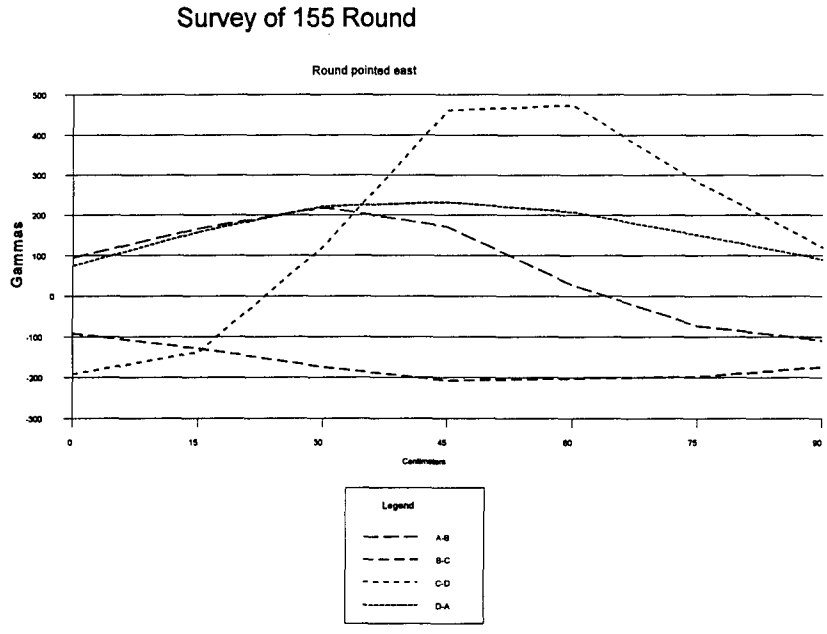

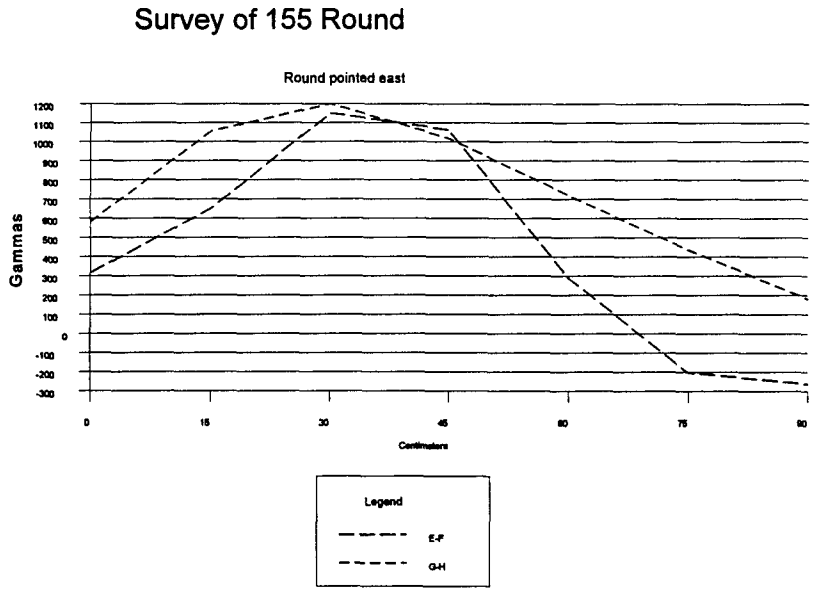

Figure 6-20. 155 East, Survey Results

Figure 6-21 compares theory and experiment for the 155 round oriented toward magnetic east using the EF scan. The total field recorded by the Geometrics magnetometer is noted on the graph along with a Mathcad prediction. The moments used in the prediction are as follows:
x-axis (horizontal,westward) ;-1250 gamma-m^3 (permanent moment toward nose)
y-axis (vertical, transverse to axis); -650 gamma-m^3 (induced)
z-axis (horizontal northward); 260 gamma-m^3 (induced moment northward)

The z-directed moment has been calculated by ratioing it to the induced y moment in the same proportion as the earth field components.

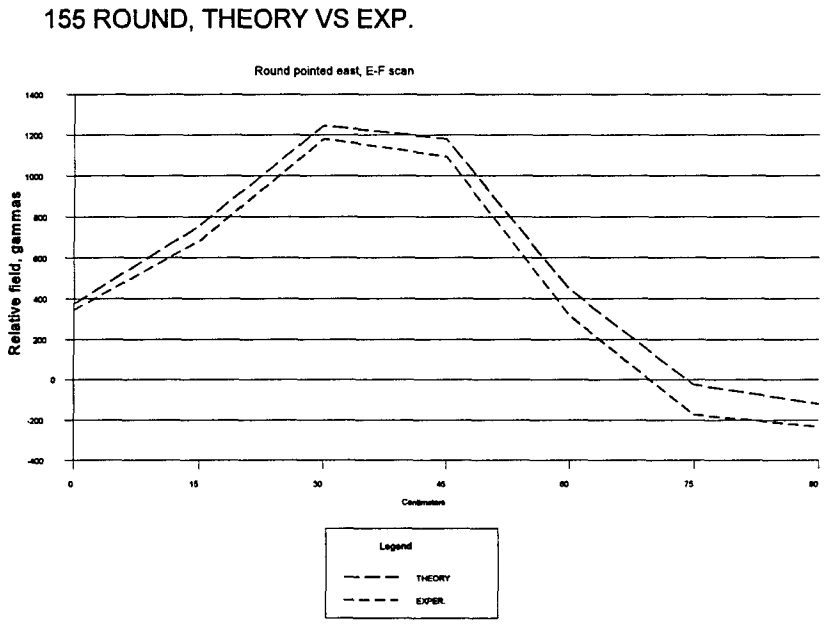

Figure 6-21. 155 Round East, Theory vs. Experiment, EF Survey

Theory and experiment are in good agreement for this survey.

6.1.4.3 The 155 North Survey

This survey was taken 9-28-95. A 155 round (#2554) was oriented toward magnetic north while resting at ground level. The survey was taken around a square 90 cm on a side and at a height of 50 cm above the ground (42.5 cm above the round centerline). The survey results in gammas are first tabulated below in Table 6-9.

Table 6-9. 155 Round Pointed North-Data

Total field, gammas

A-B	55095	54967	54700	54411	54253	54240	54320
B-C	54311	54138	53960	53878	53975	54173	54338
C-D	54275	54136	54105	54250	54540	54856	54998
D-A	55034	55606	56602	57124	56618	55780	55190
E-F	57112	57372	56150	54535	53568	53464	53850
G-H	54266	54182	54290	54596	54623	54502	54475
	0	15	30	45	60	75	90

centimeters

Figure 6-22 shows graphs of the data, plotted relative to the ambient field.

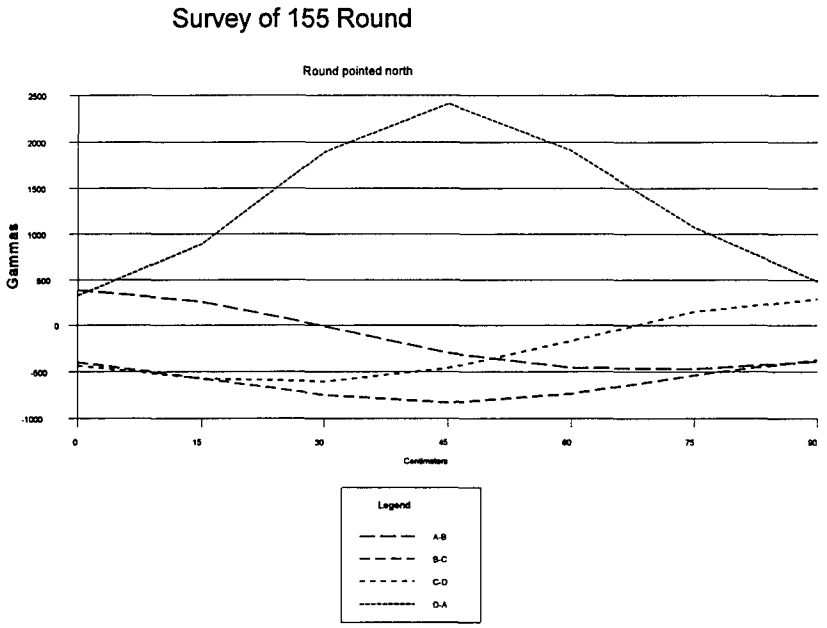

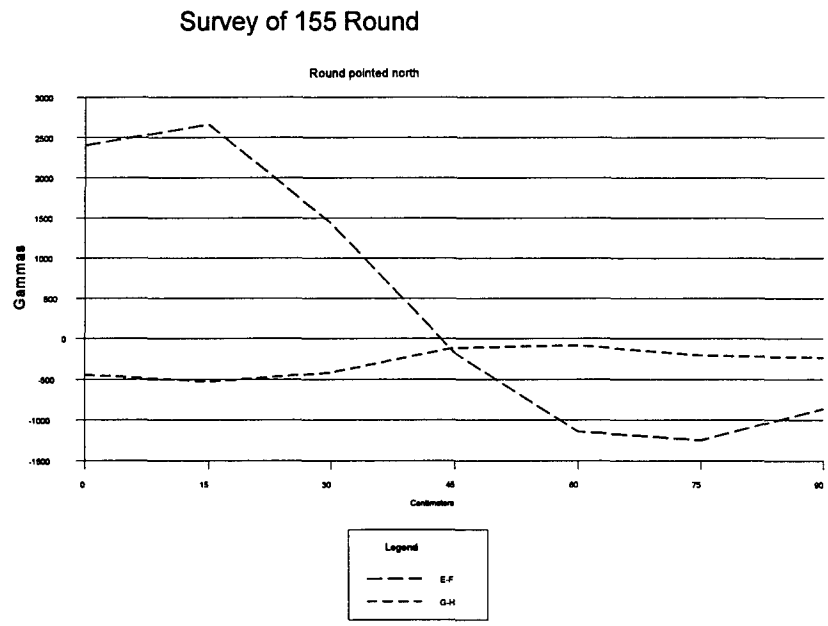

Figure 6-22. 155 North, Survey Results

Figure 6-23 compares theory and experiment for the 155 round oriented toward magnetic north using the EF scan. The moments used in the prediction are as follows:
x-axis (horizontal, transverse to axis) ; 0
y-axis (vertical, transverse to axis) ; -650 gamma-m^3
z-axis (along the axis) ;3000 gamma-m^3 (1750 induced +1250 permanent)

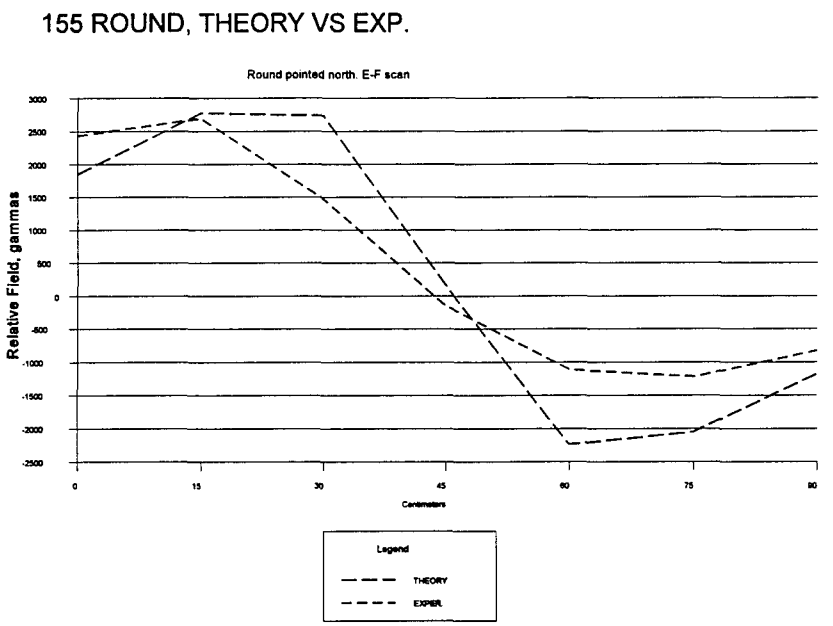

Figure 6-23. 155 North, Theory vs. Experiment, EF Survey

Figure 6-24 compares theory and experiment for the AB survey, where x=45 cm and y=-42.5 cm. All moments are as before.

155 ROUND, THEORY VS. EXPER.

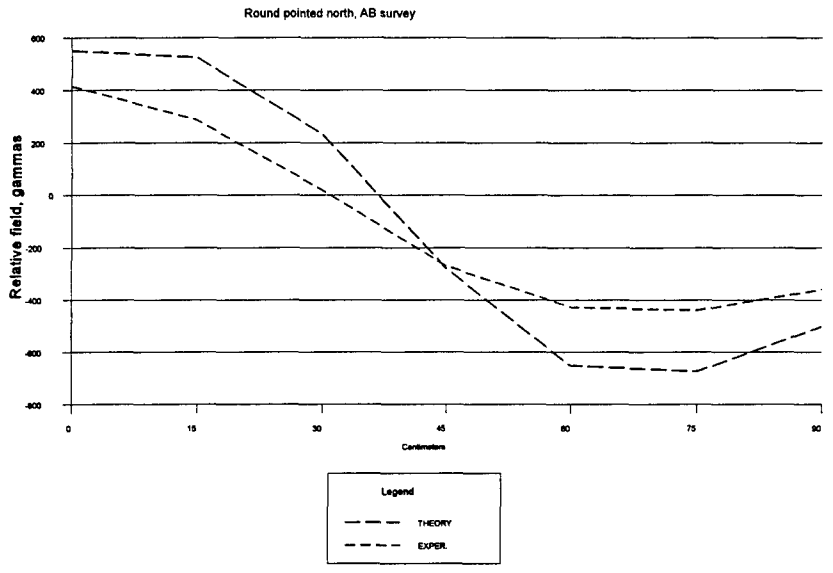

Figure 6-24. 155 North, Theory vs. Experiment, AB Survey

The signature of the surveys of the 155 have been more difficult to predict, perhaps due to the fact that the round is so long while the theory assumes a point source.

6.1.5 Measurements to Derive Moments for Vertical Rounds

A series of measurements were made with the Geometrics total field magnetometer to allow derivation of the moments of the three round types when they were vertically oriented; i.e., either pointed upward or downward. The rounds were placed in a hole to a depth that made their geometric center at the ground level of the sensor. The sensor was 45 cm distant to the east of the round. For the Mathcad 6.0 analysis, (mag5.mcd program) the x value is therefore equal to 45 cm and the y value is 0. The y-value of the moment was adjusted to give a best fit with the observations to obtain the vertical moment. The graphs of Figure 6-25 show a comparison of measurement and theory, along with the derived moments (induced and permanent). The surveys were taken along a line 45 cm east of the round from south to north (an AB survey).

For the mortar the selected vertical moments were as given in Table 6-10.

Table 6-10. Moments of Vertical Mortar

Round pointing	Total moment, gamma-m^3	induced moment, gamma-m^3	permanent moment gamma-m^3
up	-77	-73.5	3.5 (toward base)
down	-70	-73.5	3.5 (toward base)

(Remember, negative moments are directed downward in our coordinate system)

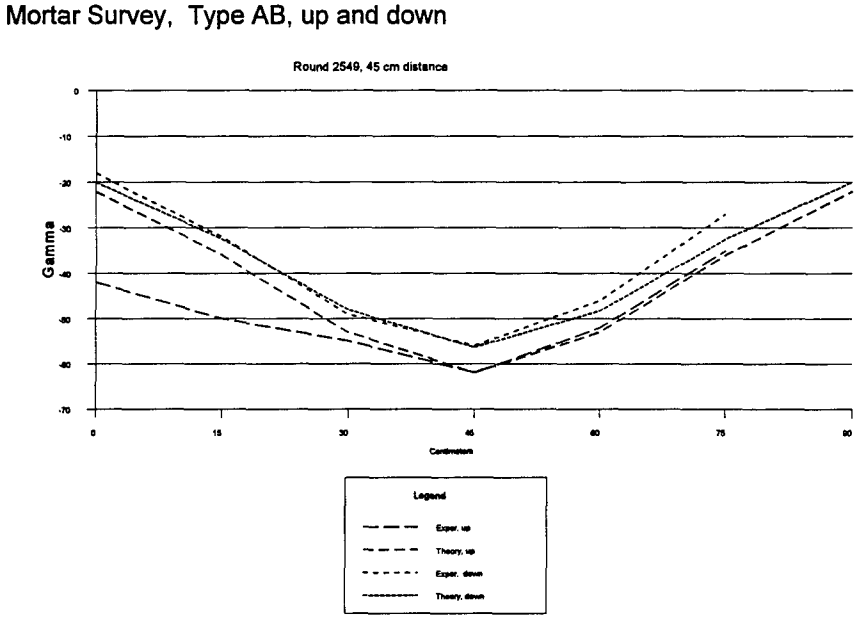

Figure 6-25. Mortar Vertical, Theory vs. Experiment, AB Survey

Table 6-11 shows the theoretical moments used to compare with experiment for a 105 Round.

Table 6-11. Moments of a Vertical 105 Round

round pointing	total moment, gamma-m^3	induced moment gamma-m^3	permanent moment gamma-m^3
up	-1874	-1154	719 (toward base)
down	-435	-1154	719 (toward base)

Figure 6-26 shows a comparison of theory and experiment for the 105 round.

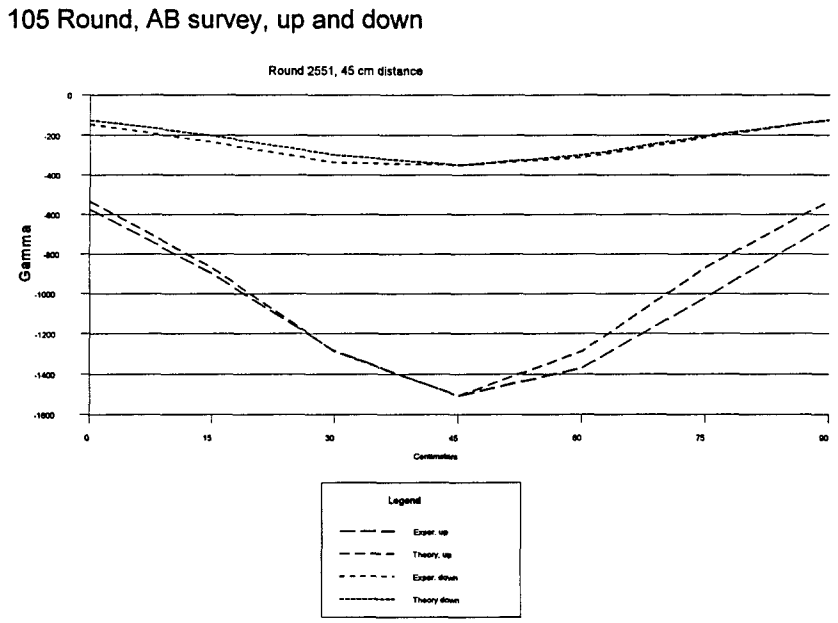

Figure 6-26. 105 Vertical, Theory vs. Experiment, AB Survey

For the 155 round, the moments of Table 6-12 were used to compare with experiment.

Table 6-12. Moments of Vertical 155 Round

pointing direction	total moment, gamma-m^3	induced moment, gamma-m^3	permanent moment gamma-m^3
up	-2091	-3403	1312 (toward nose)
down	-4715	-3403	1312 (toward nose)

Figure 6-27 shows a comparison of theory and experiment for the vertical 155 round.

It is interesting to compare the above permanent moments with those derived previously from surveys taken with the rounds horizontal. This comparison is made in the Table 6-13 below. The values compare within about 100 gamma-m^3, which is probably about the limit of accuracy for the methods employed.

Table 6-13. Moments Compared from Vertical and Horizontal Round Surveys

Round type	Permanent moment from vertical AB surveys	Permanent moment from horizontal surveys
mortar	3.5 toward base	30 toward base
105	719 toward base	825 toward base
155	1312 toward nose	1250 toward nose

155 round, AB survey, up and down

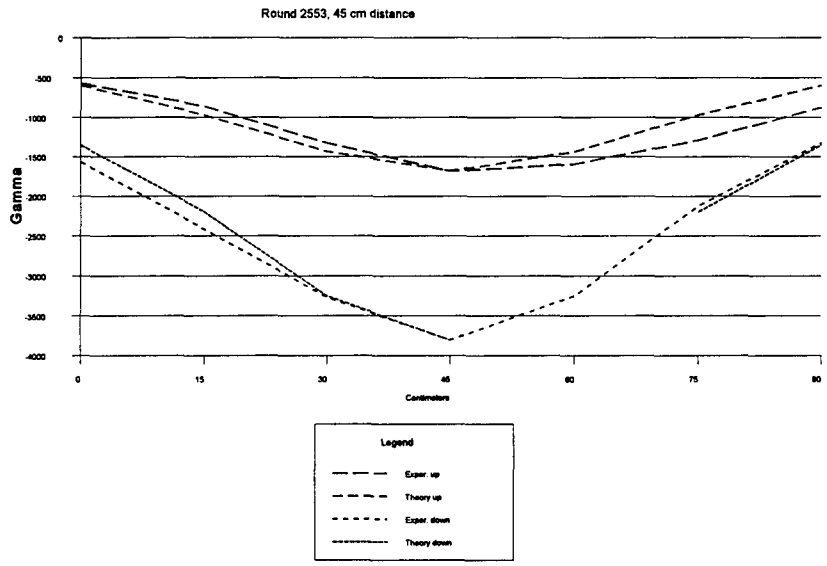

Figure 6-27. 155 Vertical, Theory vs. Experiment, AB Survey

The following subsection will tabulate all of the derived moments in summary form.

6.1.6 Summary of Derived Moments from Survey Data

Table 6-14 provides a summary of all the moments that have been used to obtain good agreement with experiment during this program. These moments were used in subsequent neural network training programs that were designed to extract information about round type and orientation.

Table 6-14. Summary Data on Round Moments (gamma-m^3)

ROUND	POINTING DIRECTION	NORTH-SOUTH COMPONENT	VERTICAL COMPONENT*	EAST-WEST COMPONENT**
Mortar	north	30 south	-55	0
	east	22 north	-55	30 west
	south	30 north	-55	0
	west	22 north	-55	30 east
	nose up	0 ***	-77	0
	nose down	0 ***	-70	0
105	north	400 south	-325	0
	east	130 north	-325	825 west
	south	1250 north	-325	0
	west	130 north	-325	825 east
	nose up	0 ***	-1874	0
	nose down	0 ***	-435	0
155	north	3000 north	-650	0
	east	260 north	-650	1250 east
	south	500 north	-650	0
	west	260 north	-650	1250 west
	nose up	0 ***	-2091	0
	nose down	0 ***	-4715	0

* A (-) sign means the moment is directed downward.
** The east-west component is caused by a permanent moment along the axis of the round when the round is pointed east or west.
*** The real value is probably not zero, but it appears to be neglible in predicting the signature of these vertical rounds..

6.2 TESTS TO TRAIN NEURAL NETWORKS

A number of surveys were conducted on grids, either 2x2 or 4x4 meters in size, so as to collect magnetic field perturbation data on the three types of rounds. These data were compiled in a neural network program so that the network could be trained to give outputs that indicated round features such as moments (north, east, or vertical), depth of the round, or distance from the sensor. Some surveys were taken with the Geometric 822 total field magnetometer while others were taken with a Vallon Iron Detector (gradiometer). First the survey grid will be described and then neural network training data and results will be provided.

6.2.1 The Survey Grid

A layout of the survey grid is shown in Figure 6-28. There were 121 data points per survey, taken at intervals of 0.2 meter for the 2x2 meter grid, and at intervals of 0.4 meter for the 4x4 meter grid. There are eleven rows of data, labeled H1 through H11. There are 11 observations per row. Row H6 passes over the round, which was at or near the center of the grid (specified for each survey). The surveys would always start at the SW corner; i.e., at H1, observation 1. Data collection would progress in a northward direction through the eleven rows, H1 to H11, then repeat for observation 2, 3, etc., and finally to observation 11.

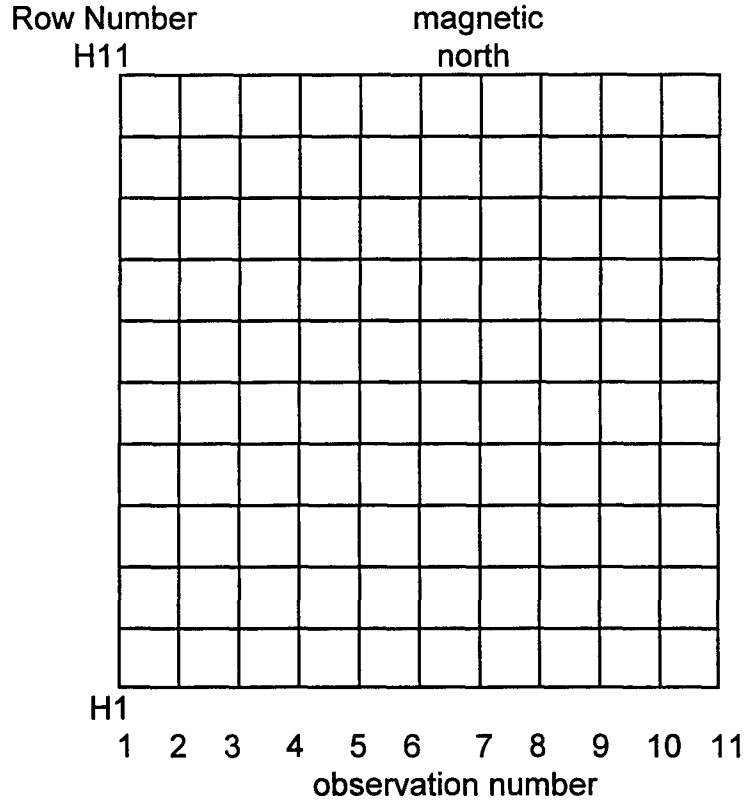

Figure 6-28. Survey Grid

6.2.2 Neural Network Training on Mortar Surveys

Six separate mortar surveys were taken on a 2x2 meter grid and then combined into one data matrix consisting of 11 rows and 66 observations. The observation numbers associated with each survey are shown below along with a Figure number where a contour plot of the data may be observed.

Observations 1-11	Mortar pointed south, depth 33 cm.	Figure 6-29
Observations 12-22	Mortar pointed north, depth 33 cm.	Figure 6-30
Observations 23-33	Mortar pointed north, depth 0 cm.	Figure 6-31
Observations 34-44	Mortar pointed east, depth 33 cm.	Figure 6-32
Observations 45-55	Mortar pointed east, depth 0 cm.	Figure 6-33
Observations 56-66	Mortar pointed south, depth 0 cm.	Figure 6-34

The contour plots were generated by insertion of each survey, consisting of 121 H-field data points, into the software programs called MAGLOC, GRID, TOPO, and PLOT. These are part of the Geometric 822 system package. The GRID/TOPO program interpolates between each pair of data points to produce a much finer resolution contour plot. The location of the geometric center of the round is located on each plot with a (+) sign.

For each of these figures, the contour plots have been limited to those values between -200 and + 200 gamma, in intervals of 20 gamma. This makes the patterns easier to compare as a function of depth and pointing angle. There are trends in these contours that are important: (1) at zero depth the negative contours extend to a greater distance from the round, and (2) when the round is at depth the positive contours are over the round. The first trend is caused by the domination of the downward moment at short range The second trend is caused by a mix of horizontal and vertical moment contributors.

Figure 6-35 shows the data plotted for each row, H1 through H11, as well as the moment data derived from the horizontal moment surveys of Section 6.1.2 (moment north , moment vertical, moment east), the distance from the round, and the depth of the round. The distance to the round is the absolute distance from the survey line (south-north line) to the geometric center of the round, in cm. The depth is the distance of the geometric center of the round below the sensor, in cm. Notice that the input data has a slight randomized component, created by the model. (If a string of numbers, all equal in value, are entered, the program will not run).

A neural network model, available on the Internet, developed by Neural Fusion, 15 Standish Avenue, Middletown, N. Y. 10940, was used for training on the data. A standard back-error-propagation option was used (MAGFIXM.BEP) with 20,000 training cycles (about 45 minutes on a 486 PC). The model was initially trained to provide an output of the magnetic moment in the north direction. Training on only one output has been found to yield much higher correlation between measured and predicted outputs.

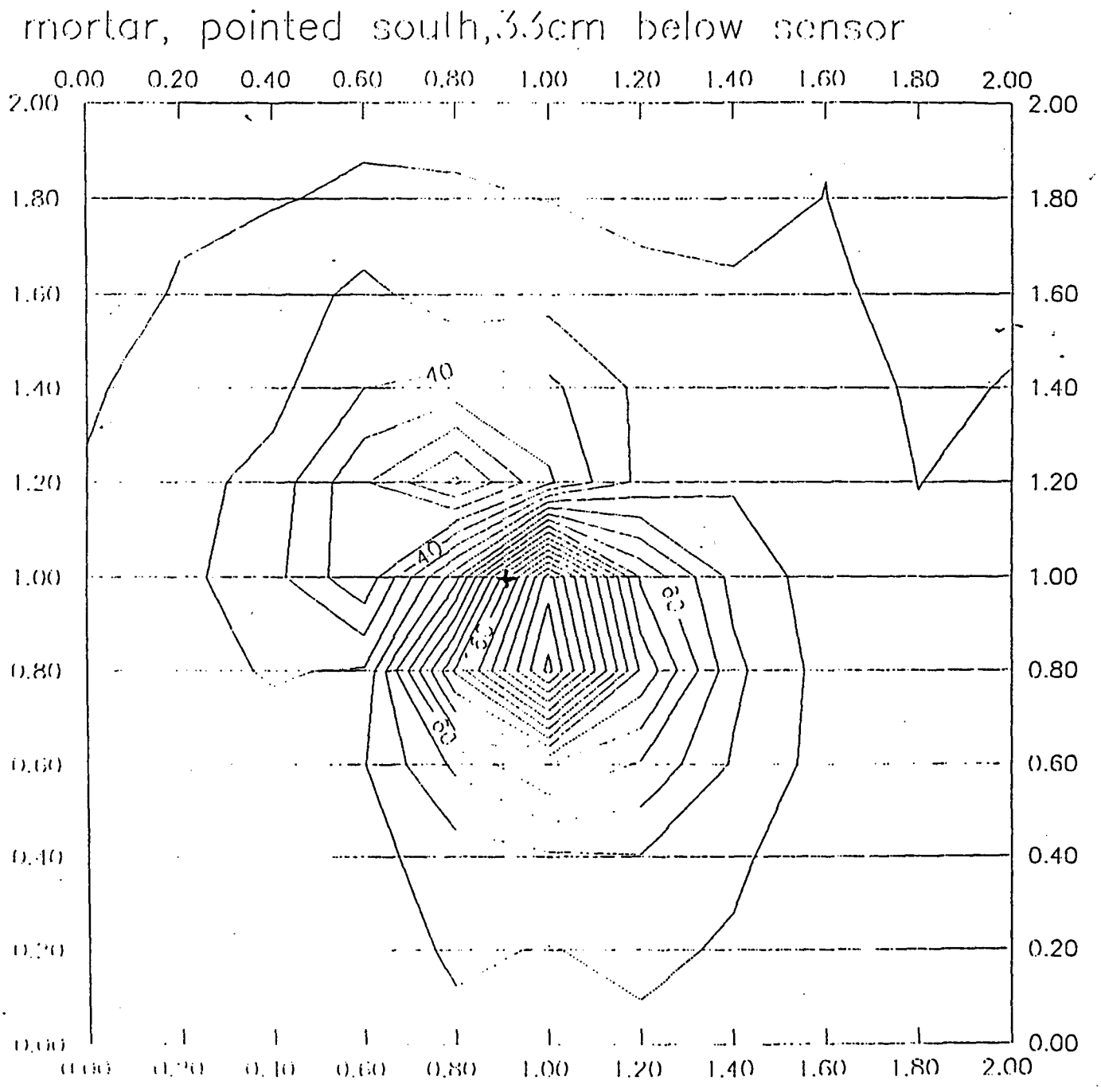

Figure 6-29. Mortar Pointed South, depth 33 cm

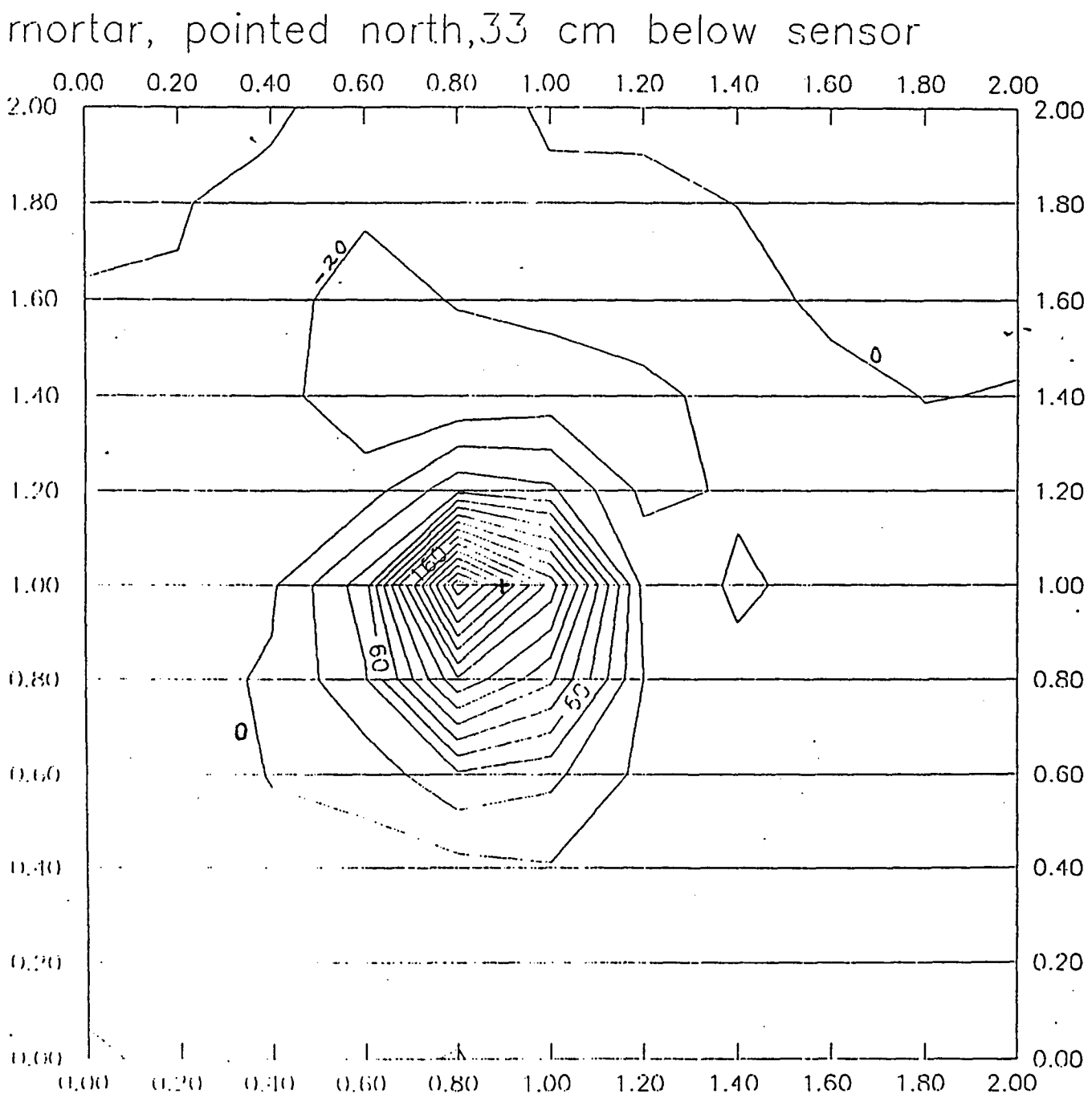

Figure 6-30. Mortar Pointed North, depth 33 cm

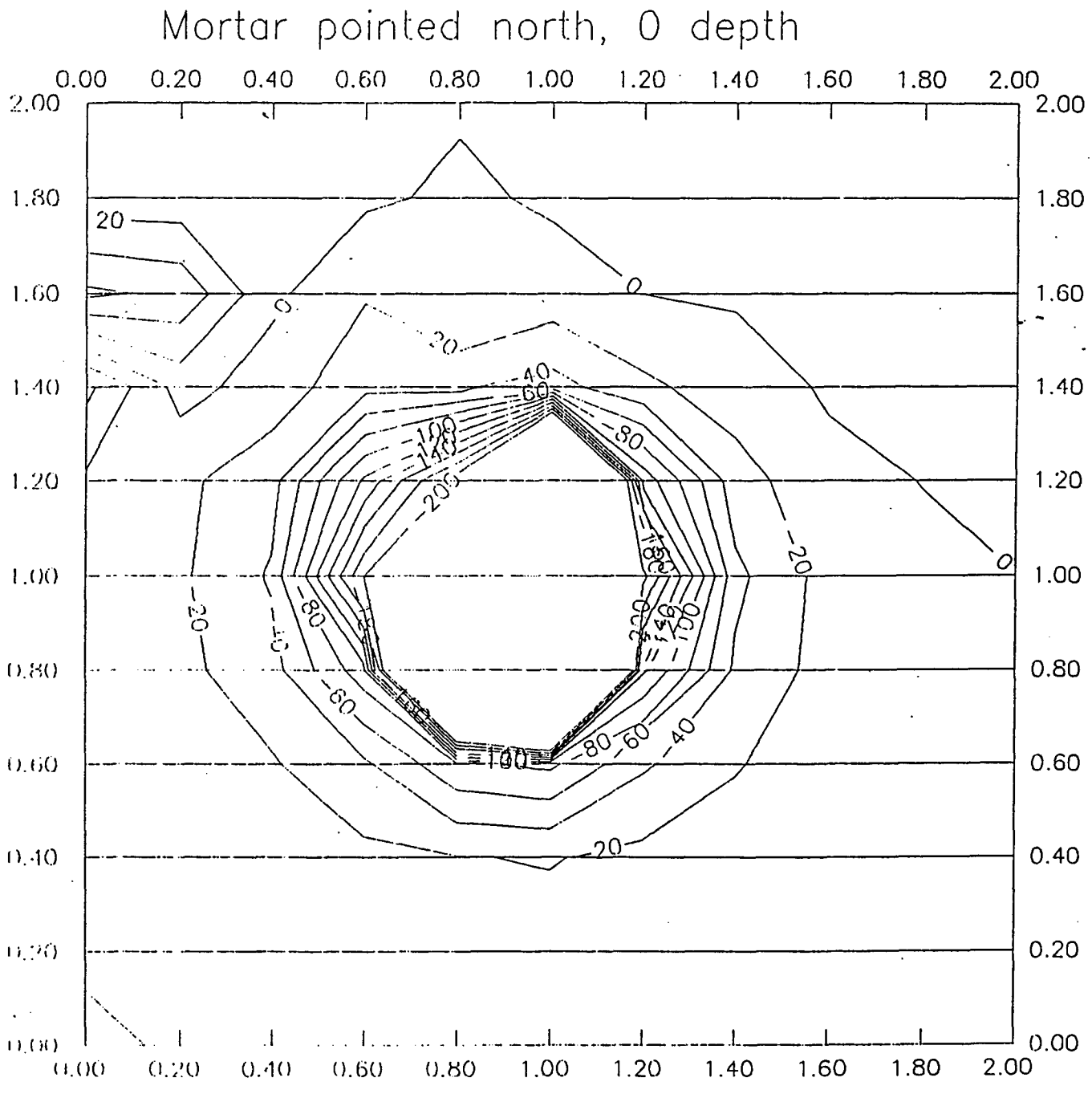

Figure 6-31. Mortar Pointed North, depth 0 cm

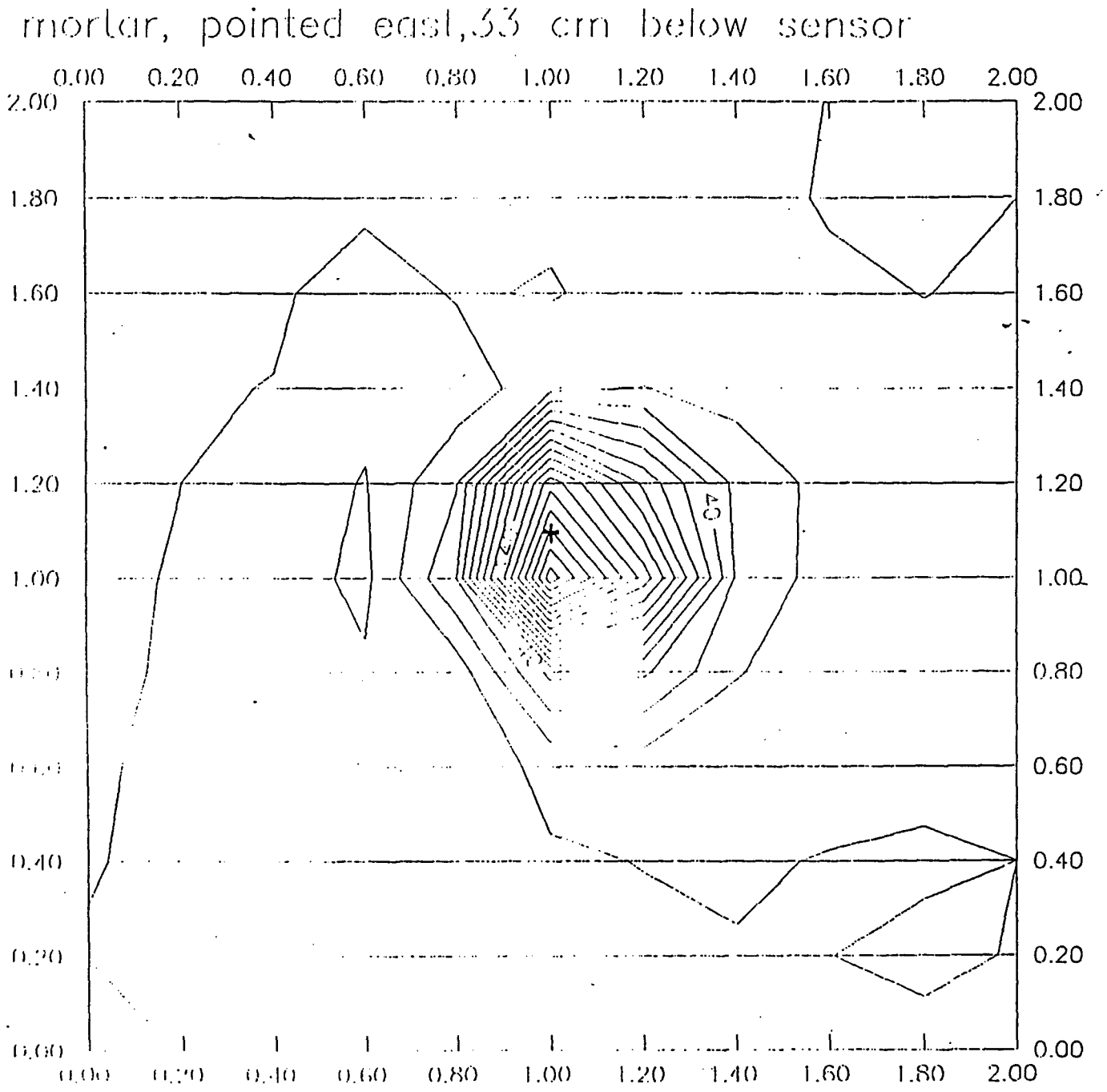

Figure 6-32. Mortar Point East, depth 33 cm

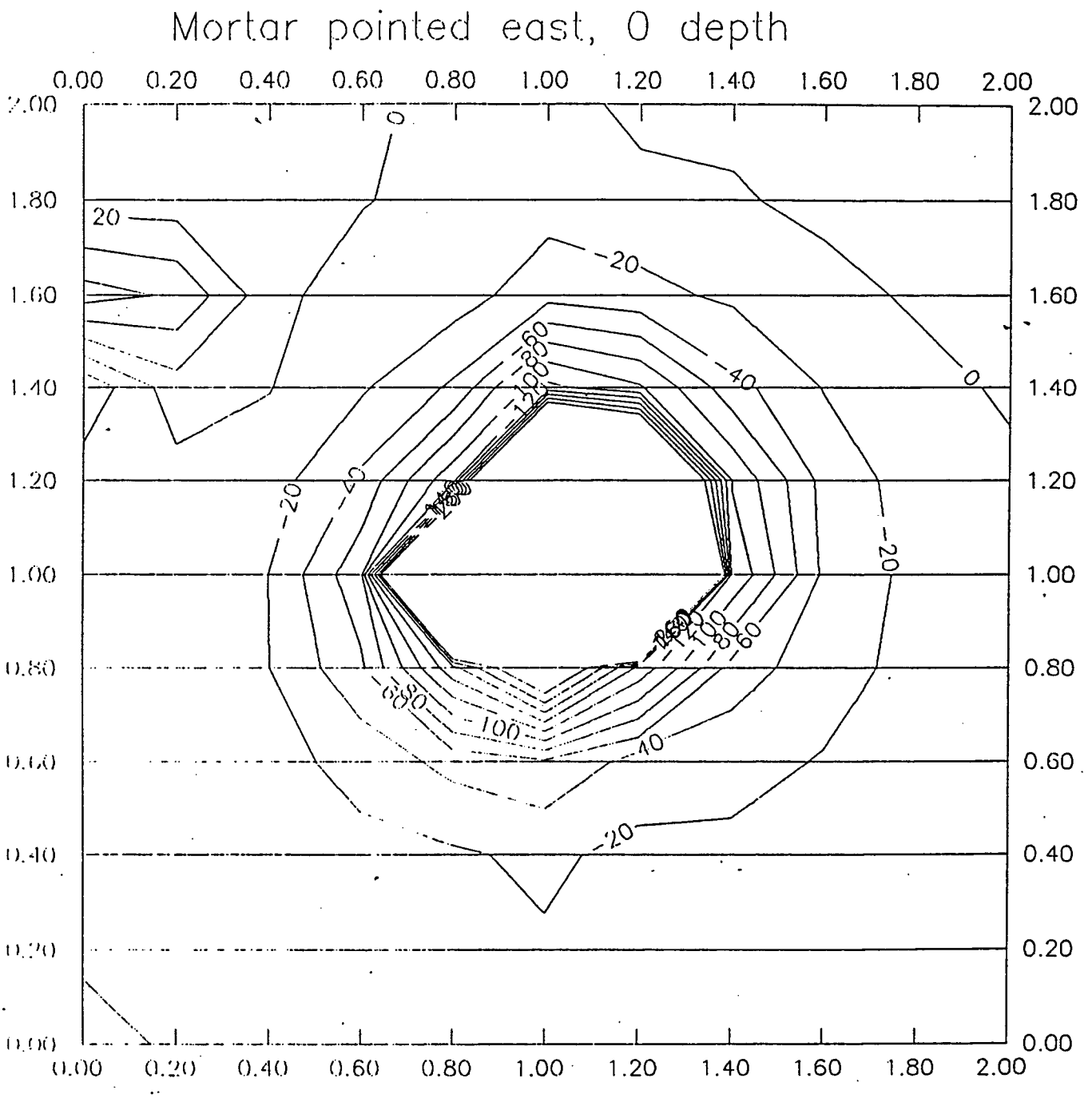

Figure 6-33. Mortar Pointed East, depth 0 cm

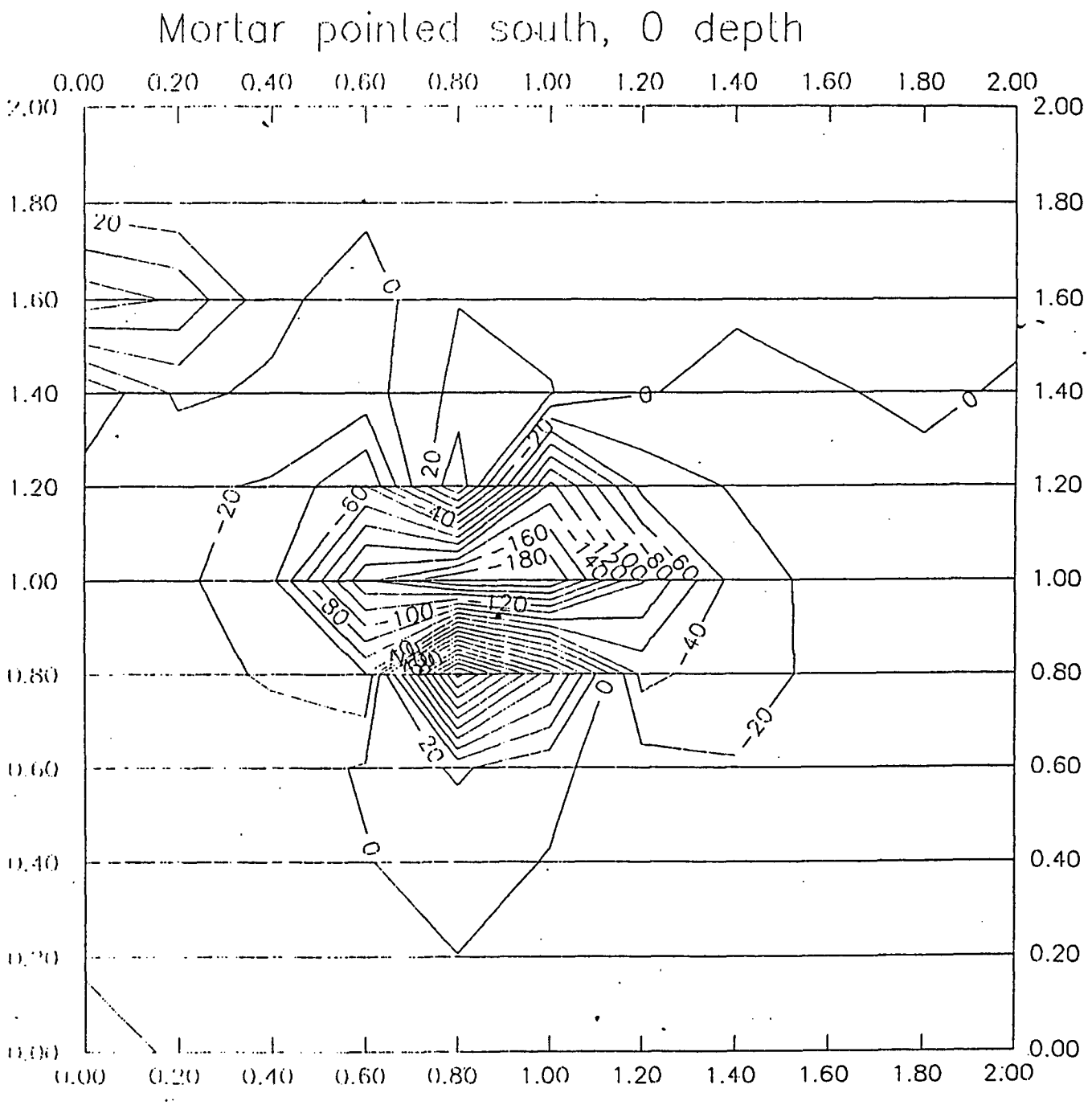

Figure 6-34. Mortar Pointed South, depth 0 cm

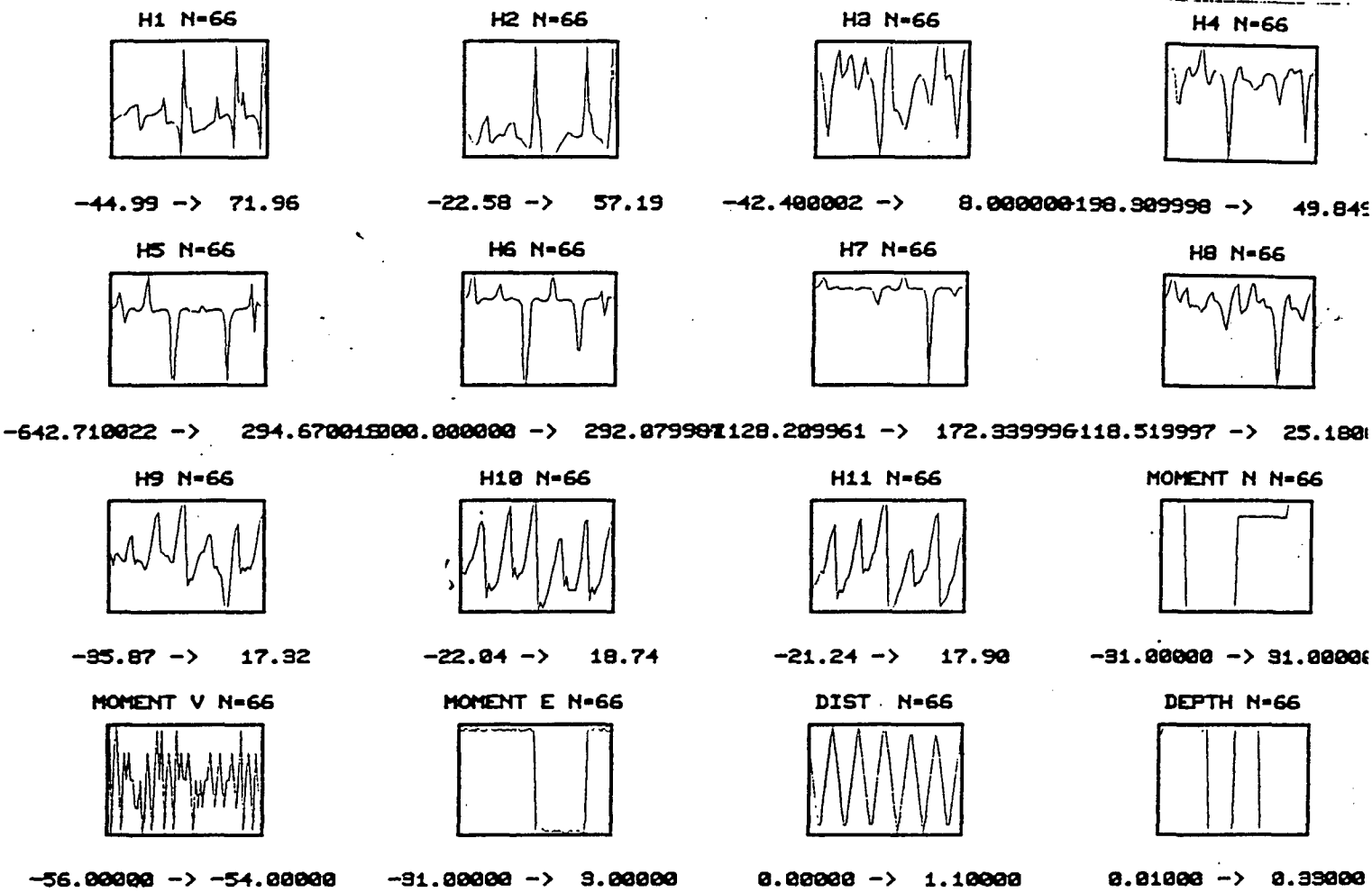

Figure 6-35. Data Summary by Row for Figures 6-29 through 6-34

Figure 6-36 shows a comparison of predicted and measured (the values entered into the program) for the magnetic moment in the north direction. A figure of merit for the comparison is the term R-square, which is a cross-correlation coefficient between predicted and measured values. For the plot of Figure 6-36 this value was R-square=0.93, a good result. For perfect agreement the value would be 1.0. The residual sum- square- error was 0.41.

The neural network program allows the collection of a variety of statistics. One of the more important diagnostics is the tabulation of the most significant input rows, measured as a percentage influence of the output. For Figure 6-36 the most significant rows were H9 and H11. The least significant were H1 and H3. We do not fully understand this result, but it will be noted that H9 and H11 are on the north side of the round, while H1 and H3 are on the south side. Frequently we have found this trend--that the more significant data lies on the north side of the round.

Another model was created, MAGFIXM1.BEP, that predicted only the east moment of the round. Figure 6-37 shows predicted and measured Moment East. The R-square was 0.914 and the sum- square- error was 0.411. The most significant rows for predicting the moment were H3 and H8. The least significant were H1 and H4. Except for H3, the trend is as before, with the least significant rows being on the south side.

The model could also be trained on the vertical moment, but this will be discussed in a later section of the report where both horizontal and vertical mortar rounds were surveyed by a Vallon gradiometer, and a new neural network training matrix was created on a larger 4x4 meter grid.

From this initial training matrix we have learned that neural network is best designed to provide a single output. For example, if the network were asked to predict the three moments, north, east and vertical, as well as distance and depth, all simultaneously, we have found that the overall R-square drops to about 0.3. Hence, it appears that neural networks should be configured in parallel so that each desired output is addressed by a single network. Ultimately neural networks should be trained on a wider variety of round orientations (or, equivalently, moments in three directions), depth, and distance than has been observed on the present program.

6.2.3. Neural Network Training on a Combination of Mortar, 105, and 155 Rounds

Thirteen surveys, each consisting of 121 data points on a 2x2 meter grid, were combined into one training matrix for the neural network. The rows , their corresponding observation numbers in the matrix, and the figure showing the contour plot of the data, are given below.

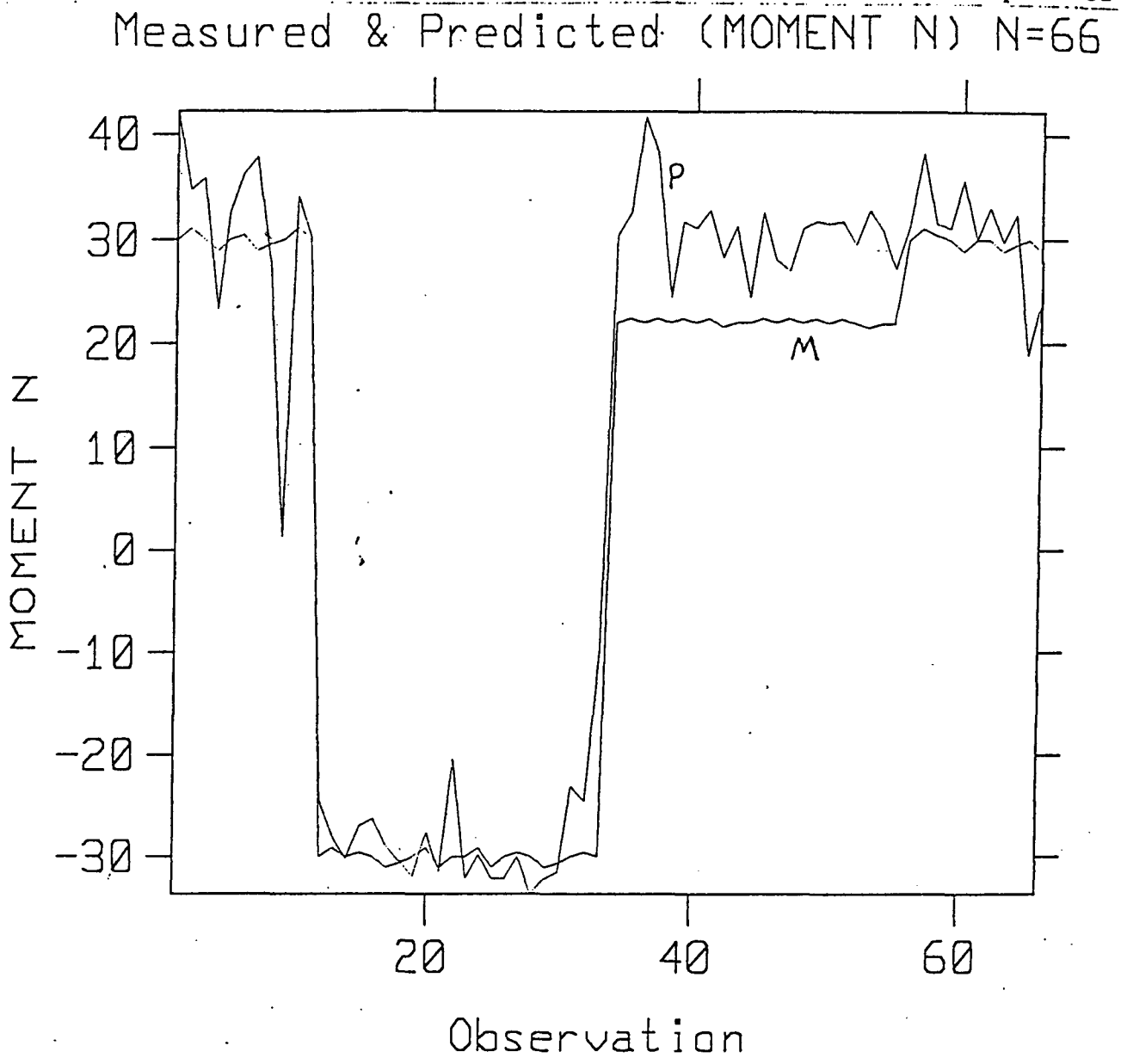

Figure 6-36. Comparison of Measured and Predicted Magnetic Moments - North

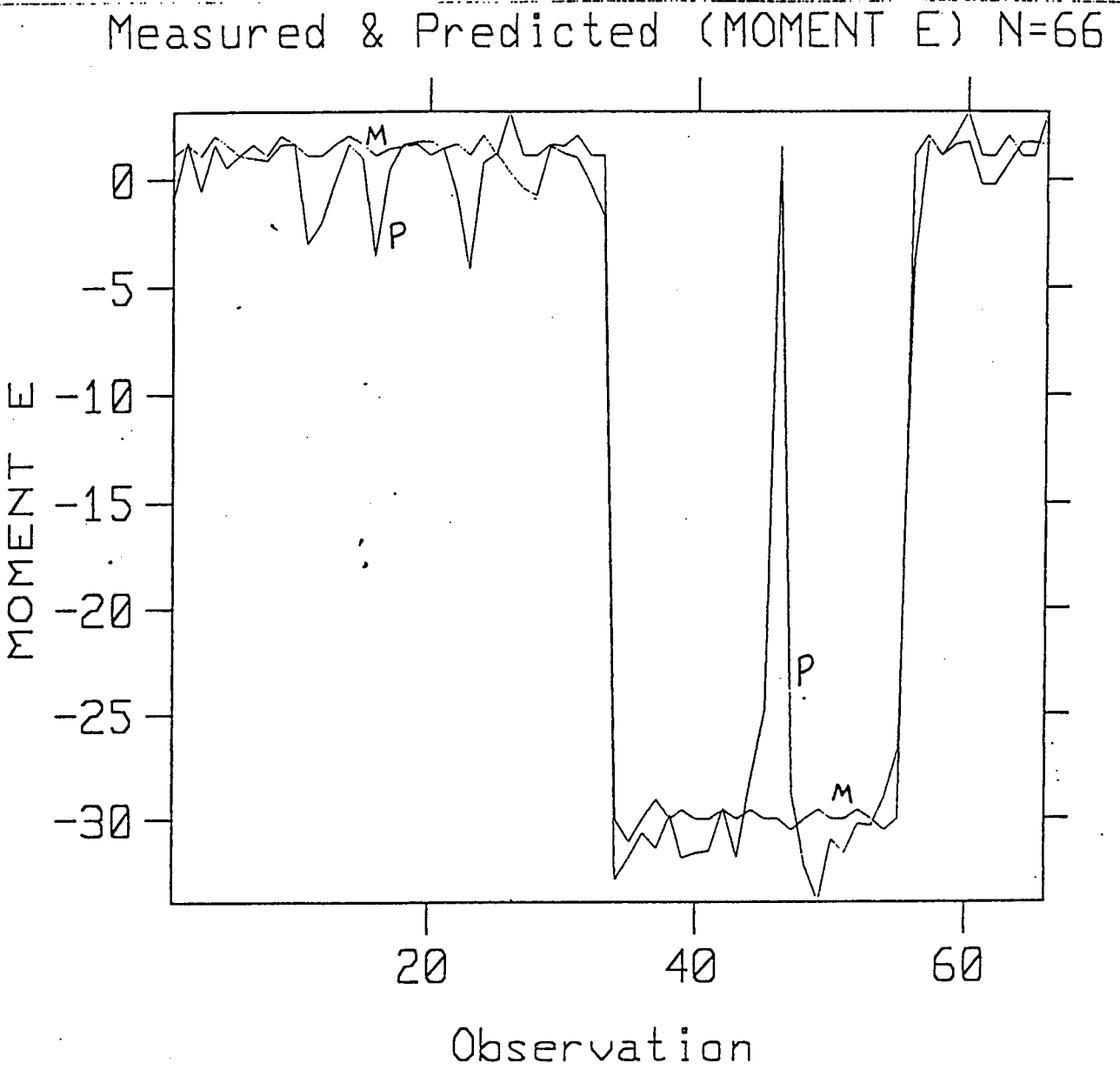

Figure 6-37. Comparison fo Measured and Predicted Magnetic Moments - East

Observations 1-11,	Mortar pointed south,	33 cm depth	Figure 6-29
Observations 12-22,	Mortar pointed north,	33 cm depth	Figure 6-30
Observations 23-33,	Mortar pointed north,	0 cm depth	Figure 6-31
Observations 34-44,	Mortar pointed east,	33 cm depth	Figure 6-32
Observations 45-55,	Mortar pointed east,	0 cm depth	Figure 6-33
Observations 56-66,	Mortar pointed south,	0 cm depth	Figure 6-34
Observations 67-77,	105 pointed south,	30 cm depth	Figure 6-38
Observations 78-88,	105 pointed east,	30 cm depth	Figure 6-39
Observations 89-99,	105 pointed north,	30 cm depth	Figure 6-40
Observations 100-110,	ambient background		Figure 6-41
Observations 111-121,	155 pointed north	30 cm depth	Figure 6-42
Observations 122-132,	155 pointed east	30 cm depth	Figure 6-43
Observations 133-143,	155 pointed south	30 cm depth	Figure 6-44

All of the above surveys, with the exception of the ambient survey (observations 100-110), will be provided to NAVEODTECHDIV in ASCII, DOS text, format (under separate cover). Figure 6-45 shows a plot of all the data, input as well as output.

The 105 contours have all been plotted from -300 to + 1000 gamma, in intervals of 100 gamma. The trends of the data in Figures 6-38 to 6-40 show that the contours are negative on the side nearest the base of the round. This is caused by the permanent moment toward the base of the round, which will cause a magnetic field that tends to subtract from the local vertical field in that direction from the round.

The ambient survey in Figure 6-41 is plotted in intervals of 2 gamma. The region is far from pristine, but this may represent the type of variation that is encountered in field operations. In a later section of the report, it will be shown that in order to remove the effect of these spatial variations, we moved the round and kept the sensor located in a fixed position when we measured detection thresholds.

The 155 contours of Figures 6-42 to 6-44 have been plotted from -1000 to + 2000 gamma in intervals of 200 gamma. The trends are different from those of the 105 round -- a fact that can be confirmed by examining Table 6-14. In this table it is shown that whether a 155 round is pointed north or south, it's net moment is to the north. This is true for the two rounds provided. We can not be certain this applies to <u>all</u> 155 rounds. This means that a buried 155 round, pointed north or south, will have negative contours on the north side of the round. Because the round has a permanent moment toward the nose of the round, a buried east-pointed round will have negative contours on the east side. This is exactly what Figures 6-42 to 6-44 show. On the other hand, Table 6-14 reveals that the 105 round has a net moment toward the south when it is pointed north, and a net moment toward the north when it is pointed south for the two rounds provided. The relative permanent moment is larger for this round and it is pointed toward the base instead of the nose, as in the 155. Hence, the horizontal,

buried 105 will have a negative contour on the side nearest the base, or conversely, a positive contour on the side nearest the nose. These results should have significant implications for future neural network training if the permanent moment trends follow those of the rounds studied .

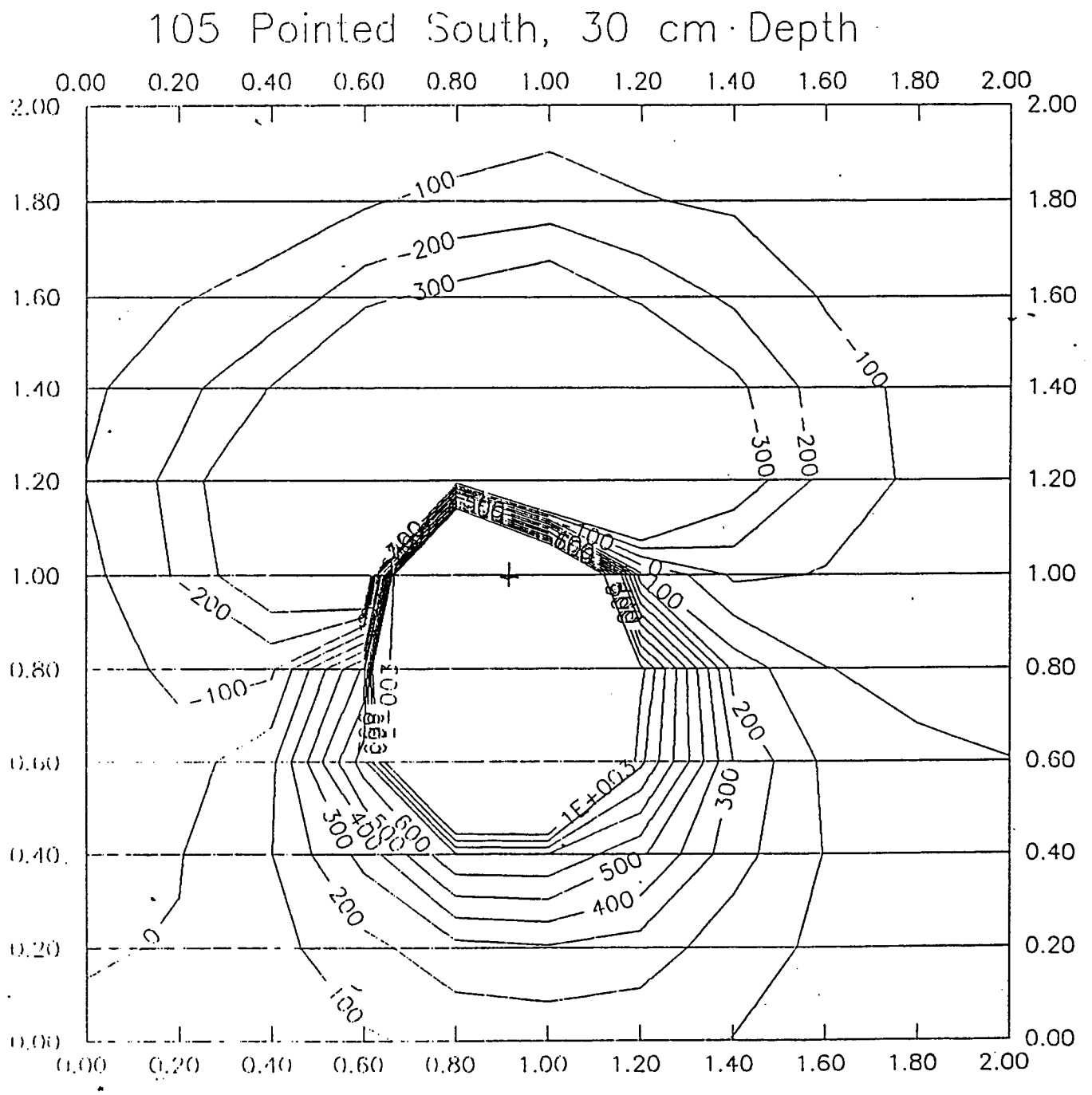

Figure 6-38. 105 Pointed South, depth 30 cm

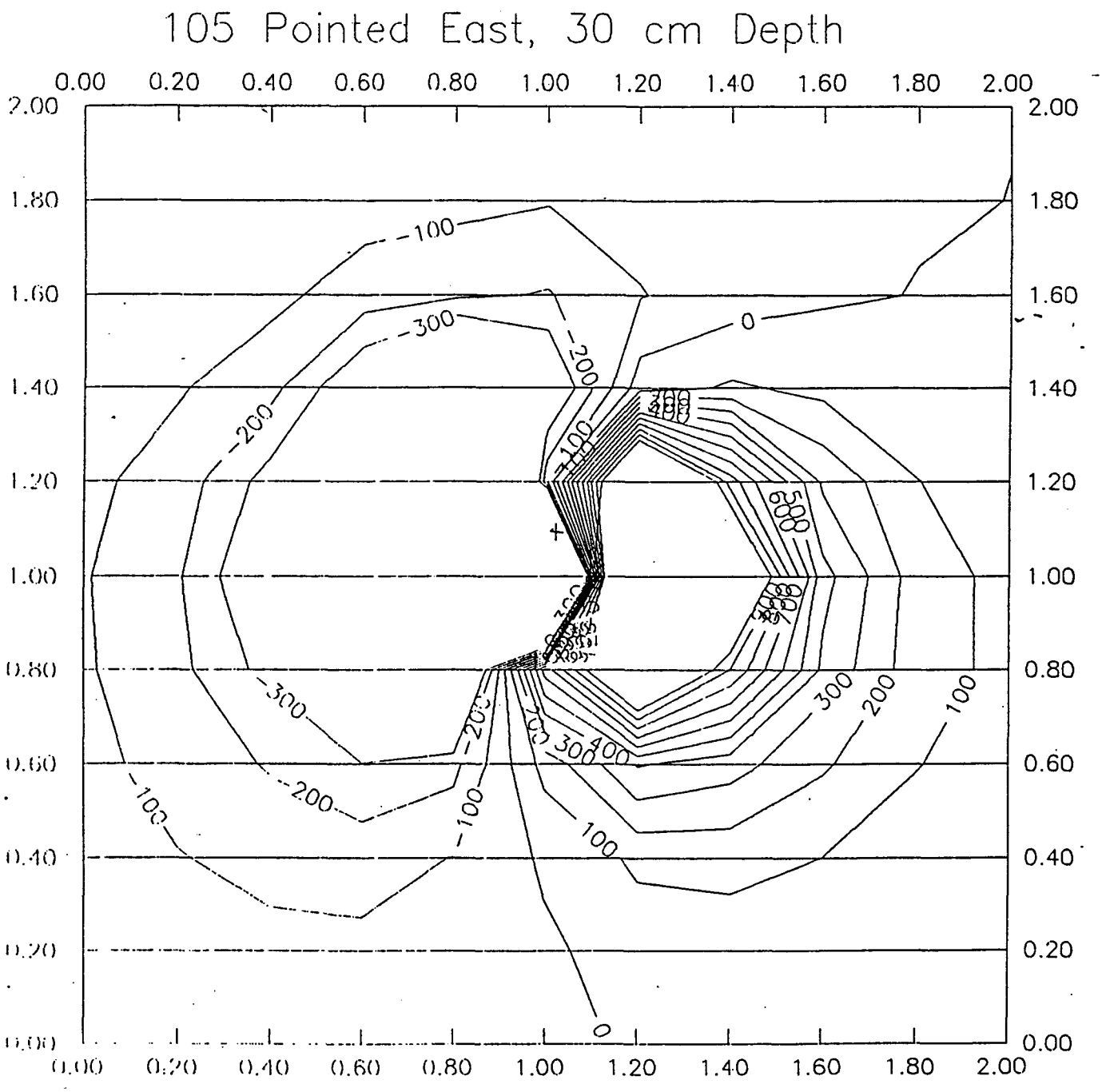

Figure 6-39. 105 Pointed East, depth 30 cm

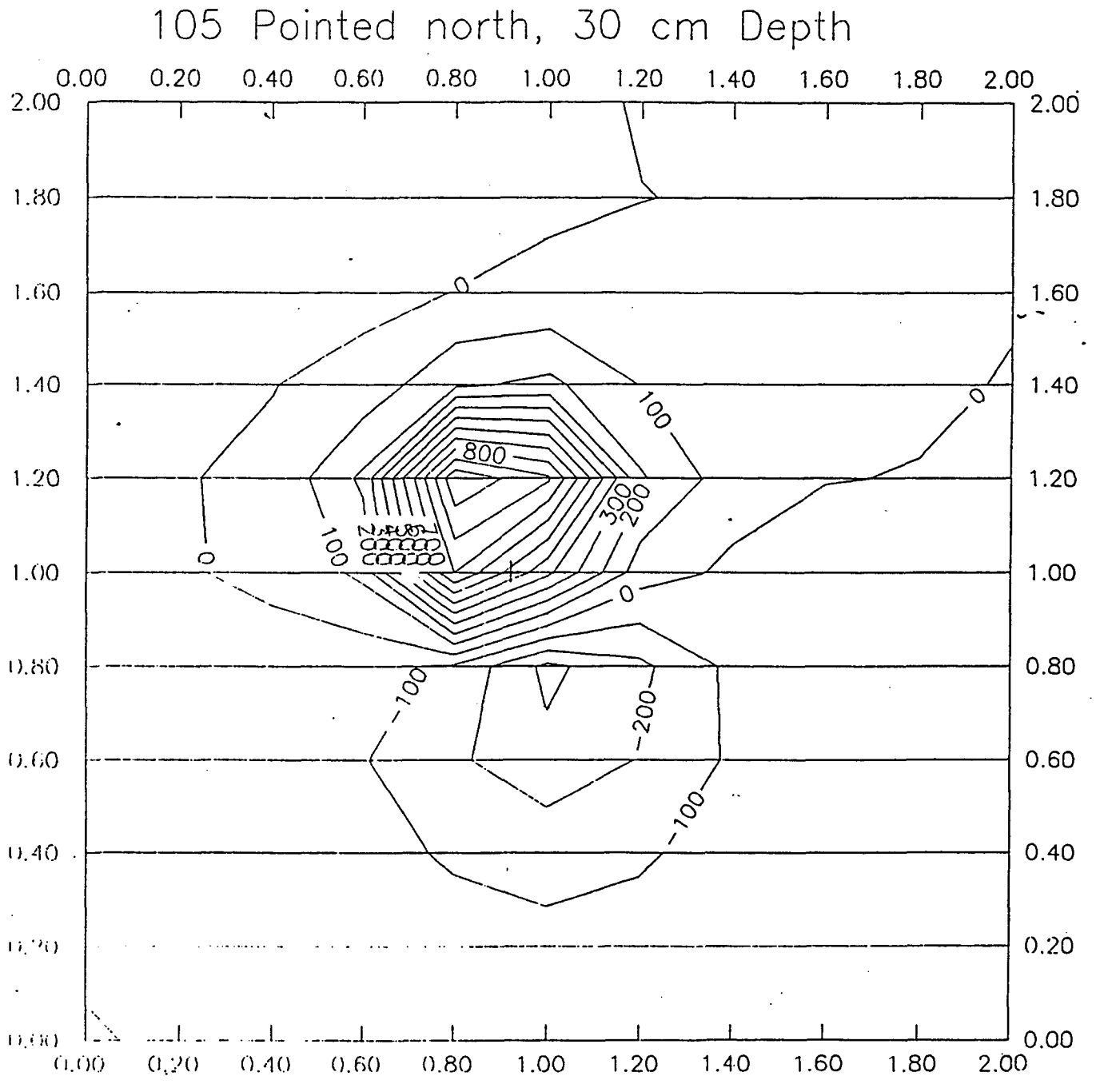

Figure 6-40. 105 Pointed North, depth 30 cm

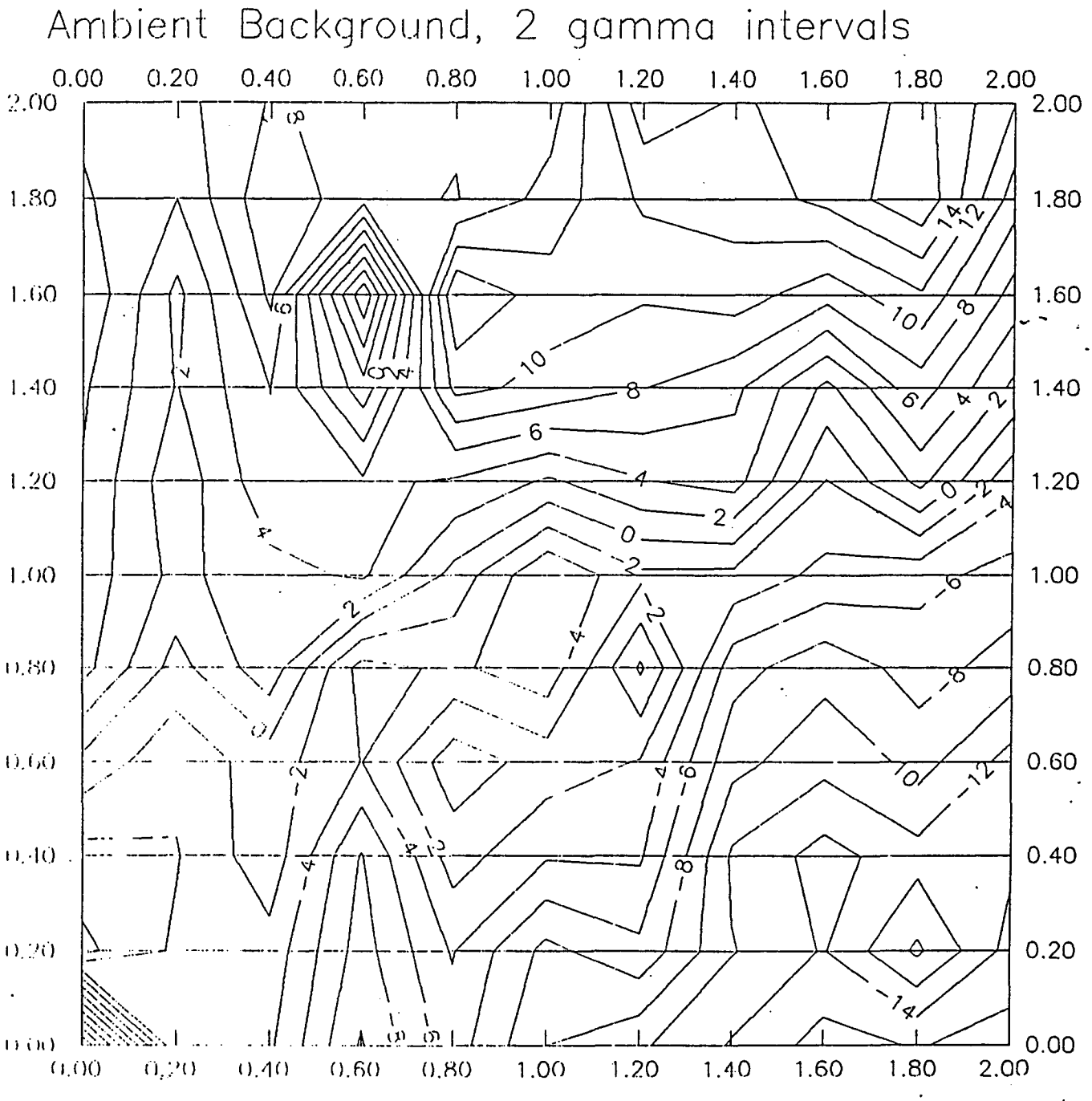

Figure 6-41. Ambient Background Survey

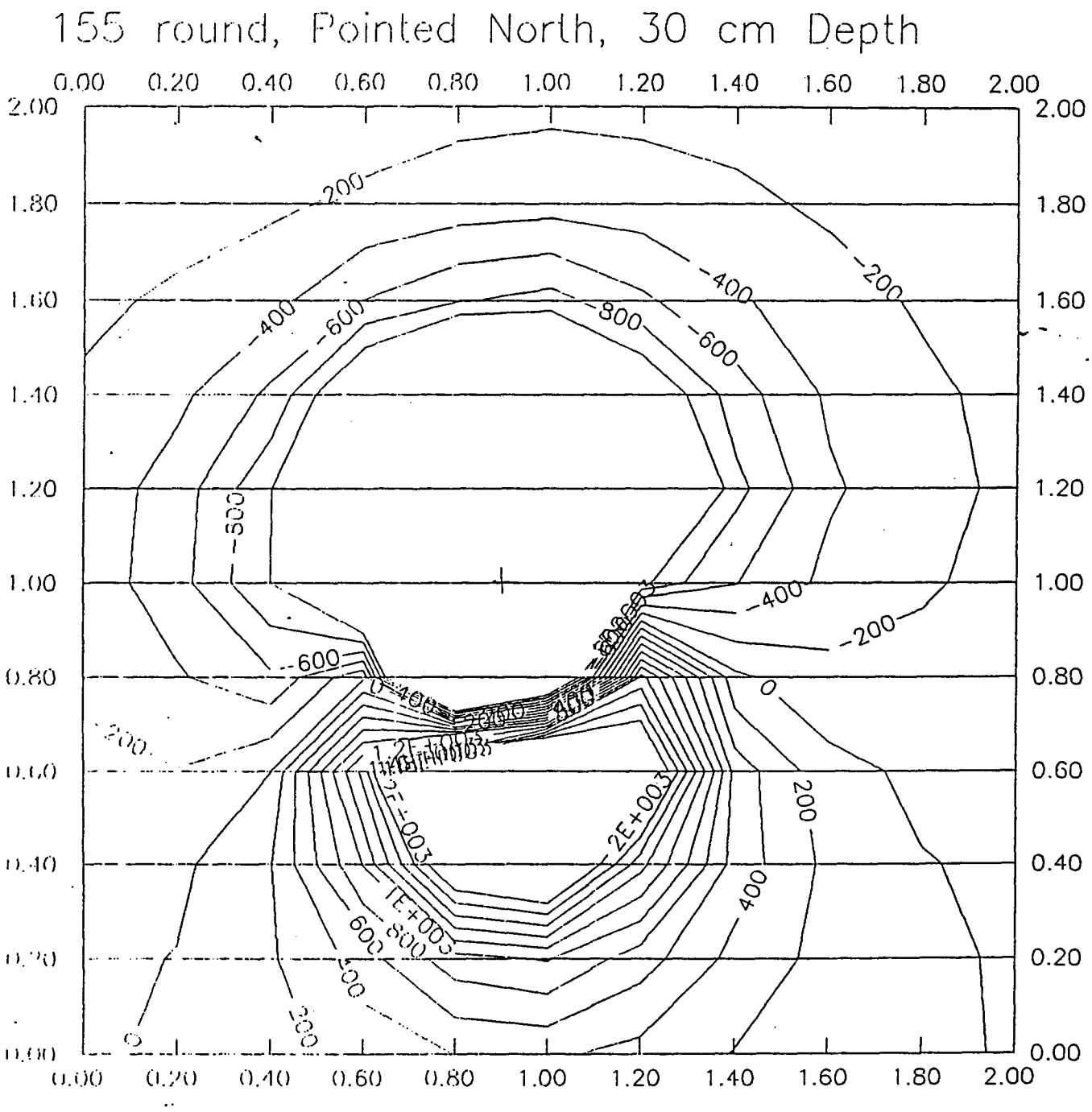

Figure 6-42. 155 Pointed North, depth 30 cm

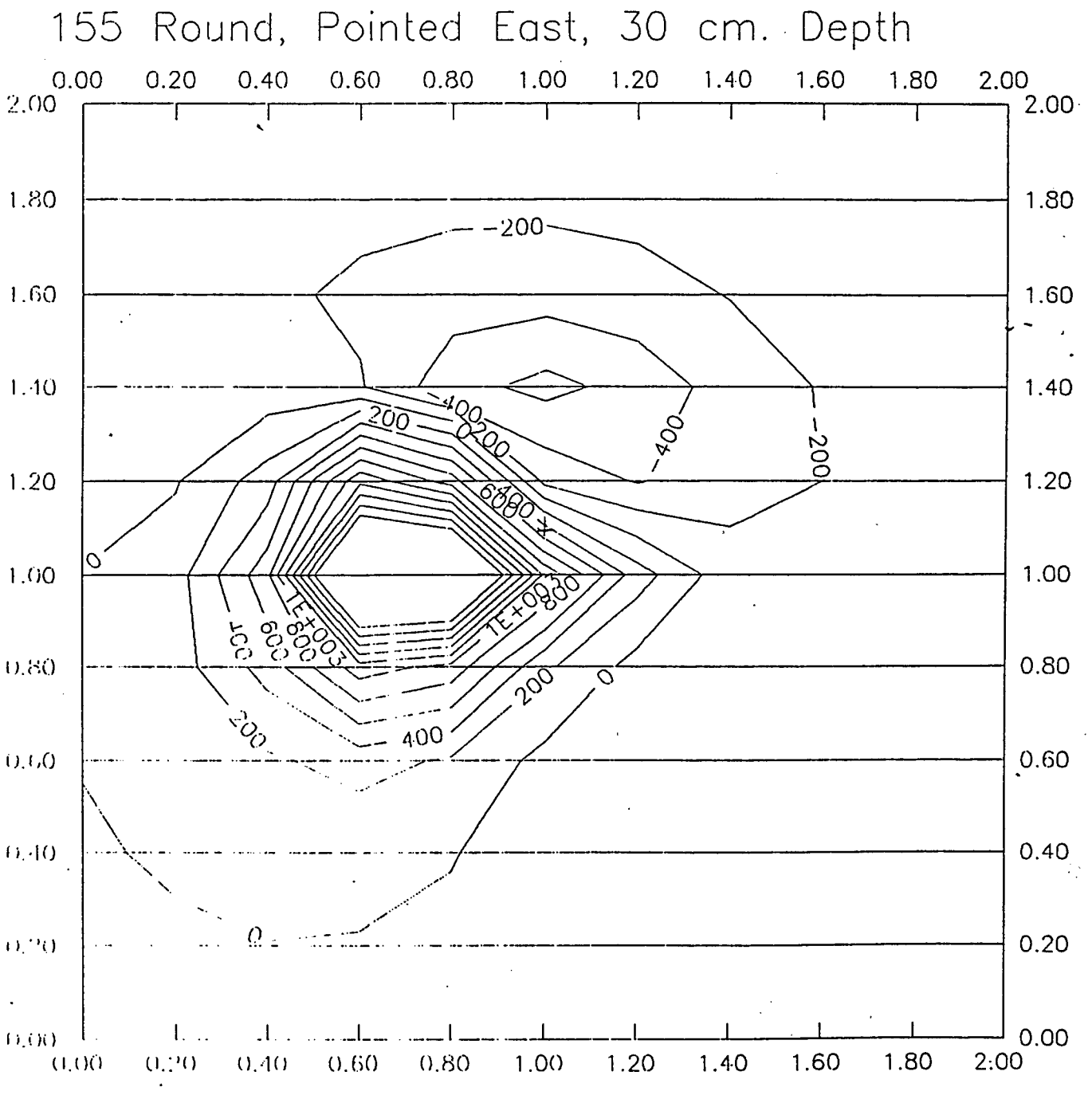

Figure 6-43. 155 Pointed East, depth 30 cm

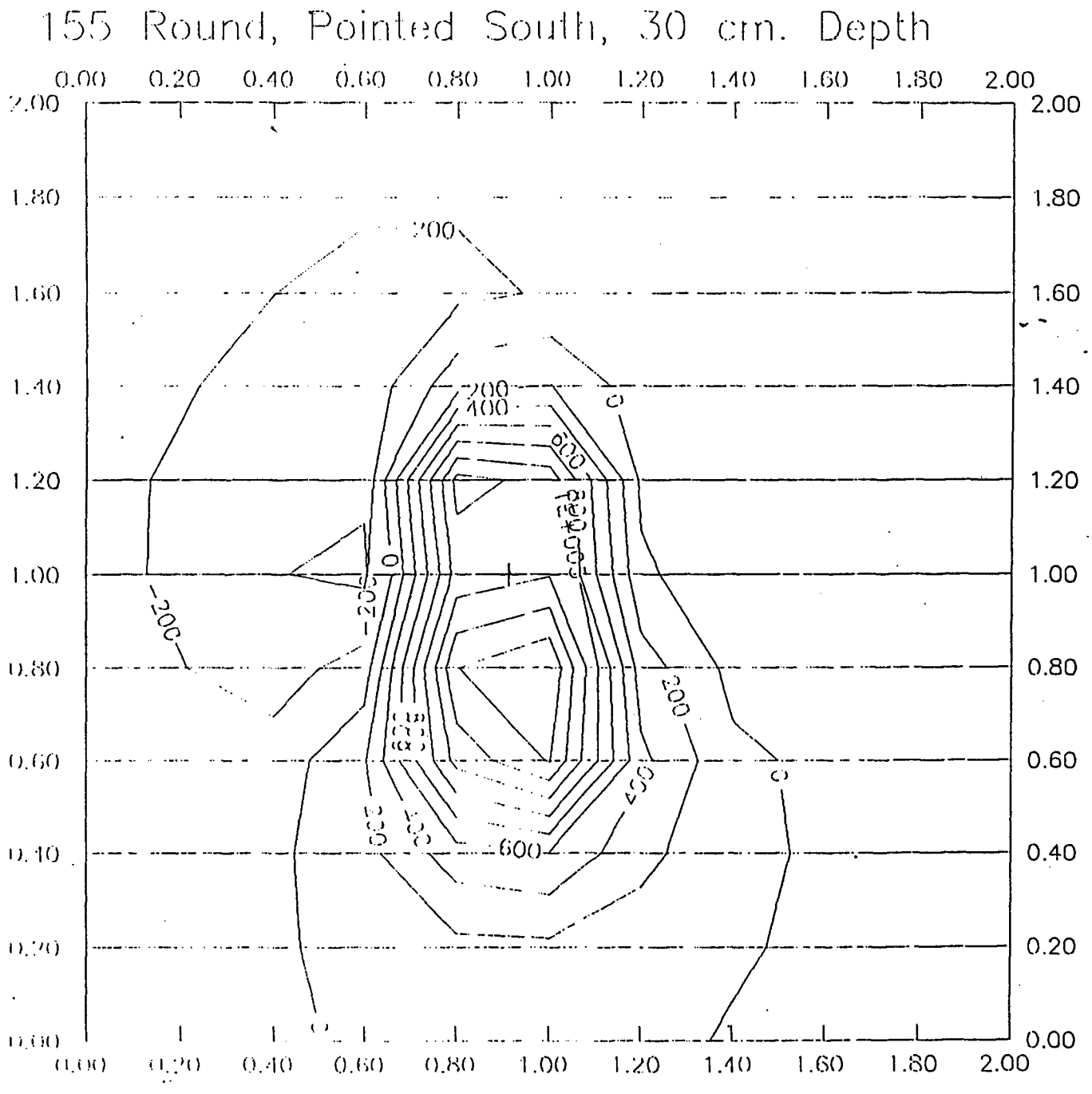

Figure 6-44. 155 Pointed South, depth 30 cm

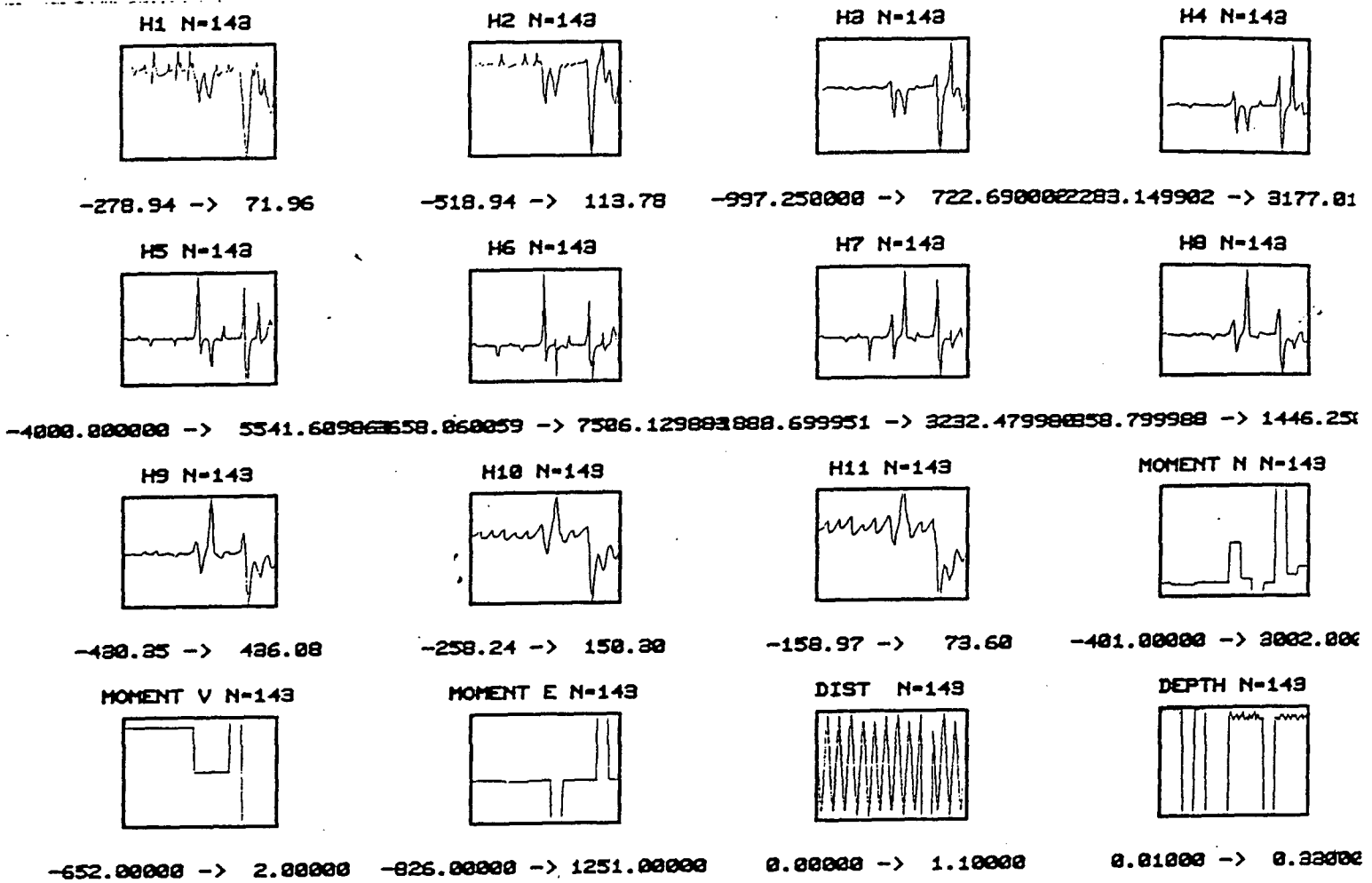

Figure 6-45. Data Summary by Row for Figures 6-29 through 6-44

A training model was established for these 143 observations (13 surveys, 11 rows each, 11 data points per row). The model MAGFIX2.BEP was trained on one output, magnetic moment north. Results of predicted and measured moment are given in Figure 6-46. The overall R-square was 0.888 and sum- square- error was 0.40. The model was trained for 20,000 cycles through the data, which required about 90 minutes. With the training limited to 10,000 the R-square was 0.738 and the sum-square- error was 0.922. The least significant row in the sensitivity analysis was row H6, over the top of the round, and the most significant row was row H10, on the north side of the round. Model MAGFIX6.BEP was used to predict the vertical moment. Results of predicted and measured moment is shown in Figure 6-47. The R-square was 0.923 and the sum-square-error was 0.422 for 20,000 training cycles. The values change to 0.807 and 1.52 for 10,000 cycles. The least significant rows were H1 and H3, on the south side of the round.

6.2.4 Neural Network Training on a 4x4 Meter Grid With a Vallon Gradiometer Sensor

The previous surveys, collected on a 2x2 meter grid with a Geometric total field magnetometer, revealed that significant magnetic field perturbations existed out to the edge of the grid and beyond. Another grid, 4x4 meters in size, with intervals of 0.4 meter, was defined. There were still 121 data points per survey. For these surveys a Vallon iron detector, or gradiometer, was used. The sensor has an analog output meter. So, rather than automatically entering the data into a lap-top computer, as was done for the Geometric total field surveys, we had to enter the data manually into the GRID program.

6.2.4.1. Surveys and Training on 105 Rounds, Vallon Sensor

The first matrix used for neural network training on the 4x4 meter grid was a collection of 5 surveys (55 observations) for a 105 round. The observation numbers, round orientation, and Figure number for the contour plot are given below:

Observations 1-11,	105 pointed west, 0 depth,	Figure 6-48
Observations 12-22,	105 pointed south, 0 depth,	Figure 6-49
Observations 23-33,	105 pointed east, 0 depth,	Figure 6-50
Observations 34-44,	105 pointed north, 0 depth,	Figure 6-51
Observations 45-55,	105 pointed down, 25 cm depth,	Figure 6-52

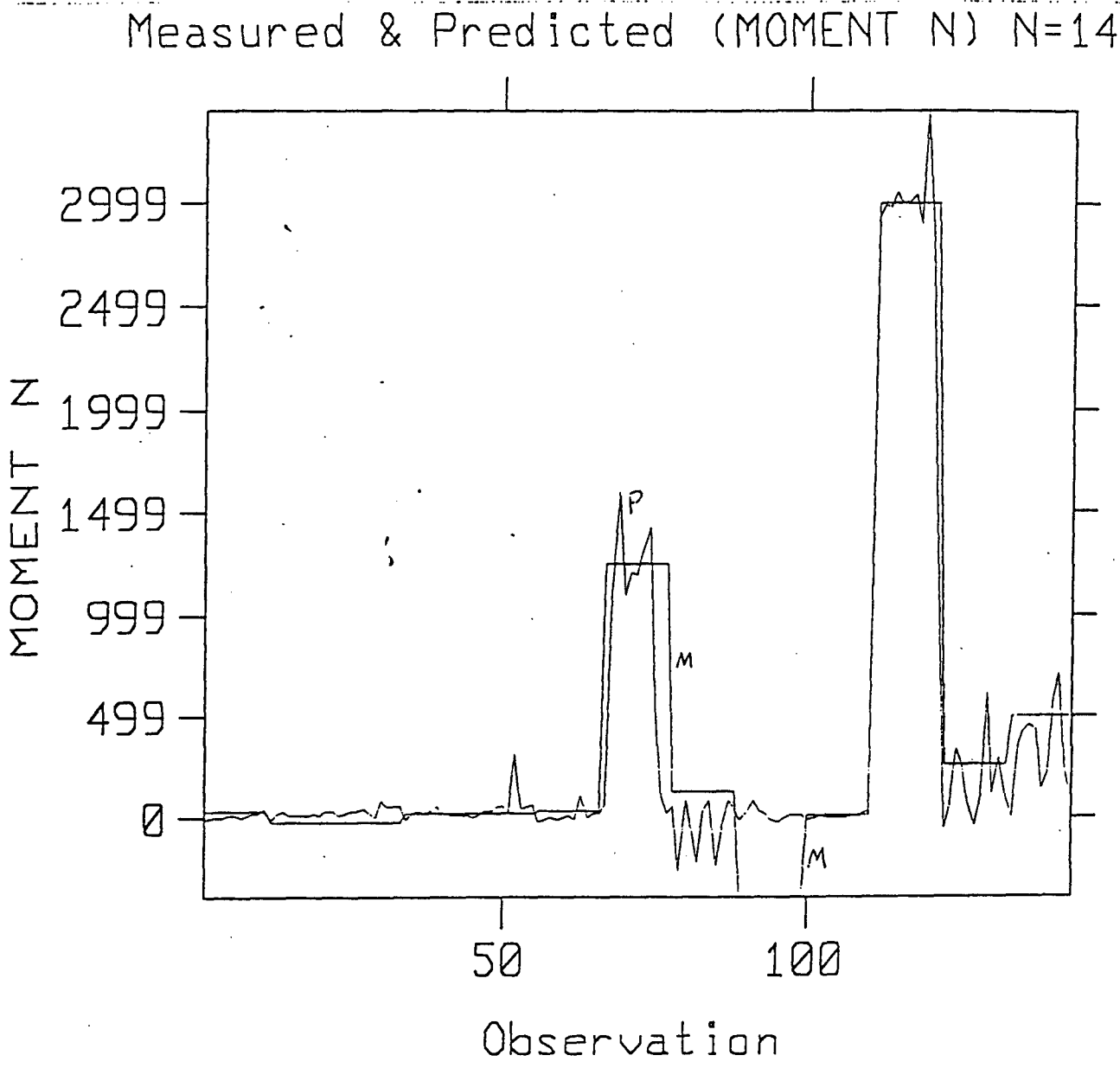

Figure 6-46. Predicted and Measured Magnetic Moments - North

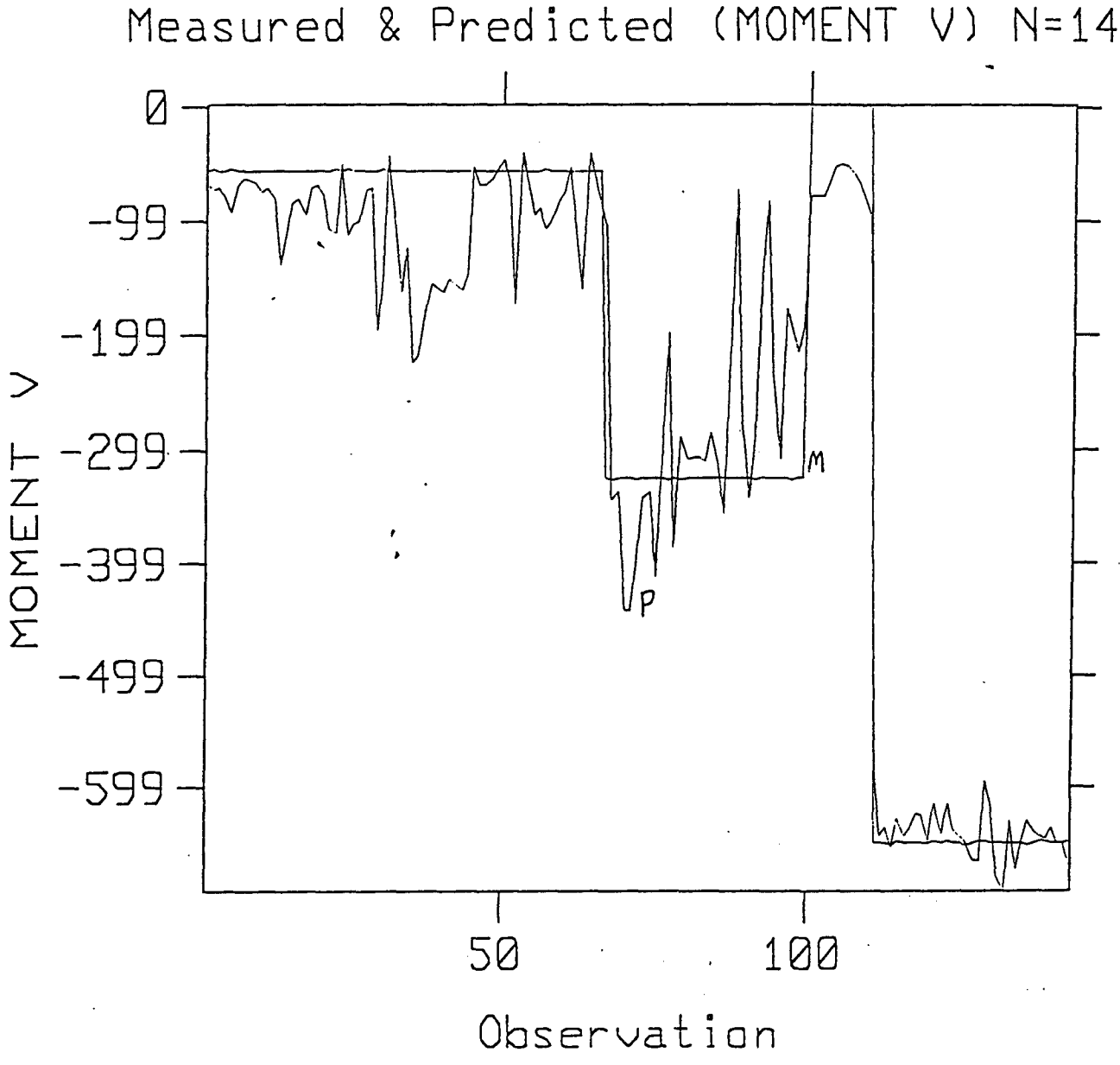

Figure 6-47. Predicted and Measured Magnetic Moments- Vertical

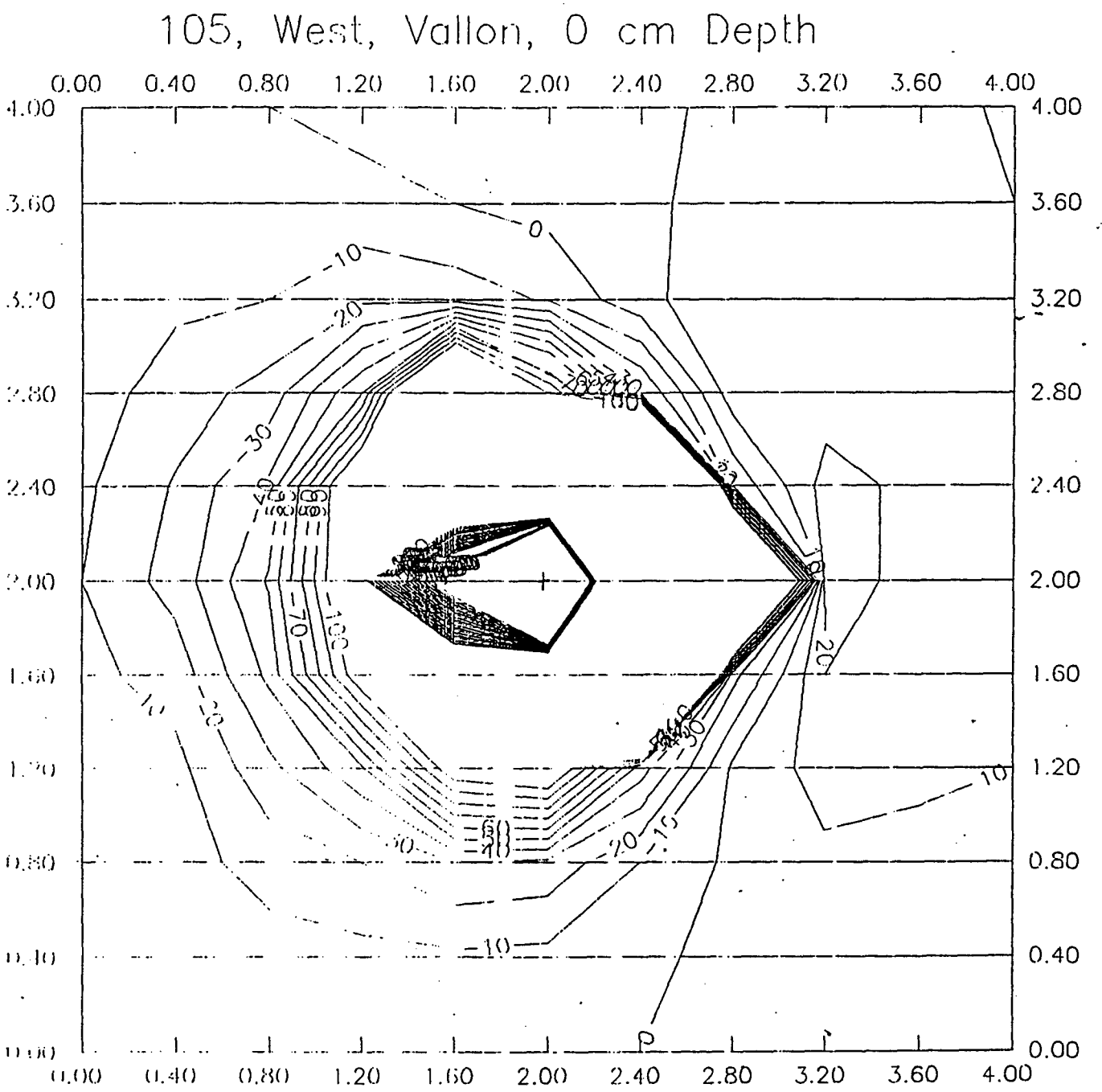

Figure 6-48. 105 Pointed West, depth 0 cm

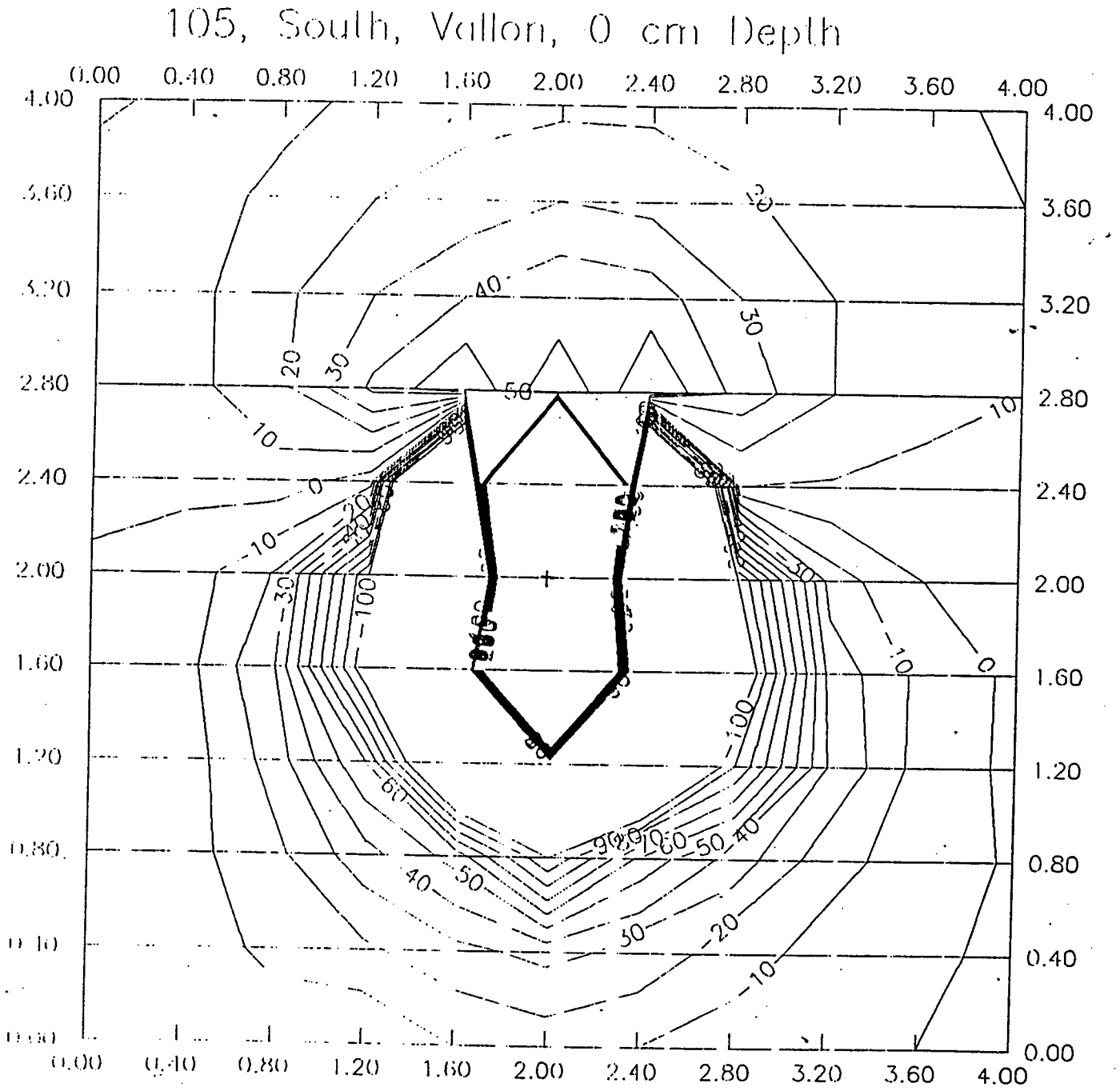

Figure 6-49. 105 Pointed South, depth 0 cm

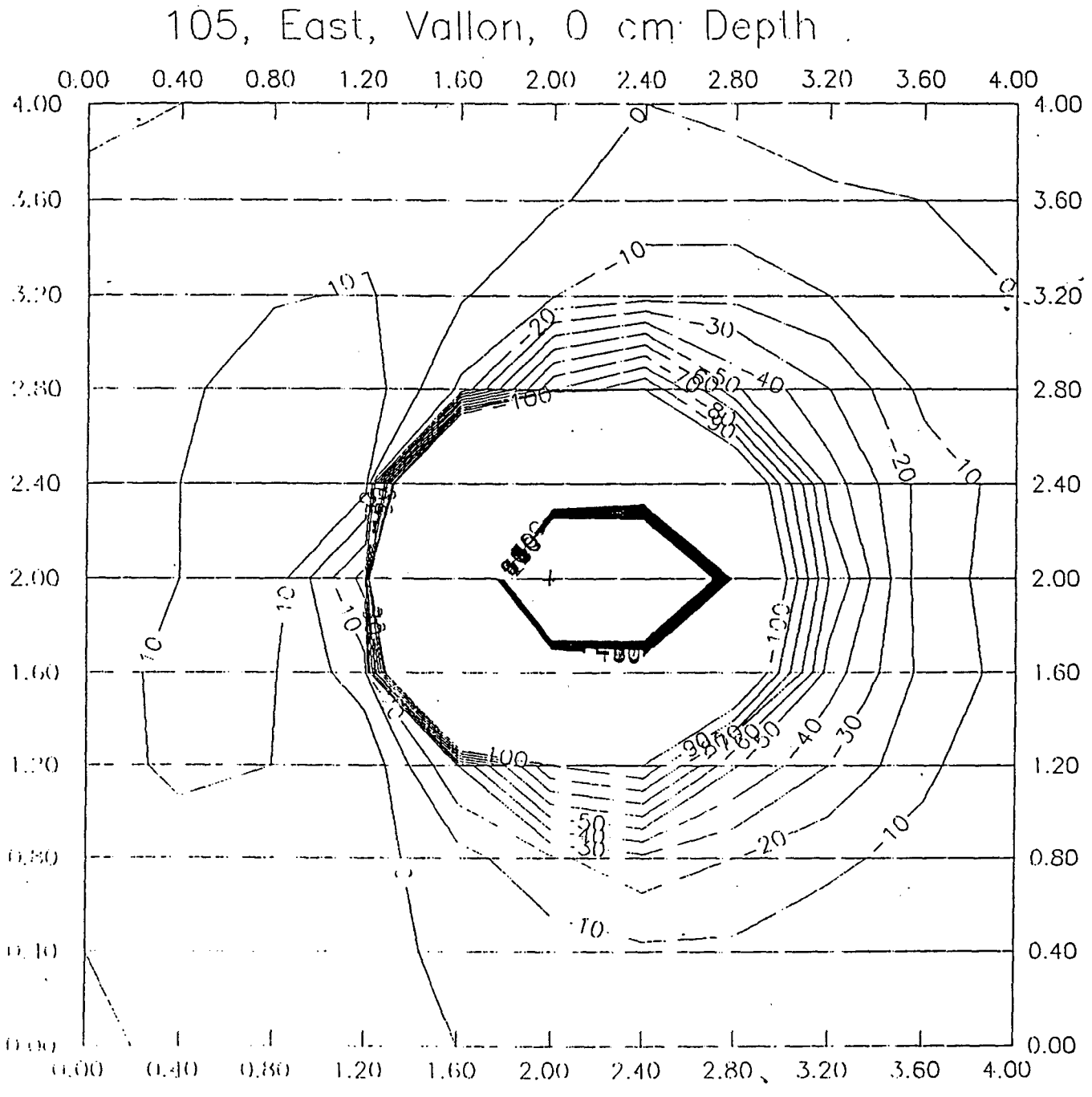

Figure 6-50. 105 Pointed East, depth 0 cm

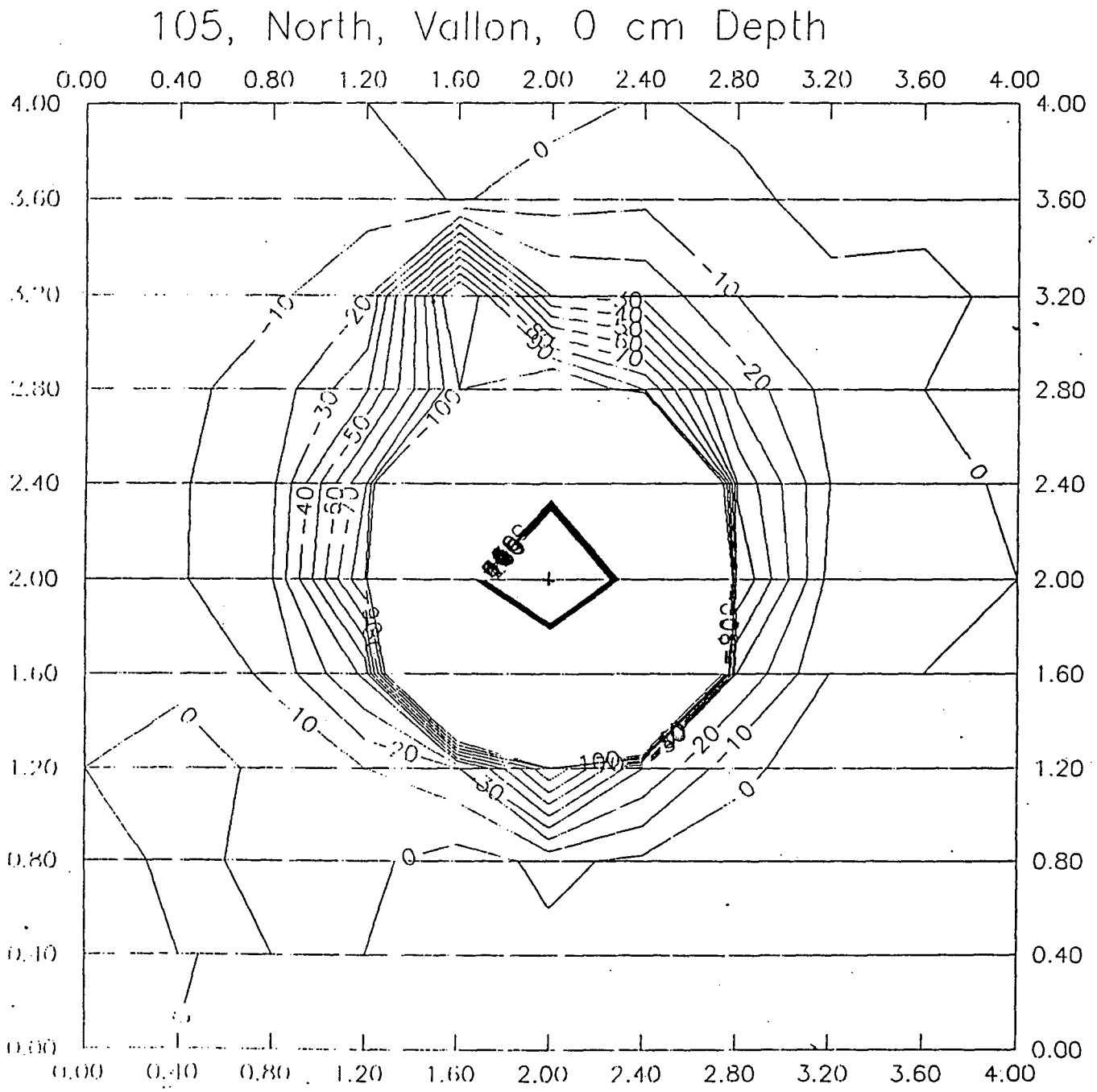

Figure 6-51. 105 Pointed North, depth 0 cm

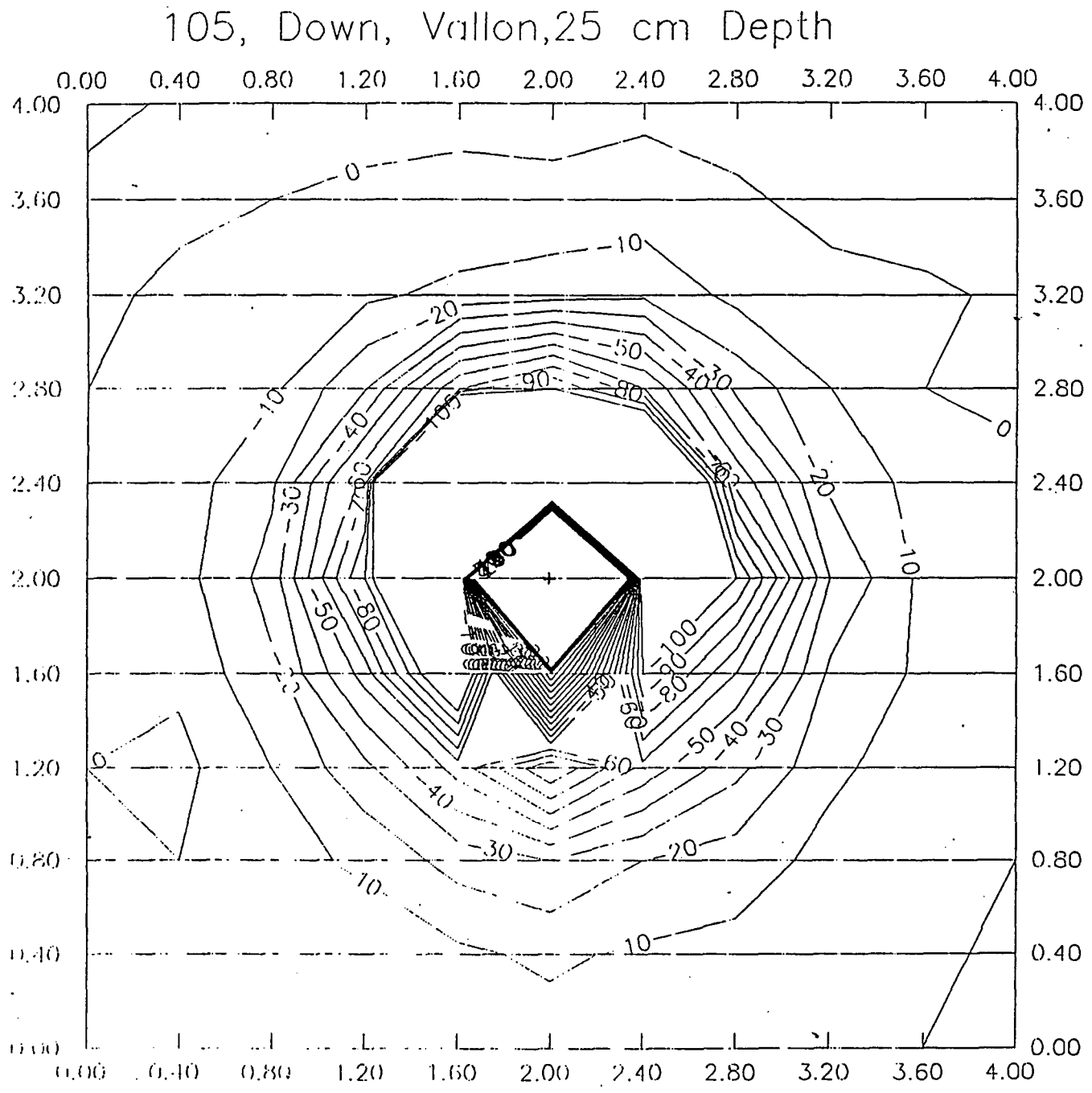

Figure 6-52. 105 Pointed Down, depth 25 cm

signals over the top of the round were in excess of 2000 gamma, the maximum reading of scale 1. The trends of the contours for the 105 round at the surface are different than those of the buried 105 rounds (discussed in subsection 6.2.3). The contours of the east- and west-pointed rounds are nearly mirror images of one another; the negative contours extending to the greatest distance on the nose side of the round. The south-pointed round has a negative contour on the south side and a positive contour on the north side. In contrast, the north-pointed round has a negative contour on both north and south sides. Notice, also, the contours indicate that detection threshold distances will be strongly dependent upon pointing direction and the azimuthal direction of approach. This latter topic will be addressed in a following section.

Figure 6-52 for the 105 pointed down shows rather symmetric contours , except very near the round on the south side. This is probably caused by a small induced moment in the north direction. 10 gamma threshold detection distances are approximately 1.5 meters for this round at 25 cm depth to it's geometric center.

A neural network training model, labeled MAGFIX9, was created. When trained for 20,000 cycles through this data of 55 rows, 11 points per row, the predicted magnetic moment north was as shown in Figure 6-53. R-square was 0.953 and sum-square-error was 0.114. The training time was 25 minutes on the 486 PC. The most significant row was H7, on the north side, and the least significant row was H3 on the south side.

A second training model was used to predict the moment in the vertical direction. This result is shown in Figure 6-54. R-square was increased to 0.988 and the sum-square-error was down to 0.039. This condition results from the fact that there is very little variation in the vertical moment throughout the matrix of data. In fact there are only two values, one for horizontal and one for a downward pointed round. The most significant row was H9 and the least significant was H4.

Training model MAGFIX10 was used to predict the magnetic moment in the east direction. Figure 6-55 shows the result. R-square increased to 0.991 and the error reduced to 0.016. This an unusually good result, again perhaps caused by the fact that there are not a large number of variations in the east moment. All of the above training occurred over 20,000 cycles, a number that seems sufficient in that no further improvements could be expected.

6.2.4.2 Training on Surveys of a Mortar Round, Vallon Sensor

A matrix of 9 surveys, 99 observations, was compiled to train the neural network on mortar detection. The observation numbers, round orientation, depth, and the Figure number for the contour plot are given below.

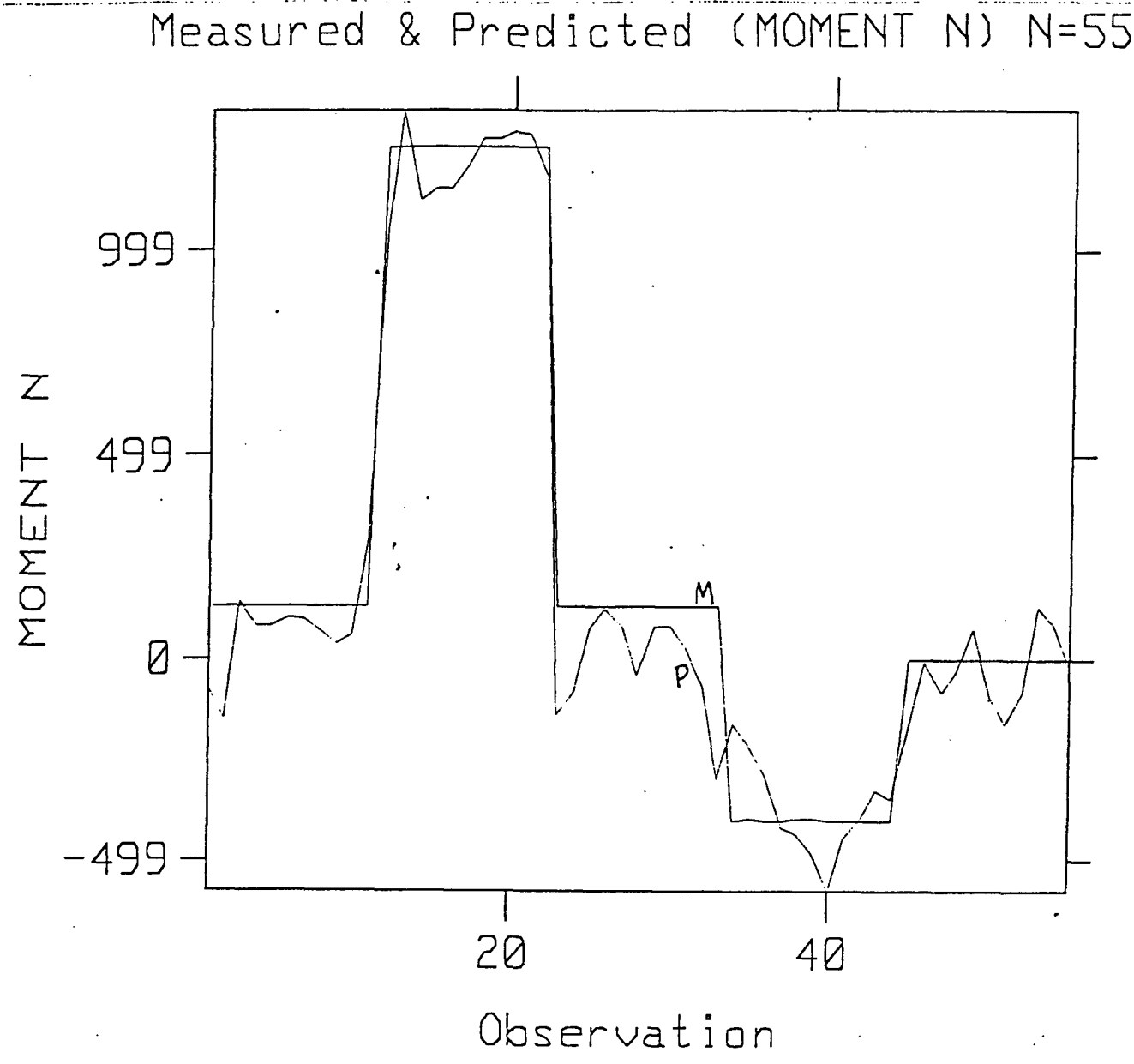

Figure 6-53. Measured and Predicted Magnetic Moment - North

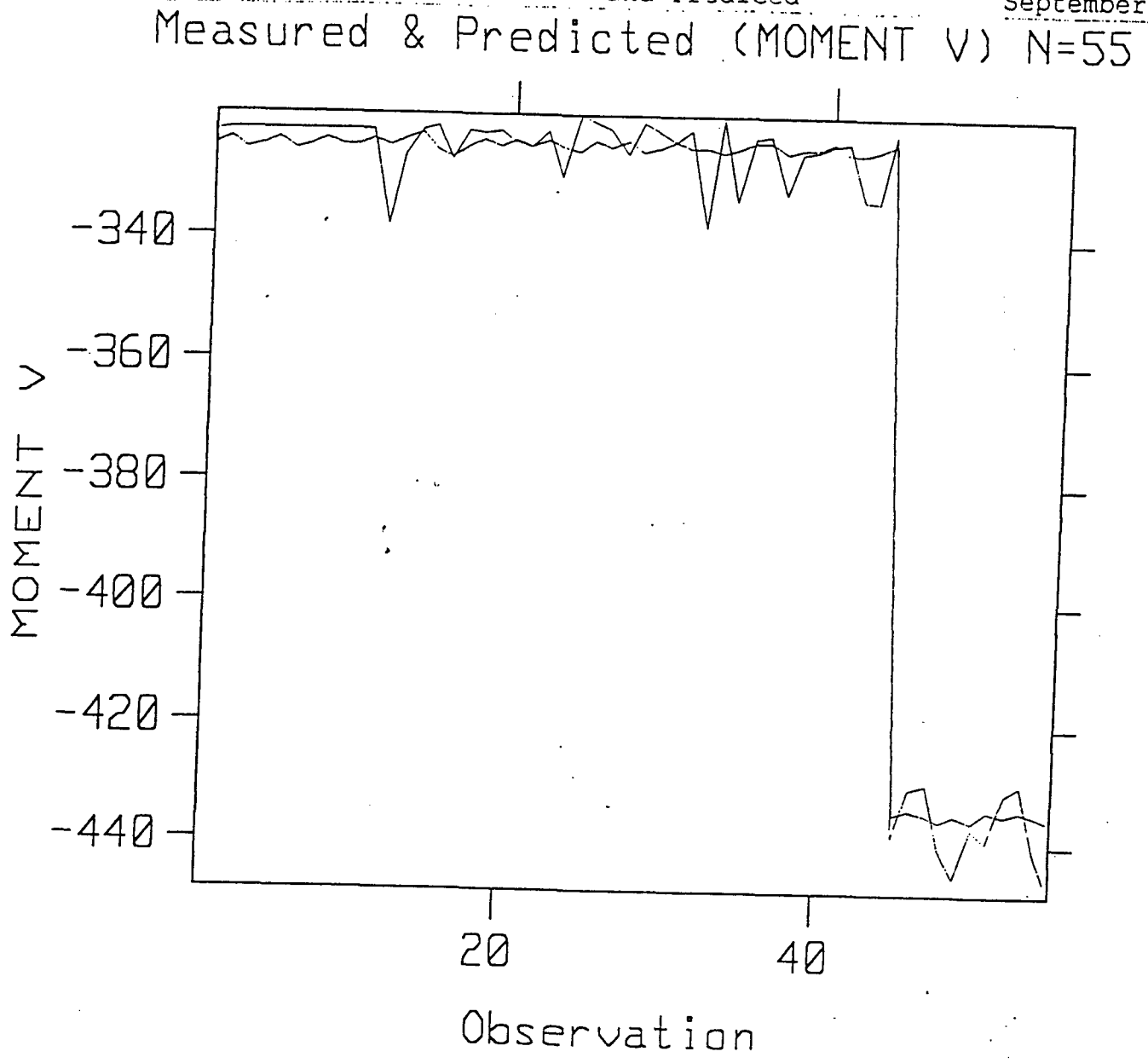

Figure 6-54. Measured and Predicted Magnetic Moment - Vertical

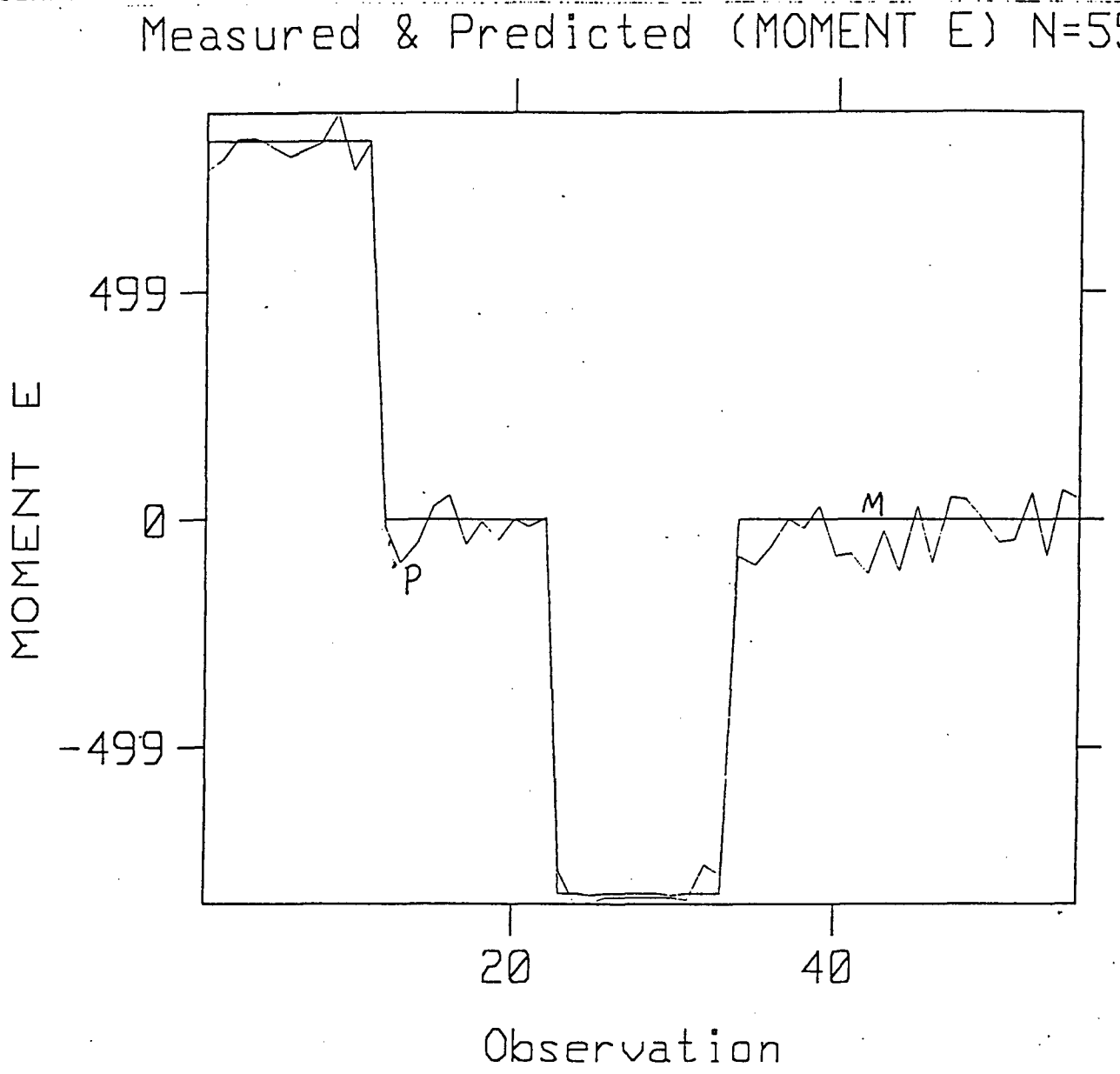

Figure 6-55. Measured and Predicted Magnetic Moment - East

Observations 1-11,	mortar down,	25 cm depth,	Figure 6-56
Observations 12-22,	mortar west,	0 cm depth,	Figure 6-57
Observations 23-33,	mortar south,	0 cm depth,	Figure 6-58
Observations 34-44,	mortar east,	0 cm depth,	Figure 6-59
Observations 45-55,	mortar north,	0 cm depth,	Figure 6-60
Observations 56-66,	mortar west,	40 cm depth,	Figure 6-61
Observations 67-77,	mortar south,	40 cm depth,	Figure 6-62
Observations 78-88,	mortar east,	40 cm depth,	Figure 6-63
Observations 89-99,	mortar north,	40 cm depth,	Figure 6-64

All of the contour plots have been shown from -100 to 100 gamma in intervals of 10 gamma. For each survey of a horizontal round the pin in the nose of the round was pointed upward. For the downward-pointed round the pin was toward the south. These effects of rotation about the round's long axis will be discussed later in the report.

The contours of Figure 6-56 are not as symmetric as those for the 105 round pointed downward. We do not fully understand this result, but it may be related to greater influence of the pin in the nose of the mortar, or it's inner asymmetry. The contours of Figures 6-57 through 6-60, for the round at the surface, show negative contours on all sides of the round. For the buried mortar round, Figures 6-61 through 6-64, the contours are largely positive on all sides of the round.

The neural network model, labeled MORTARDV, was trained for 20 cycles on the data of Figure 6-65. The results for predicting the moment north are given in Figure 6-66. R-square was 0.926 and the error was 0.363. Training time was 56 minutes. The most significant row was H9 and the least significant was H2. The model converged rapidly and 10,000 cycles would have produced almost the same result.

Model MORTRDV1 was used to predict the moment east. Figure 6-67 shows the result. R-square was down to 0.7 and the sum-square-error was up to 1.09. This illustrates that the east moment is harder to predict, possibly because it contributes a smaller amount to the overall signal, as compared to the vertical and north moments.

Figure 6-68 shows the result of predicting the vertical moment using model MORTRDV2. Here only two values occur for the moment, and the R-square increased to 0.982. The error was down to 0.050. The most significant row was H10, and the least was H5

We believe the neural network offers promise for ordnance classification and detection at field sites. The results to date, on a limited collection of data, indicate that a separate network should be trained for each desired output; such as, moment north, vertical, or east, and the distance and depth outputs, if desired. It is likely an overall supervisory network, looking at the outputs from the separate designated networks,

would be needed to make an overall, best estimate of the ordnance classification, pointing direction and location.

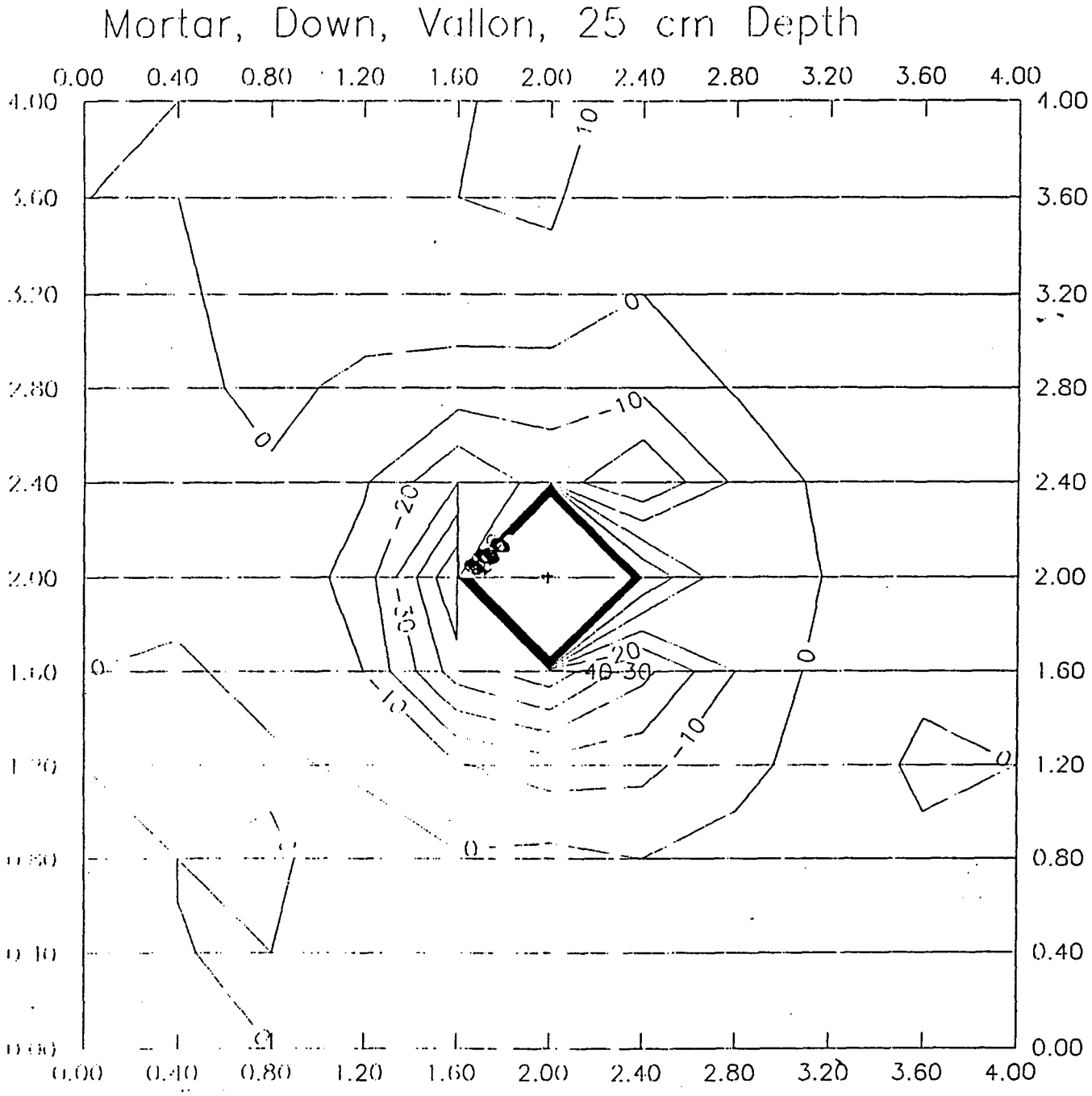

Figure 6-56. Mortar Pointed Down, depth 25 cm

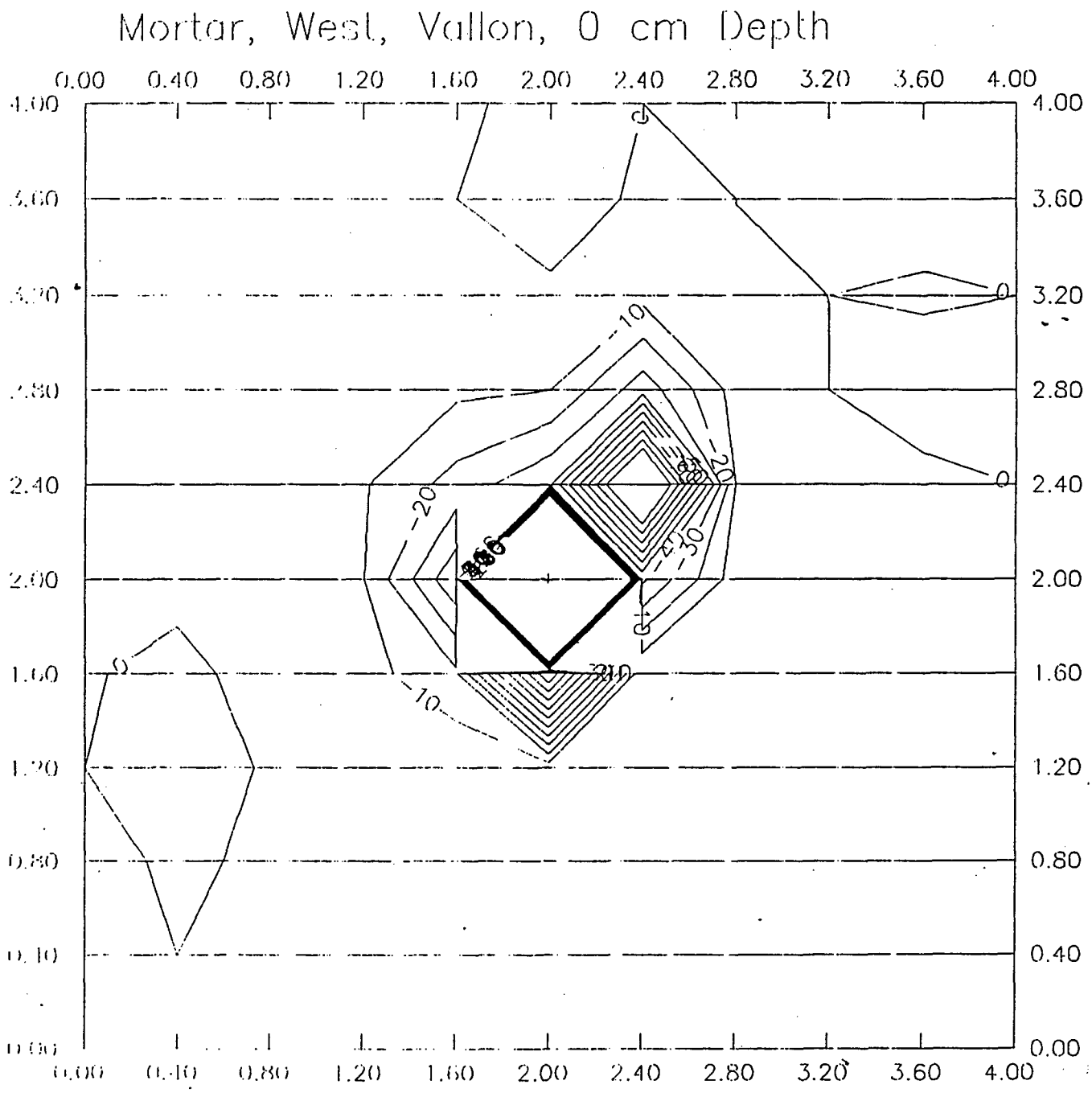

Figure 6-57. Mortar Pointed West, depth 0 cm

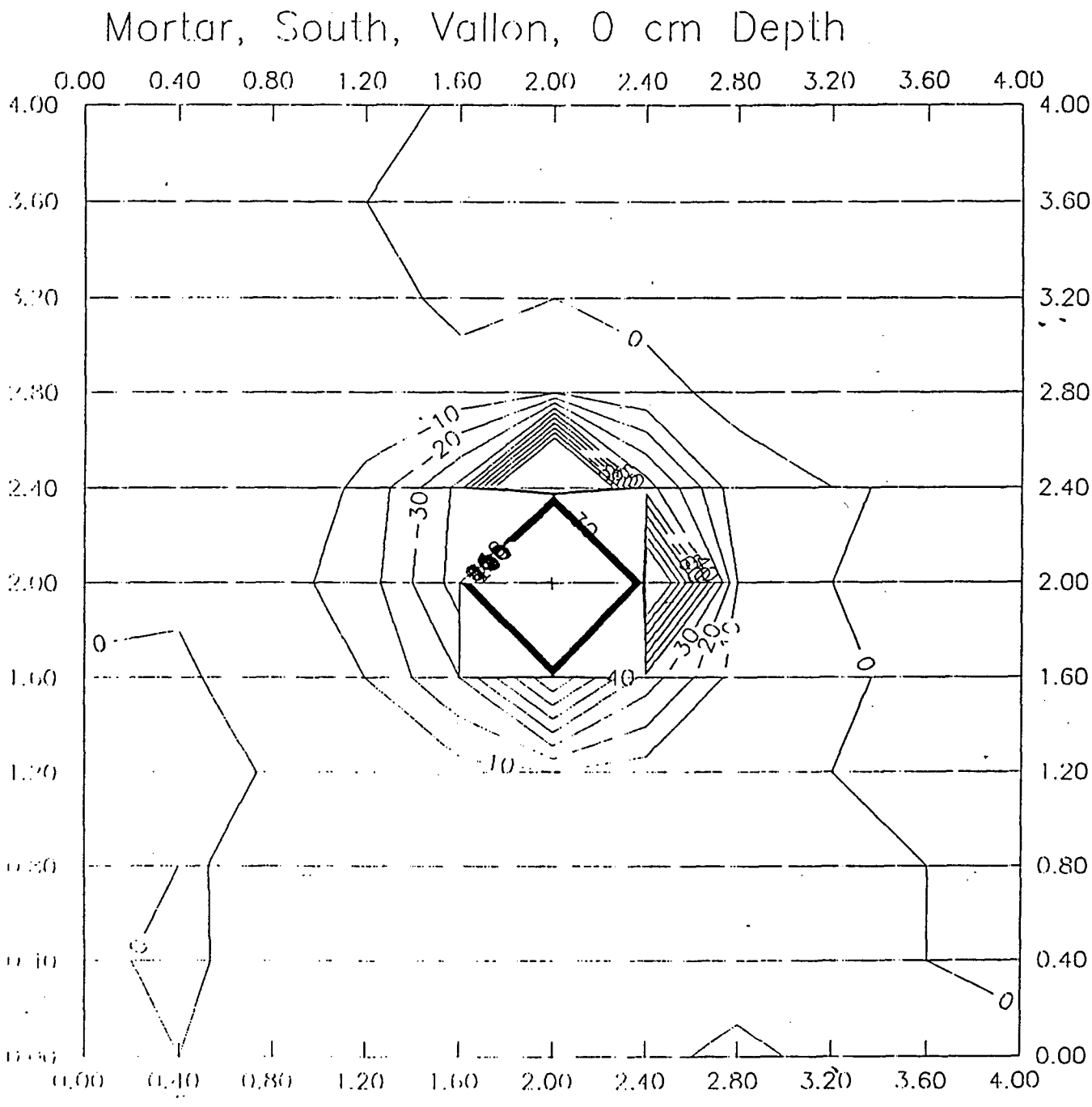

Figure 6-58. Mortar Pointed South, depth 25 cm

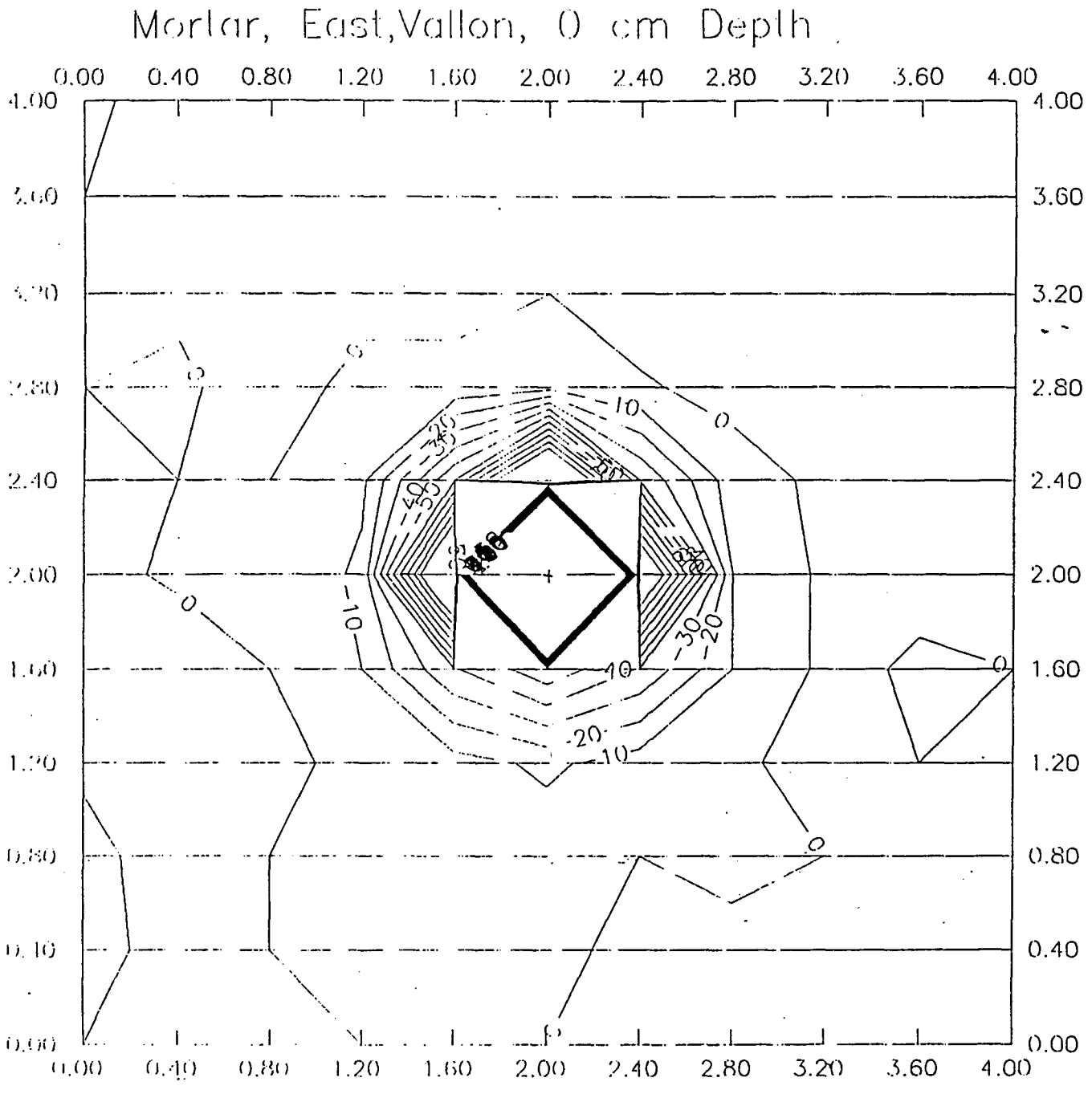

Figure 6-59. Mortar Pointed East, depth 0 cm

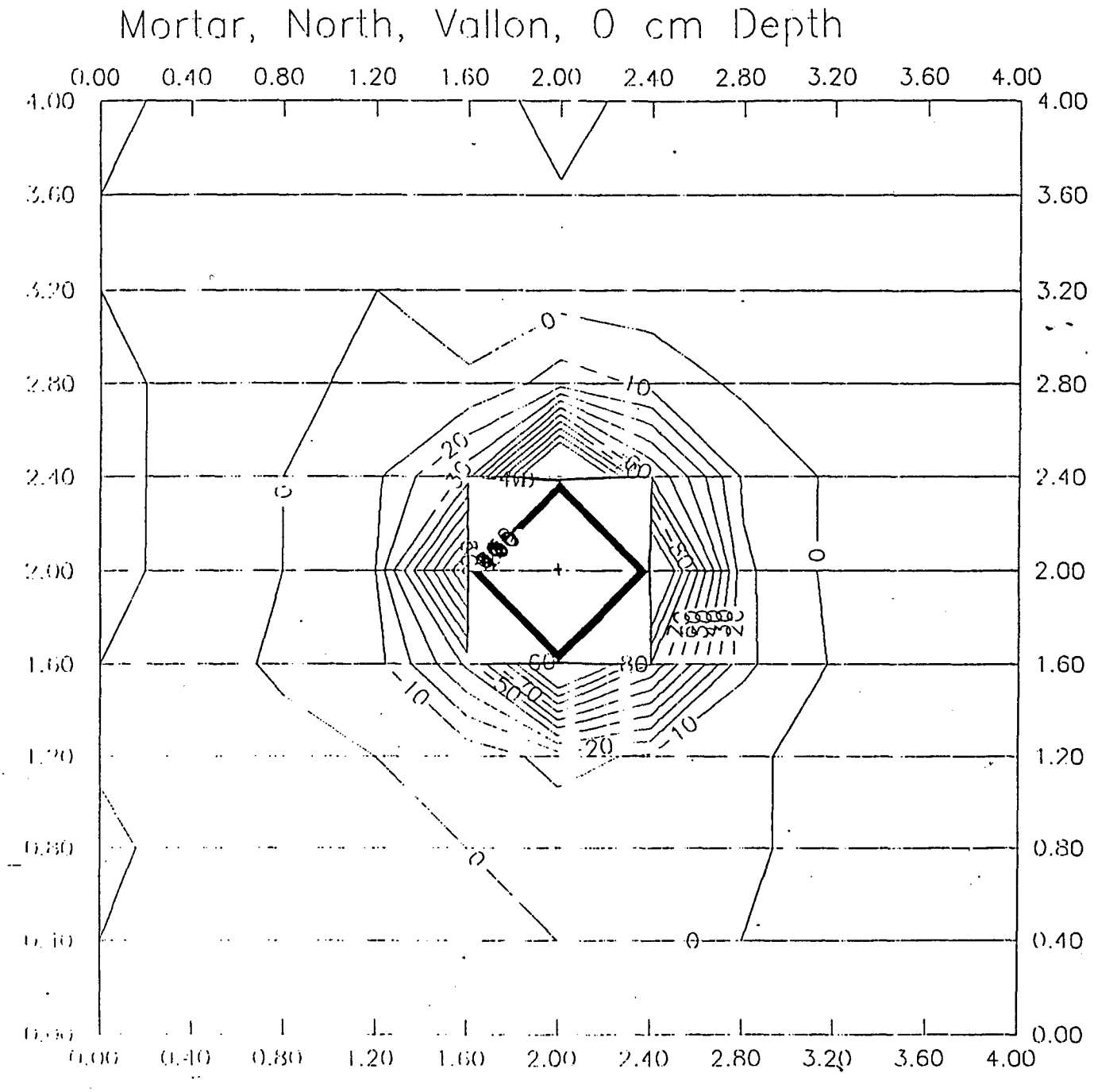

Figure 6-60. Mortar Pointed North, depth 0 cm

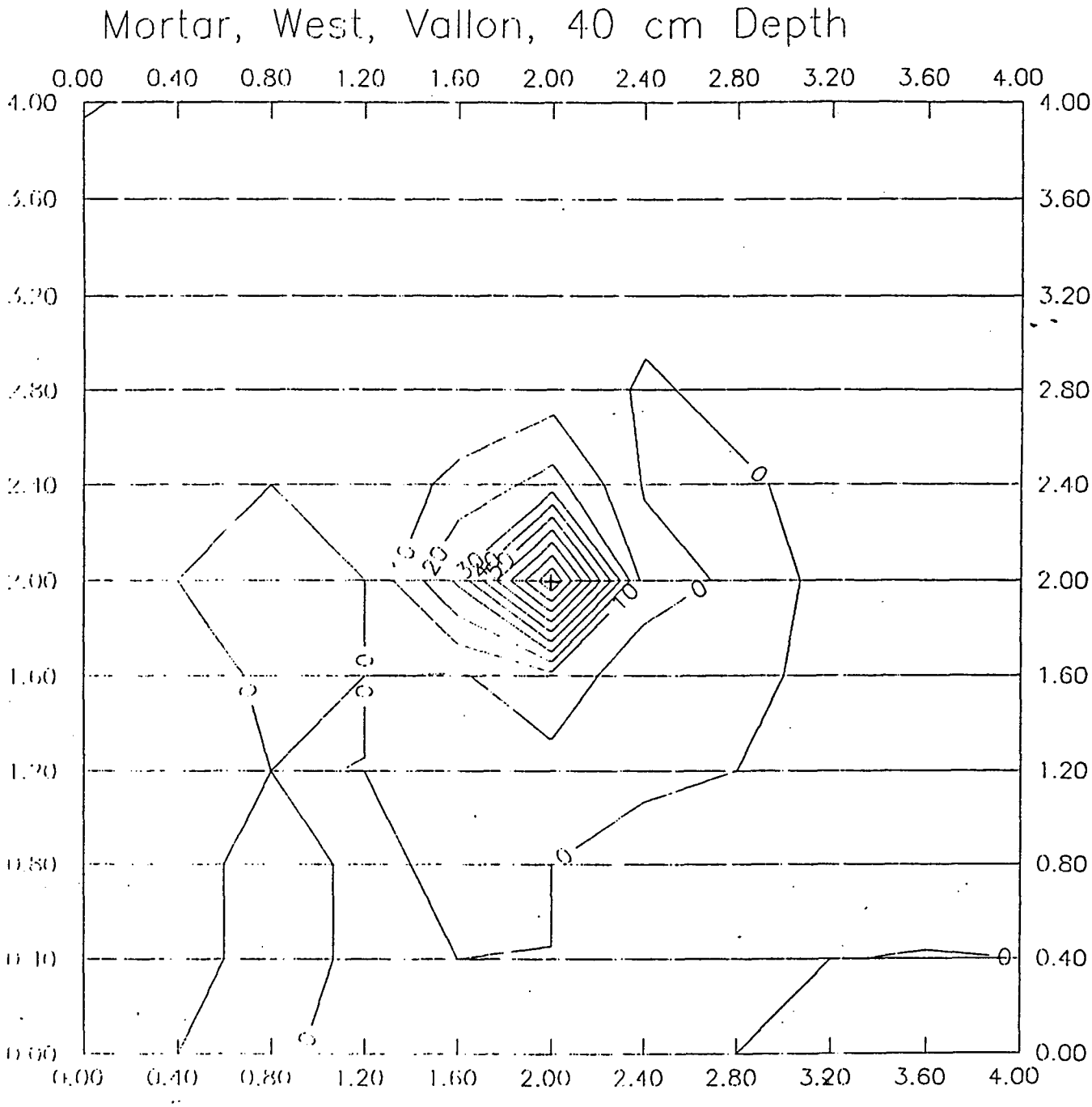

Figure 6-61. Mortar Pointed West, depth 40 cm

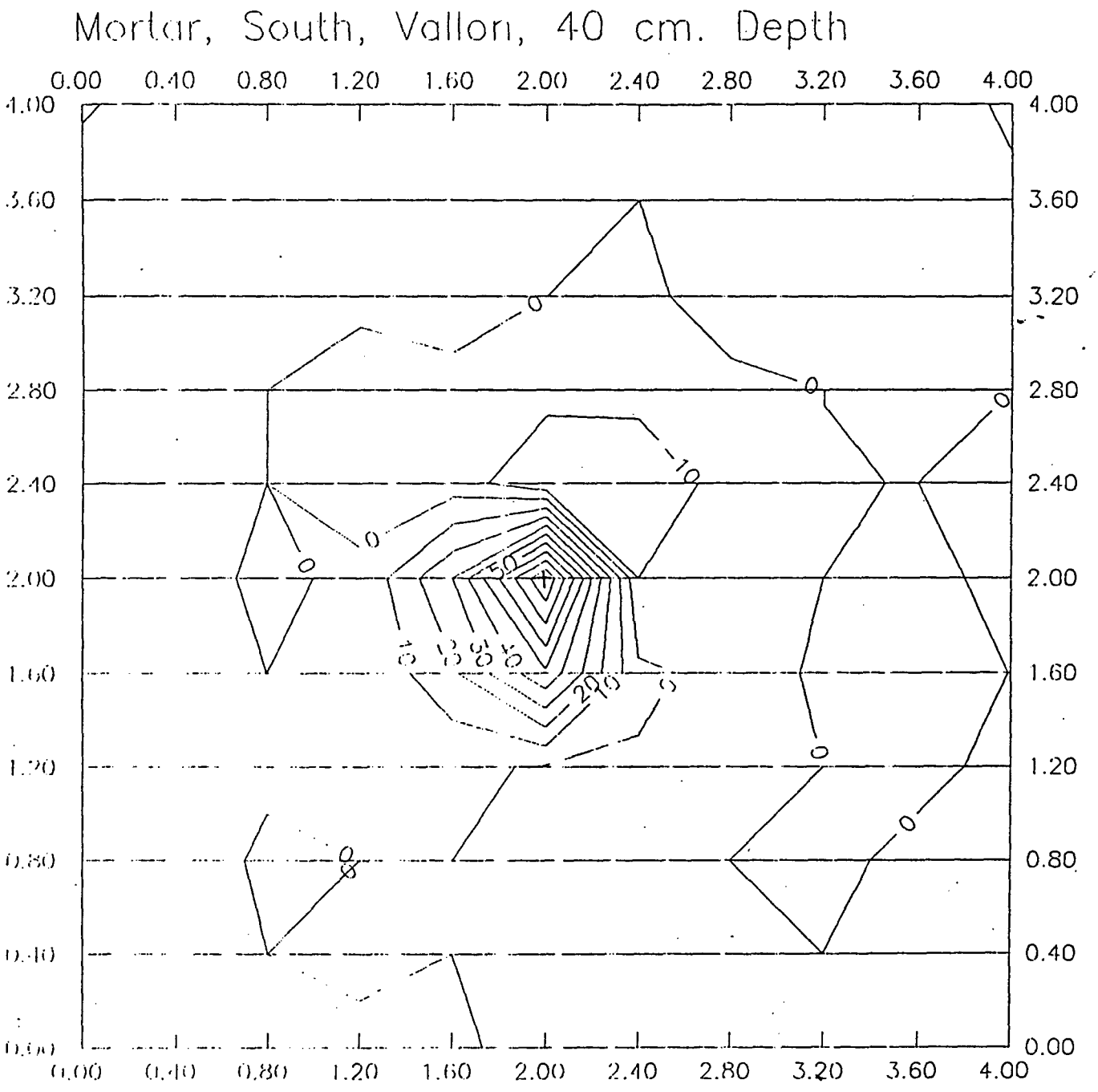

Figure 6-62. Mortar Pointed South, depth 40 cm

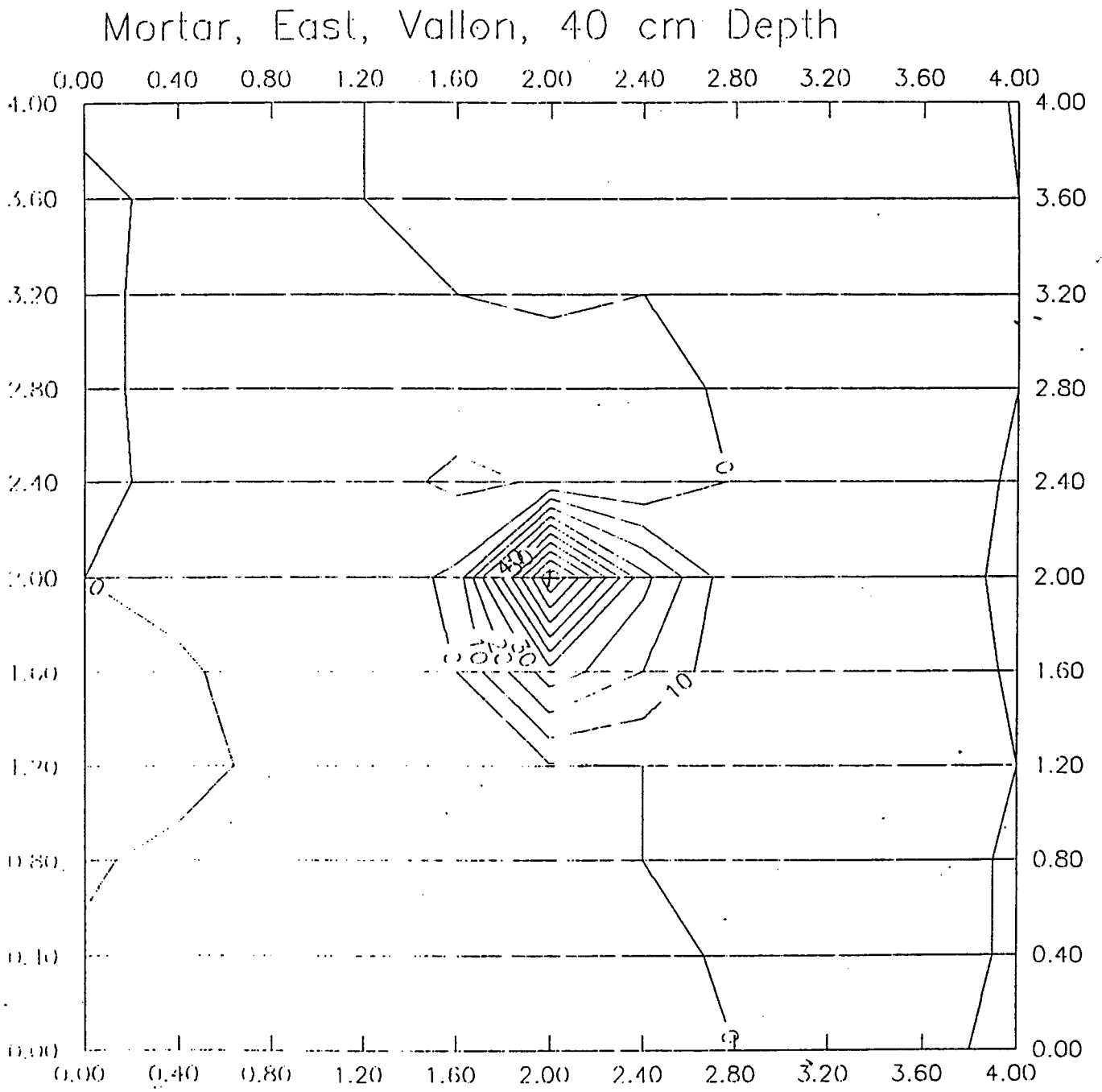

Figure 6-63. Morter Pointed East, depth 25 cm

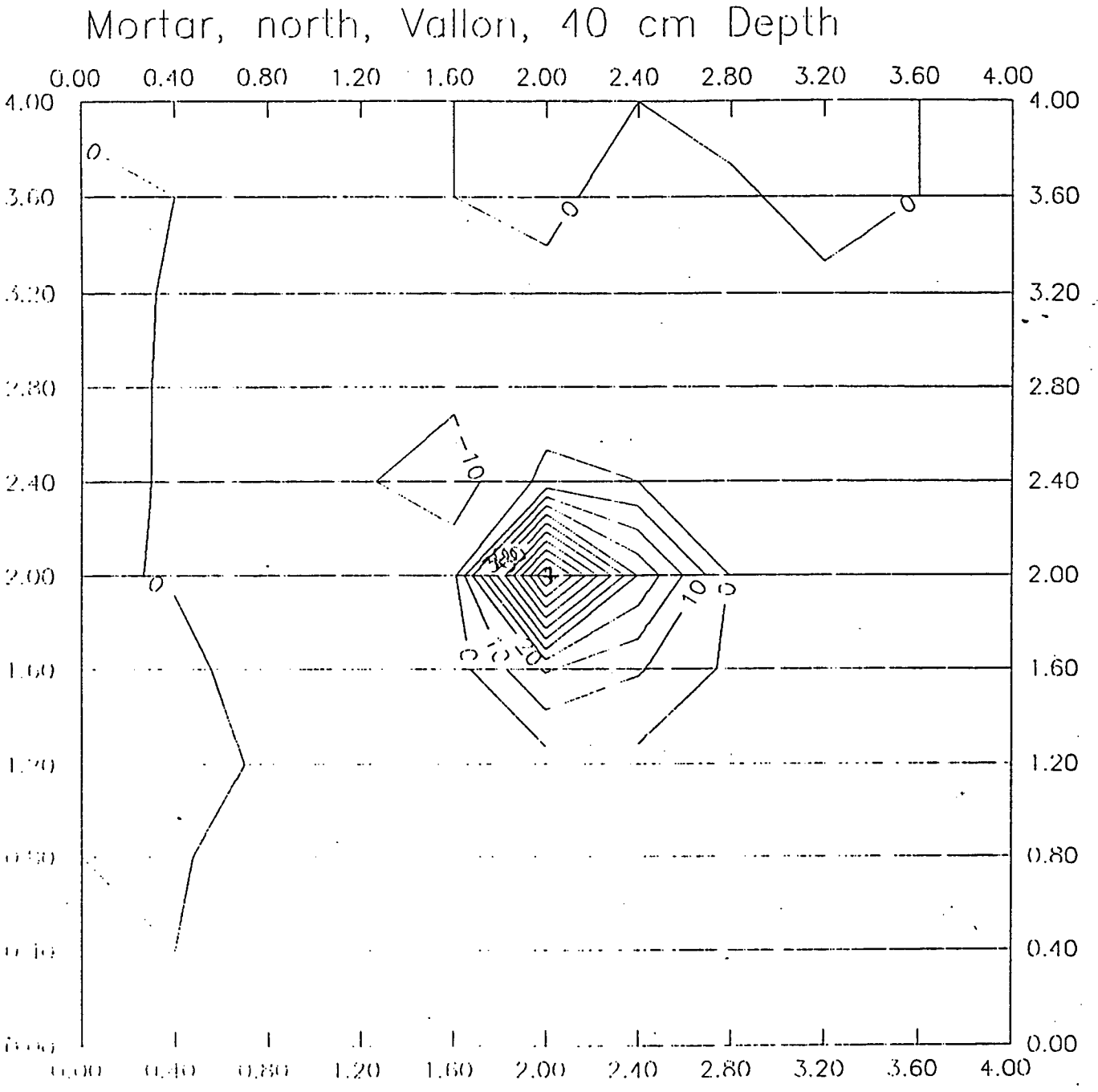

Figure 6-64. Mortar Pointed North, depth 40 cm

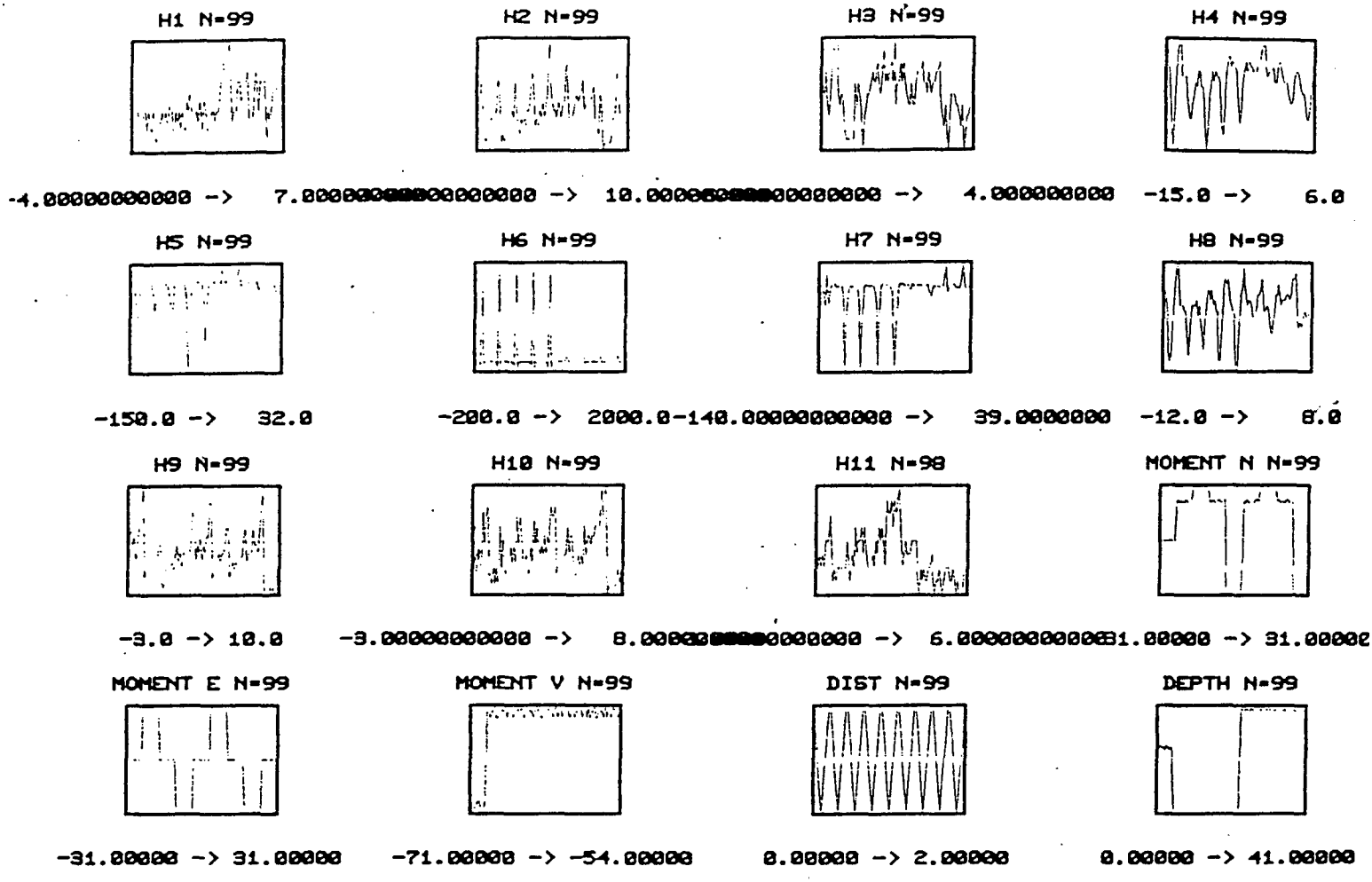

Figure 6-65. Data Summary for the Mortar

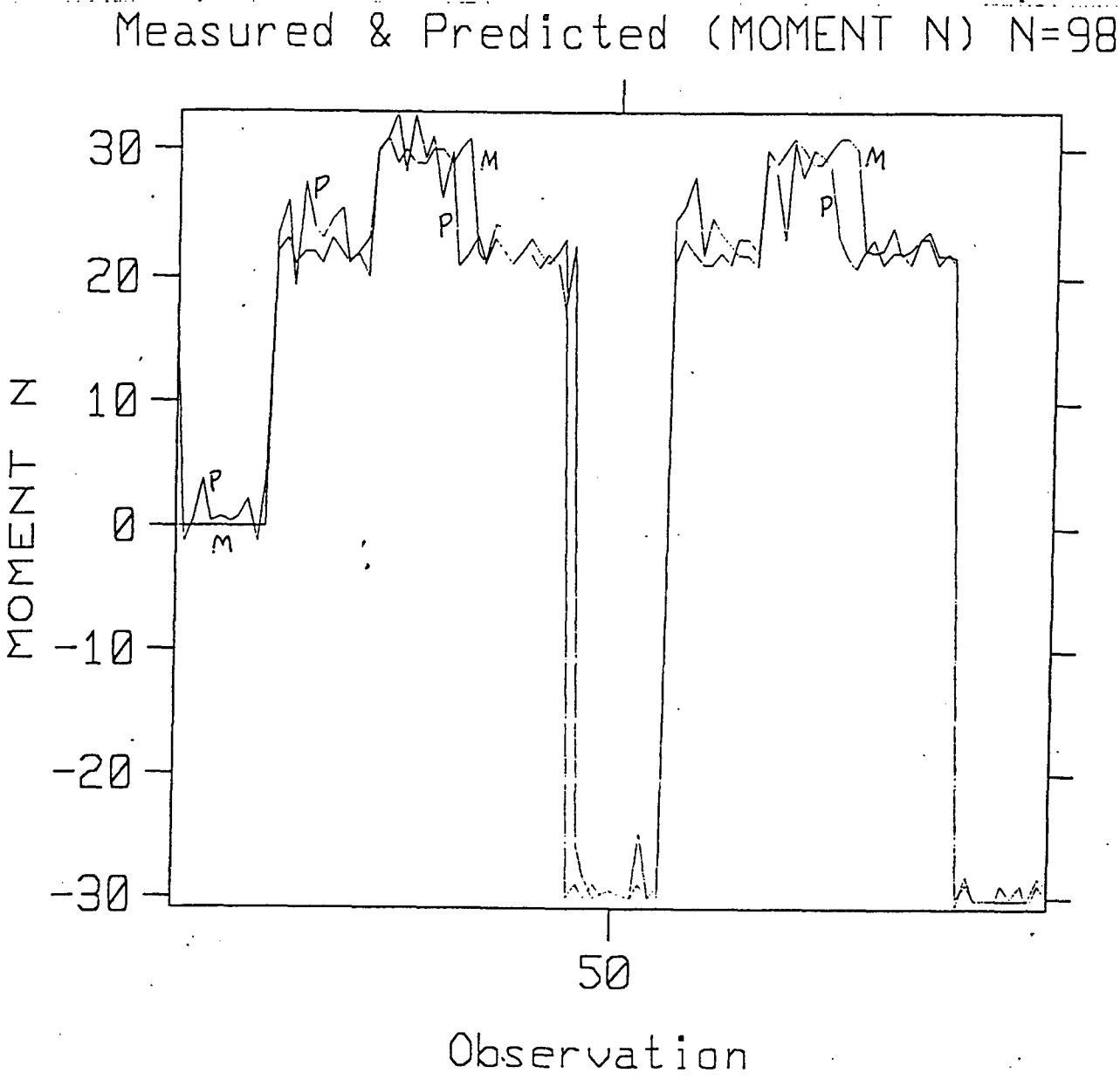

Figure 6-66. Measured and Predicted Magnetic Moment - North

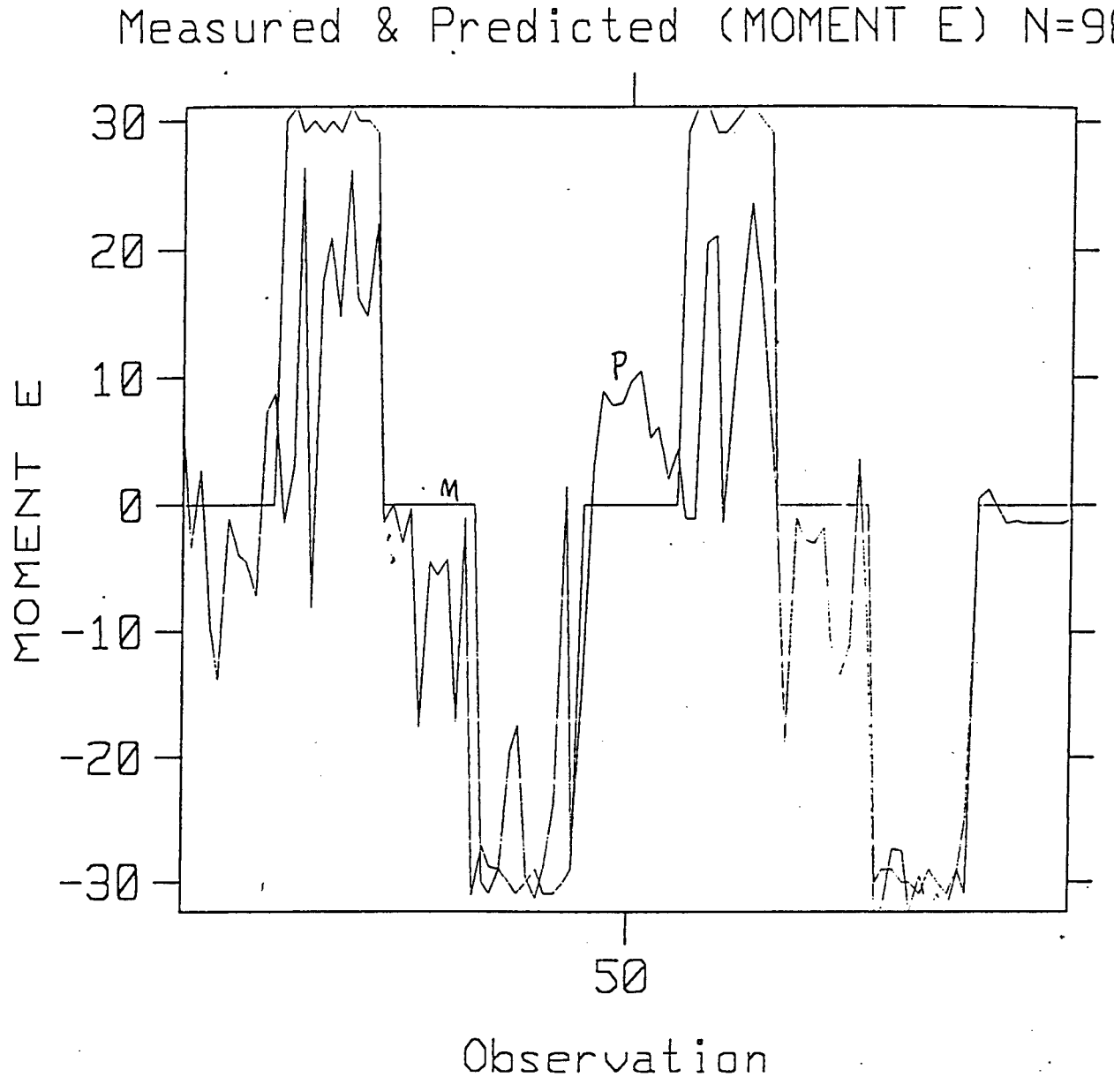

Figure 6-67. Measured and Predicted Magnetic Moment - East

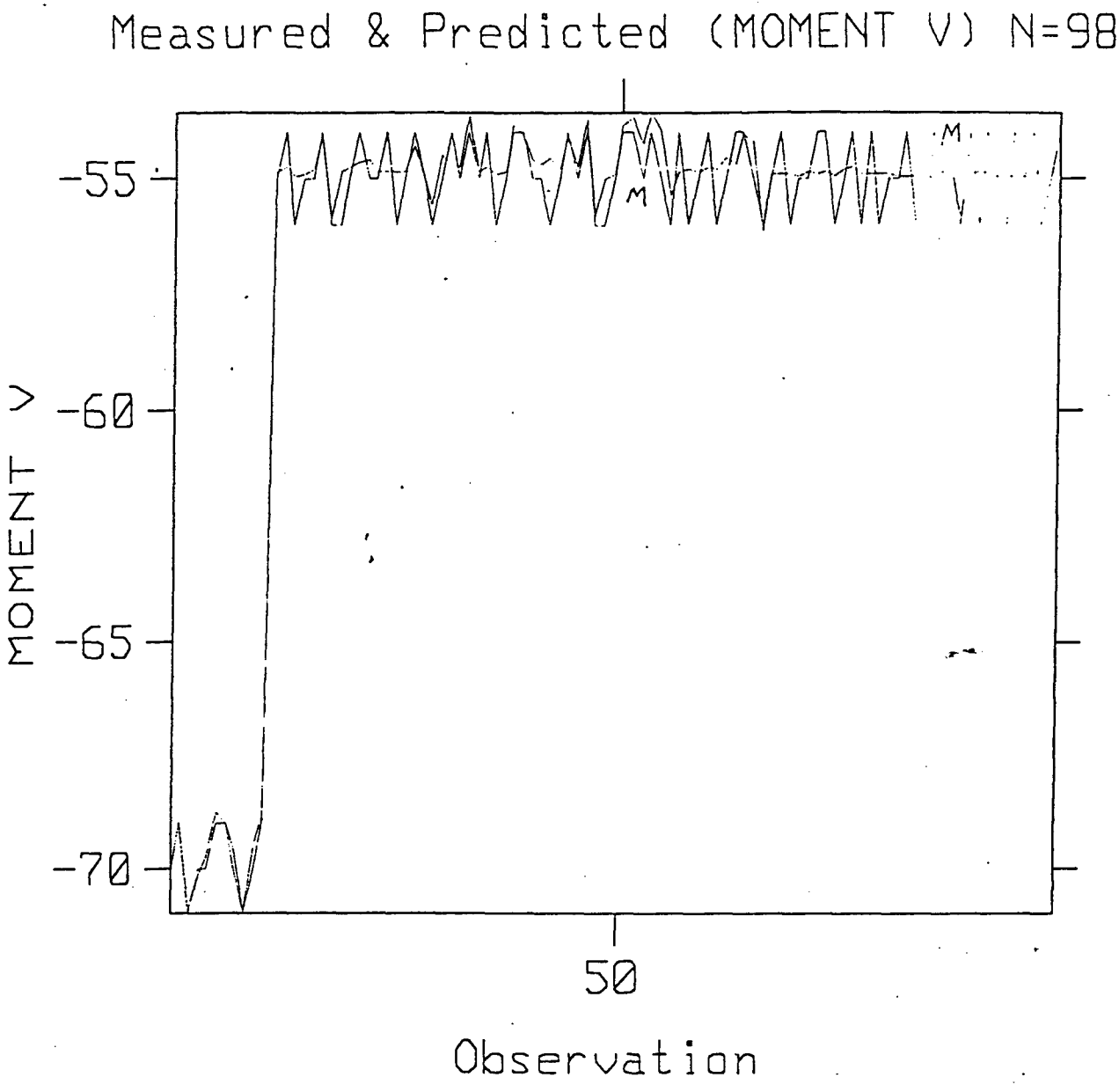

Figure 6-68. Measured and Predicted Magnetic Moment -Vertical

6.3 TESTS TO DETERMINE DETECTION THRESHOLDS

Although the detection range can be inferred from the contour plots of the previous section, it was considered more accurate to measure the detection thresholds more directly for 5, 10, and 20 gamma perturbations in the earth's field. Initially the rounds were positioned with a known orientation and the sensor was moved along lines of constant azimuth to approach the round. The ambient field was measured at a large distance, and then the locations of the sensor as it recorded + or - changes of 5, 10, and 20 gamma were marked with wooden pins. This procedure only takes about 2-3 minutes per line of approach so diurnal variations are minimized. However it was noted that in this procedure we are including the spatial variations of the test site, which can be a significant part of the threshold signal being sought. (See Figure 6-41 for an example of the variations on the test site) To remove this effect it was decided to conduct the experiment with the sensor at a fixed site and then move the round along lines of constant azimuth toward the sensor. This procedure revealed another problem-- the signal from the round was found to depend upon the rotation angle of the round about it's longitudinal axis. This means that there are ferromagnetic components within the round that are not symmetric about the long axis. The mortar round is particularly obvious in this respect with it's steel pin in the side of the nose. The 105 and 155 rounds have the same magnetic asymmetry, but the cause of this is not visible to the eye. The rotation effects are first reported below in Section 6.3.1, and then the detection threshold results are summarized in Section 6.3.2.

6.3.1 Rotation Effects

The first rotation experiments were conducted on the mortar round. Because the mortar round has a pin and screw in its nose at right angles to the longitudinal axis, the perturbation in the earth's magnetic field, caused by the presence of the round, is sensitive to rotation of the round about it's axis. The field perturbation was measured at distances of 65 and 83 centimeters from the geometric center of the round to the sensor. These distances are the approximate ones for magnetic field perturbations of 10 and 5 gamma, respectively, based on earlier studies with random orientations of the mortar round. The ambient field was 54653 gamma.

The sensor was located in the magnetic north direction from the round. The round was pointed north or east (round 2549) and north, east, or west for round 2550. The rotation angle of the round is clockwise as the observer looks from the tail of the round toward the nose. A rotation angle of 0 degrees is indexed with the head of the screw vertically upward as the round lays horizontally. All measurements were taken with both the sensor and the round at ground level. The sensor was a Geometric 822 total field magnetometer.

Figures 6-69 and 6-70 show the results for round 2549 at distances of 83 and 65 cm,

6.3 TESTS TO DETERMINE DETECTION THRESHOLDS

Although the detection range can be inferred from the contour plots of the previous section, it was considered more accurate to measure the detection thresholds more directly for 5, 10, and 20 gamma perturbations in the earth's field. Initially the rounds were positioned with a known orientation and the sensor was moved along lines of constant azimuth to approach the round. The ambient field was measured at a large distance, and then the locations of the sensor as it recorded + or - changes of 5, 10, and 20 gamma were marked with wooden pins. This procedure only takes about 2-3 minutes per line of approach so diurnal variations are minimized. However it was noted that in this procedure we are including the spatial variations of the test site, which can be a significant part of the threshold signal being sought. (See Figure 6-41 for an example of the variations on the test site) To remove this effect it was decided to conduct the experiment with the sensor at a fixed site and then move the round along lines of constant azimuth toward the sensor. This procedure revealed another problem-- the signal from the round was found to depend upon the rotation angle of the round about it's longitudinal axis. This means that there are ferromagnetic components within the round that are not symmetric about the long axis. The mortar round is particularly obvious in this respect with it's steel pin in the side of the nose. The 105 and 155 rounds have the same magnetic asymmetry, but the cause of this is not visible to the eye. The rotation effects are first reported below in Section 6.3.1, and then the detection threshold results are summarized in Section 6.3.2.

6.3.1 Rotation Effects

The first rotation experiments were conducted on the mortar round. Because the mortar round has a pin and screw in its nose at right angles to the longitudinal axis, the perturbation in the earth's magnetic field, caused by the presence of the round, is sensitive to rotation of the round about it's axis. The field perturbation was measured at distances of 65 and 83 centimeters from the geometric center of the round to the sensor. These distances are the approximate ones for magnetic field perturbations of 10 and 5 gamma, respectively, based on earlier studies with random orientations of the mortar round. The ambient field was 54653 gamma.

The sensor was located in the magnetic north direction from the round. The round was pointed north or east (round 2549) and north, east, or west for round 2550. The rotation angle of the round is clockwise as the observer looks from the tail of the round toward the nose. A rotation angle of 0 degrees is indexed with the head of the screw vertically upward as the round lays horizontally. All measurements were taken with both the sensor and the round at ground level. The sensor was a Geometric 822 total field magnetometer.

Figures 6-69 and 6-70 show the results for round 2549 at distances of 83 and 65 cm,

respectively. If the amplitude of the rotation effect is h, then the effective moment that causes it is given by $M = 4\pi hr^3$.

The effective moment for these two cases is on the order of M= 50 gamma-m^3.

Field Perturbation, Mortar Round 2549

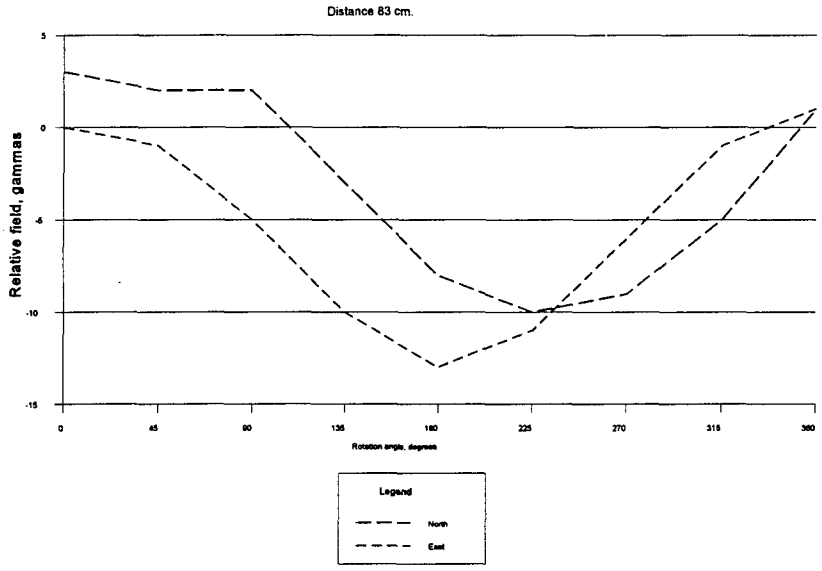

Figure 6-69. Rotation Effects on Mortar Round, 83 cm Distance

Field Perturbation, Mortar Round 2549

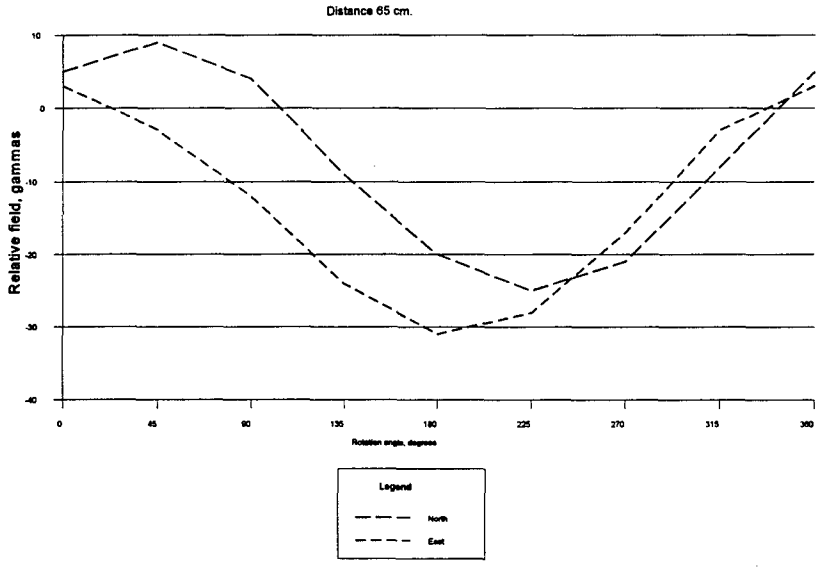

Figure 6-70. Mortar Round Rotation Effects, 65 cm Distance

Figures 6-71 and 6-72 show results for round 2550. The amplitude of these rotation effects is consistent with a moment on the order of 70 gamma-m^3.

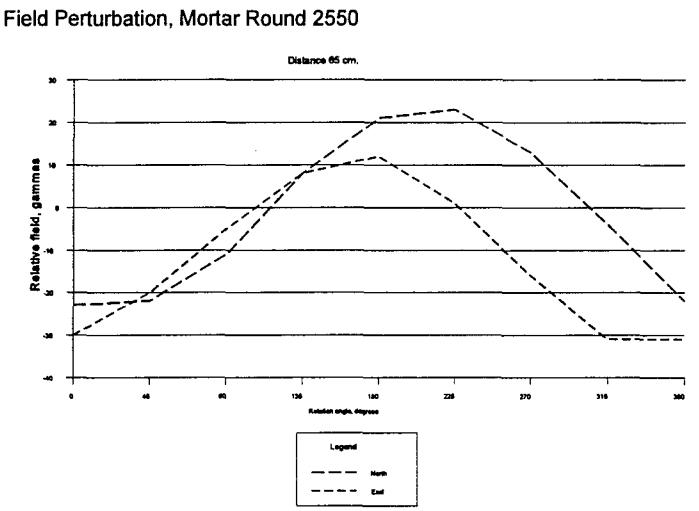

Figure 6-71. Rotation Effects on Round 2550, 65 cm

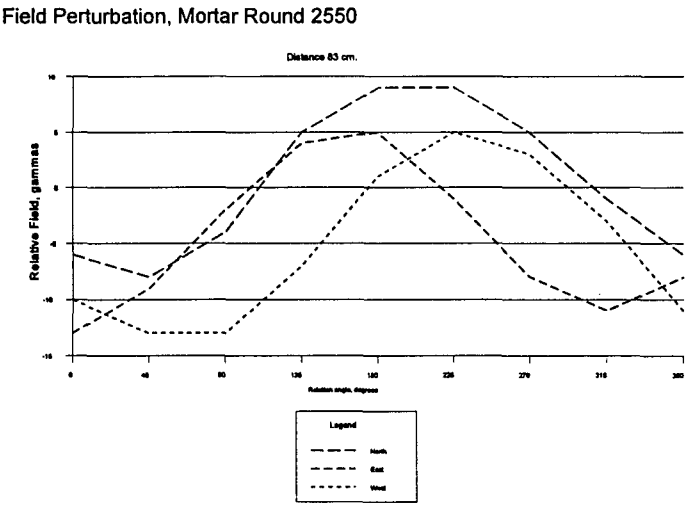

Figure 6-72. Rotation Effects on Round 2550, 83 cm

Additional measurements were made with a Vallon gradiometer instead of the Geometric sensor. The mortar round was placed horizontal on the ground, pointed east, and located 0.8 meter north of a Vallon gradiometer. The round was then rotated about it's long axis in increments of 45 degrees clockwise as seen from the base. The zero degree reference was with the nose pin pointed upward. Similarly the 105 round, pointed east, was 1.2 meters from the Vallon gradiometer. The zero degree reference was with the serial number tag upward.

Data are tabulated in Table 6-15 and then plotted below.

Table 6-15. Rotation Effects on Mortar and 105 Rounds

	rotation angle, degrees								
	0	45	90	135	180	225	270	315	360
mortar	-17	-15	-7	3	8	8	-4	-11	-16
105	4	2	-6	-15	-19	-19	-14	-2	2

Field readings are in gamma.

These readings are consistent with an off-axis moment of 77 gamma-m^3 for the mortar and a moment of 250 gamma-m^3 for the 105 round.

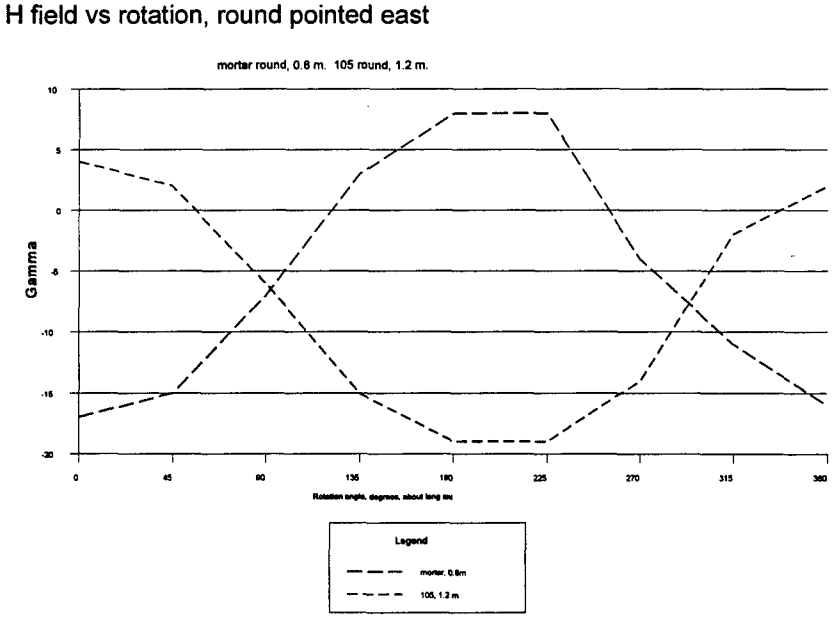

Figure 6-73. Rotation Effects on Mortar and 105, Vallon Sensor

105 round #2552 was studied further for effects of pointing angle in the four cardinal directions.

The round was located at ground level at a distance of 0.5 meter from a total field magnetometer (Geometric 822), which also was at ground level. The round was pointed toward magnetic north, east, south, or west and then rotated in 45 degree increments about it's long axis. The field perturbation is shown below in Figure 6-74. All readings are in gamma, relative to the ambient total field of 54675 gamma. The results show that the amplitude of the rotation perturbation is roughly independent of the pointing angle, except for a south-pointed round where the effect is larger. The greatest effect of pointing angle is to establish the mean level of the field.

105 ROUND, ROTATION EFFECTS

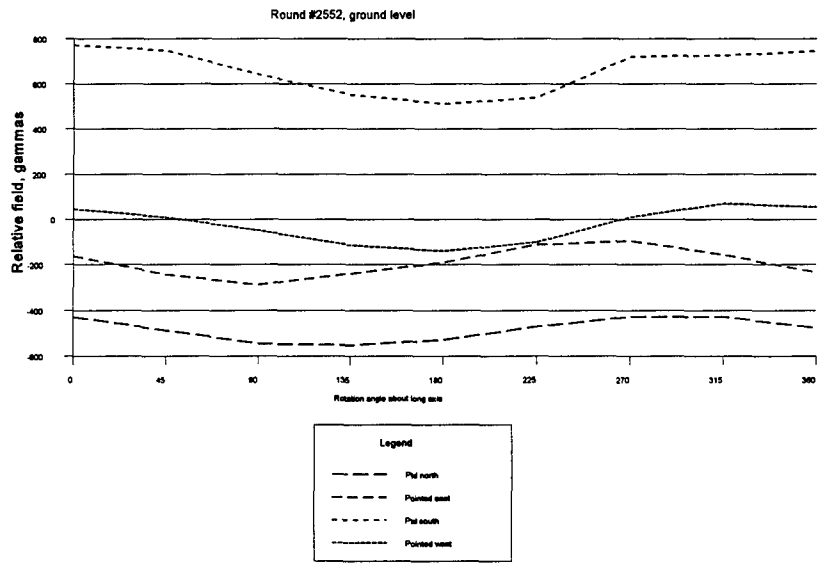

Figure 6-74. 105 Rotation Effects with Pointing Direction

Next a 155 round (#2553) was placed in a horizontal position at ground level and 76 cm from the Geometric 822 total field magnetometer (also at ground level). The round was rotated clockwise, as viewed from the base looking toward the nose. The 2553 tag in

an upward position was the reference 0 degree position. Results are plotted below in Figure 6-75. They show that the 155 rotation perturbation varies considerably with pointing angle, being as small as 80 gamma-m^3 for the east direction and as large as 400 gamma-m^3 for the south direction.

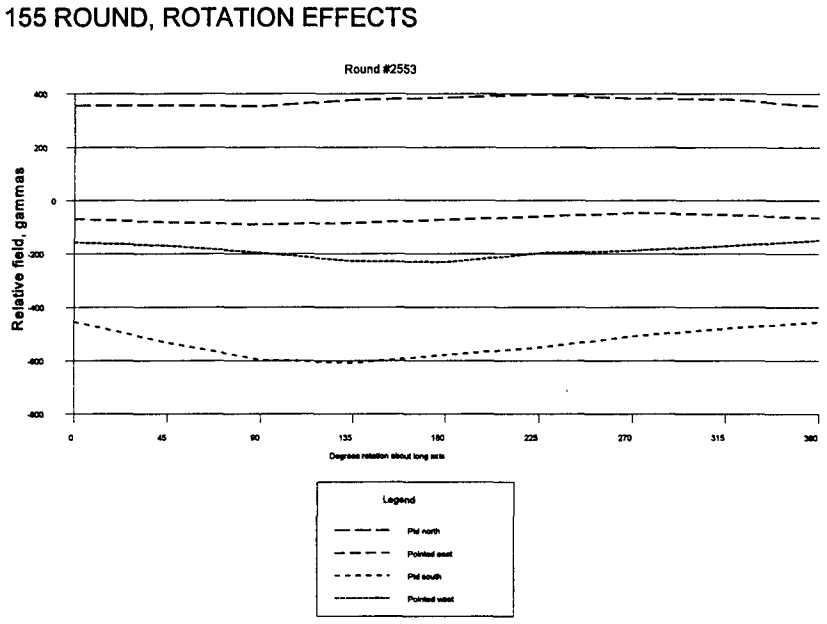

Figure 6-75. 155 Round Rotation Effects, 76 cm Distance

6.3.2 Detection Threshold Experiments

The distance that a round can be detected, for threshold changes in the earth's field of + or - 5, 10, and 20 gamma, were measured. For rounds located at ground level it was found best to keep the round at a fixed location and then move the total field sensor until the thresholds were crossed. This procedure removes the spatial field variations that can add or subtract from the round signal. The sensor was located at known azimuth angles from the round, relative to magnetic north. First the round would be moved away from the sensor at a considerable distance (10 meters or more), and then it would be moved progressively toward the sensor until a 5, 10, or 20 gamma signal change was noted. The reference reading was the total field at the time the round was

well removed from the sensor. Hence, the diurnal variations are not a factor since the three threshold crossings can be located at a given azimuth angle in approximately one to two minutes. Wooden markers were placed at each crossing and then their distances, measured along the ground, were subsequently measured and recorded. Data were recorded for round pointing directions of north, east, south, and west.

When the rounds were buried in the ground, it was not possible to move the round. For these cases the sensor was moved along a constant azimuth angle and the threshold distances were noted. These data will contain more variation due to the ground magnetic anomalies. Some data, however, were obtained with the sensor elevated above the ground and the round moved at the proper angle along the ground. Here the round is effectively "buried" by the distance that the sensor is elevated. In all cases the data on any given azimuth angle was obtained rapidly and all data are relative to the local magnetic field at the start of each threshold run through 5, 10, and 20 gamma changes.

The mean and standard deviation of the threshold distances were calculated and reported in Table 6-15. Note that the 5 gamma threshold has the largest standard deviation. This is to be expected since the noise level of the sensor is about + or - 1 gamma. The overall standard deviations of the threshold distances are large because we are computing data across all azimuth angles. The threshold distance will clearly depend upon the angular variation of the magnetic field perturbation from the round. In practice this angle from the round to the sensor is not known. Hence, we have averaged and computed standard deviations over all angles to obtain a more realistic, real-world value. The data are reported as mean/standard deviation. All dimensions are in centimeters. Appendix provides an example of the MathCad program that calculates the mean and standard deviation of these measurements.

Figure 6-76 shows a scatter plot of the data in Table 6-15. All the mean values for the 5, 10, and 20 gamma threshold detection distances have been shown, regardless of the orientation of the round. There is considerable scatter in the data, and there are cases where a round gives a greater detection range when it is buried. However, the standard deviations are also large, so the data are really falling within the expected variations. The first two rows of Table 6-15 are interesting to compare. Here a Geometric magnetometer and a Vallon gradiometer have been used to observe the same condition--a 105 round at the surface. Notice that the detection ranges are only slightly different, and they fall well within one standard deviation of one another. A similar comparison and result occur in rows four and five where a mortar round is involved.

It is also evident that the detection ranges are not significantly different for cases where the round was moved or where the sensor was moved. This is caused, we believe, by the fact that the detection range is more dependent upon the azimuth angle of

approach than it is on the spatial variations of the site. The larger standard deviation of the angle effect is the one that dominates.

The above trends are important for eventual measurements at clean-up sites because they help set a measurement interval for searches at ground level. However, considerably more data is needed at greater depths, particularly for the 105 and 155 rounds.

Table 6-15. Summary of 105, 155,and Mortar Detection Thresholds

			Detection Threshold			
File No.& type	Depth, cm	Pointing direction	5 Gamma	10 Gamma	20 Gamma	Comments
105det sensor moved	0	n,e,s,w 32 readings	189.3/60.7	151.3/29.6	126.5/27.4	Geometric 0 to 315 degrees
105det2 round moved	0	n,e,s,w 16 readings	174.4/47.1	146.7/42.5	120/35.7	Vallon, tag up, 0 to 315 degrees
105det1 round moved	76	n,e,s,w 12 readings	210.9/56.5	159.5/46.3	119.2/45.6	Geometric 0 to 225 degrees
mtrdet round moved	0	n,e,s,w	83.7/18.6	65.1/13.8	not meas.	Geometric 0 to 315 degrees
mordet3 round moved	0	n,e,s,w	91.3/18.5	76.6/12.3	62.3/10	Vallon, 0 to 315 degrees, pin up

mtrdet2 round moved	30	north	68.3/27.2	52.1/7.6	40.7/7.3	Geometric 0 to 315 degrees
mrtdet4 round moved	40	north	90/22.2	66.2/18.2	44.4/10.7	Vallon, 0 to 315 degrees
105down sensor moved	46	down 5 readings	307 mean 27 stdev	241 mean 14 stdev	178 mean 19 stdev	Geometric 0 to 315 degrees
105down1 round moved	63.5	down 8 readings	200 mean 14 stdev	134 mean 17 stdev	81 mean stdev 17	Geometric 0 to 315 degrees
105down3 round moved	183	down 8 readings	88 mean 33 stdev	40 mrsn 24 stdev	not observable	Geometric 0 to 315 degrees
155det round moved	73.6	n,e,s,w 32 readings	254 mean 83 stdev	196 mean 55 stdev	151 mean 45 stdev	Geometric 0 to 315 degrees
155down round moved	46	down 8 readings	413 mean 30 stdev	347 mean 26 stdev	269 mean 26 stdev	Geometric 0 to 315 degrees
155down1 round moved	170	down 8 readings	226 mean 48 stdev	197 mean 45 stdev	167 mean 38 stdev	Geometric 0 to 315 degrees

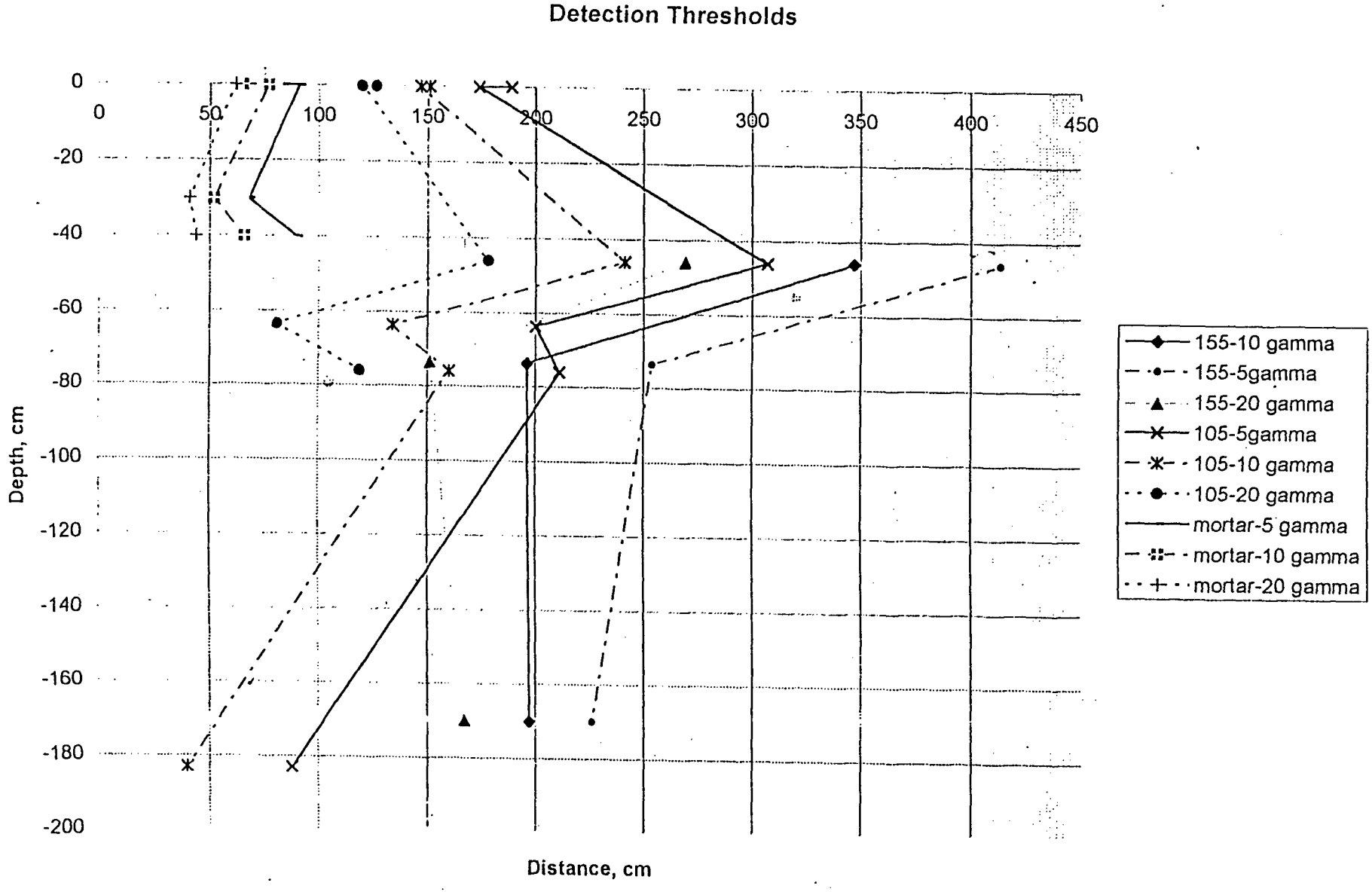

Figure 6-76. Detection Thresholds for the Mortar, 105 and 155

6.4 MEASUREMENTS OF THE DIURNAL VARIATIONS AND SENSOR NOISE

The Geometric total field magnetometer was used to record the diurnal drift over an eight hour period, which is typically the time that a battery pack will provide power. Figure 6-77 shows the result.

The most severe change occurred around 10:15, where the ambient field decreases 7 gamma in about 30 minutes. A similar magnitude rise occurs later in that same hour. This illustrates that detection measurements need to be conducted in short time intervals between calibrations of the ambient field. For the case of our experiments, we referenced the ambient field after each series of measurements-- at intervals of no more than 10 minutes and frequently as often as 3 minutes when measuring detection thresholds.

The Vallon gradiometer was operated over several minutes while readings were observed on scales 6 and 7 (0.3 and 0.1 gamma per division, respectively). As long as the instrument is stationary the readings do not fluctuate more than about + or - 0.15 gamma. A more severe test , however, is to repeatedly move the instrument to a fixed site, observe the reading, move away, and then return to take another reading. We have found that this test becomes a measure of the operator's ability to hold the sensor rod vertical and to maintain mechanical nulling. Typically the readings could be maintained the same, from measurement to measurement, within about + or - 1 gamma. This, we believe, is a more realistic test of the effective Vallon noise level.

The Geometric sensor is not subject to any sensitivity to orientation, being a total field magnetometer. We have typically observed peak-to-peak fluctuations on the order of 3 gamma with the sensor stationary, which can be interpreted to mean a standard deviation of about 0.5 gamma if the peak-to-peak spread represents + and - three standard deviation. This is also in the range of the manufacture's specifications.

6.5 CONCLUSIONS DRAWN FROM THE EXPERIMENTS

There a number of conclusions that can be made from these experiments and the supporting analysis. They are itemized below.

- Meaningful magnetic moments for the rounds can be derived from experiments conducted with well- defined geometry. The values derived are estimated to be accurate to within about + or - 50 gamma. This is about a 10% error for the larger rounds, but easily a 100% error for a mortar round. The errors are largely caused by the finite length of the rounds, while the theory assumes a point source.

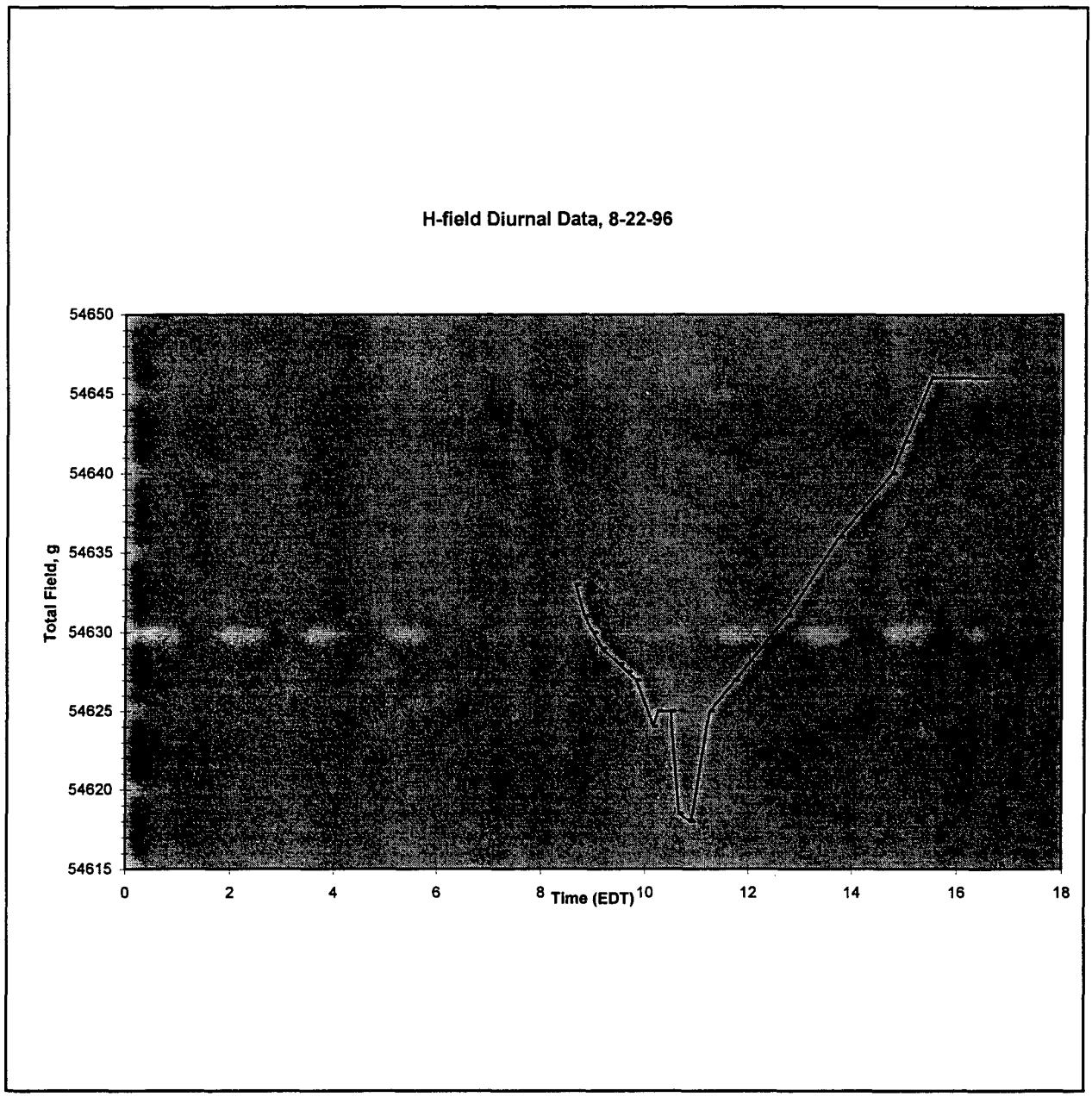

Figure 6-77. Diurnal Drift of the Ambient Magnetic Field

- All of the rounds showed the presence of a permanent magnetic moment along the longitudinal axis of the round. For the mortar and 105, this moment is directed toward the base. For the 155 this moment is directed toward the nose. We have been able to summarize all of the these moments, plus the induced moments, for the various orientations of the rounds. Permanent moments can be caused by various ferrous objects withing the rounds and their history of exposure to magnetic fields during manufacturing, shipment and storage. We can not determine the exact source without disassembly of the round.

- Surveys were taken on grids at intervals of 0.2 or 0.4 meters, and the data was compiled into training matrices for neural networks. Matrices varied from 605 to 1573 input data points. It was found that a neural network can predict output variables, such as the moments in three directions, distance, and depth, if one network is designated for each output. Correlation with experiment can be in the range of 0.7 to 0.99, depending on the output. We believe neural networks have promise for buried object detection and classification if they can be trained on very large data sets--at least larger that those compiled on this program. The networks were found to converge on the solution after about 20,000 looks, or cycles, through the data matrix. The time required to perform the training was about 90 minutes for 20,000 looks at a matrix of 1573 data inputs on a 486 PC. Proportionately longer times will be required for larger matrices.

- Detection ranges, measured along the surface of the round, have been measured under conditions where the rounds were pointed in a variety of directions. The data were analyzed to yield mean and standard deviations for detection threshold distances. The standard deviations are relatively large because there is a strong dependence of the threshold detection on the azimuth angle of the sensor from the round. In practice, at field sites for clean-up operations, the orientation of the round is largely unknown, so it was appropriate to average and analyze the data over a variety of round orientations and angles to the sensor. This has been done and tabulated for each round.

- The Geometric and Vallon sensors are reliable and relatively easy to use. The Geometric unit was supplied with valuable processing software such as Magloc, Grid, Surf, Topo, and Plot that allowed us to rapidly collect and analyze the data. The Topo plots of magnetic field contours were particularly revealing as they showed distinct patterns that were dependent upon round orientation. The Vallon sensor, operating in a gradiometer mode but with a direct output in relative magnetic field, showed similar detection threshold trends as the Geometric unit.

7.0 CONCLUSIONS AND RECOMMENDATIONS

The mortar, 105, and 155 rounds have been examined in considerable detail for their magnetic signatures. A total field magnetometer, the Geometrics 822, along with moment equations analyzed on MathCad, have been successful in obtaining both permanent and induced moments of the rounds under controlled geometries with a variety of round orientations. Table 6-14, shown earlier in the report, summarizes these derived moments. The moments are considered to be accurate within + or - 5% for the larger rounds and about + or - 100% for the mortar. In principal these results could be improved with the use of a 3-axis magnetometer, but the unit provided on this program would not operate properly. We feel the results with the total field magnetometer are adequate and they explain some of the effects that previous workers have found (see J. R. McDonald and Richard Robertson, "Magnetic Sensor Field Tests and Evaluations for Towed Array Systems", NRL/PU/6110-96-303.)

One effect noted on all rounds was the fact that they all contain an asymmetric component of their magnetic moment around their longitudinal axis. The result is, that as the round is rotated about this axis, the magnetic signal goes through a cyclic behavior with rotation angle. This may have a direct bearing on McDonald and Robertson's comment "A disappointing result of this analysis is the lack of consistency of multiple measurements of individual targets made for different heights. These often reflect a factor of two difference in relative values." (page 49, of previous reference). Unless the rotation angle of the round is known or controlled, considerable variation in magnetic signal may result.

We have also found that the detection threshold distances vary considerably with the azimuth direction from the round to the sensor as well as the pointing direction of the round. Table 6-16 and Figure 6-76 have summarized these results. From Table 6-14 we have calculated an overall average total vector moment of the rounds, using the four cardinal pointing directions for the horizontal rounds and the two vertical (down and up) data points. The result is shown in Table 7-1.

Table 7-1. Average Total Moment of the Rounds

ROUND	Average total moment, gamma-m^3
Mortar	67.5
105	984
155	2260

Figure 7-1 is a plot of moment versus measured weight of the rounds that we used(containing no explosive). The moment correlates well with weight.

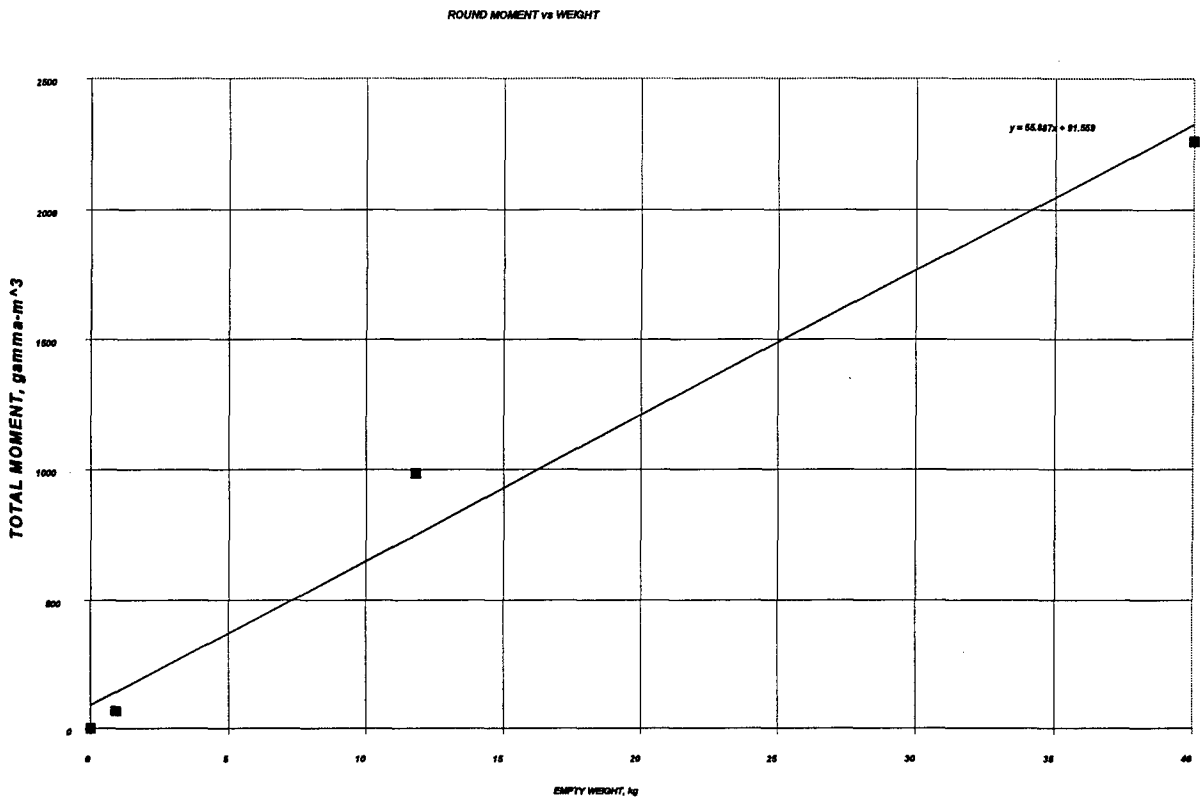

Figure 7-1. Magnetic Moment Versus Measured Weight of Rounds

From these average moments, reflecting a wide range of possible orientations, we have derived recommended sensor array spacings for ordnance detection with a 5, 10 or 15 gamma threshold. This was done by using a simple expression relating measured H-field perturbation to the average moment of Table 7-1.

$$r^3 = M/4\pi H$$

$$x = \sqrt{(r^2 - d^2)}$$

where M = the average moment, gamma-m^3,
H = 5 gamma, 10 or 15 gammas
d = depth of round, meters
x = horizontal distance along ground for threshold detection

Figures 7-2, 7-3 and 7-4 provide the recommended array spacing, x, for the three rounds at various depths as function of the desired signal level based on the results of our measurements.

Notice in the figures that there is a rapid reduction in array spacing as the depth approaches that maximum value where detection is no longer possible--because of the diminishing signal. It is also noted that these results are in contrast with the recommended array spacings given by McDonald and Robertson, page 82. They recommend array spacings that increase with depth of the round, while we recommend spacings that must decrease with depth because of the signal dependence upon r^-3. We believe our interpretation is the proper one, and it roughly follows the trend of Figure 6-76, where detection threshold distance tended in an overall sense to decrease with depth.

The data in Figures 7-2, 7-3 and 7-4 have been plotted versus desired signal level. However if the rms noise level N is known the data may be interpolated versus S/N. For example if N=2.5 gamma, the curve of Figure 7-2 labeled 5 gamma represents a S/N of 2. The curve labeled 10 gamma represents a S/N of 4, etc. N will be the square root of the sum of the squares from all sources including clutter contributions from the measurement site, sensor noise , diurnal variation during the measurement time, senor/platform motion induced currents and sensor orientation errors caused by platform random motions

We have trained neural networks on the H-field data collected on square arrays of 2x2 meter of 4x4 meter size. It is recommended that arrays of 6x6 meters, or larger, be used in the future since the 155 detection ranges exceed 3 meters in some cases. The neural networks show promise for ordnance detection and classification, but the

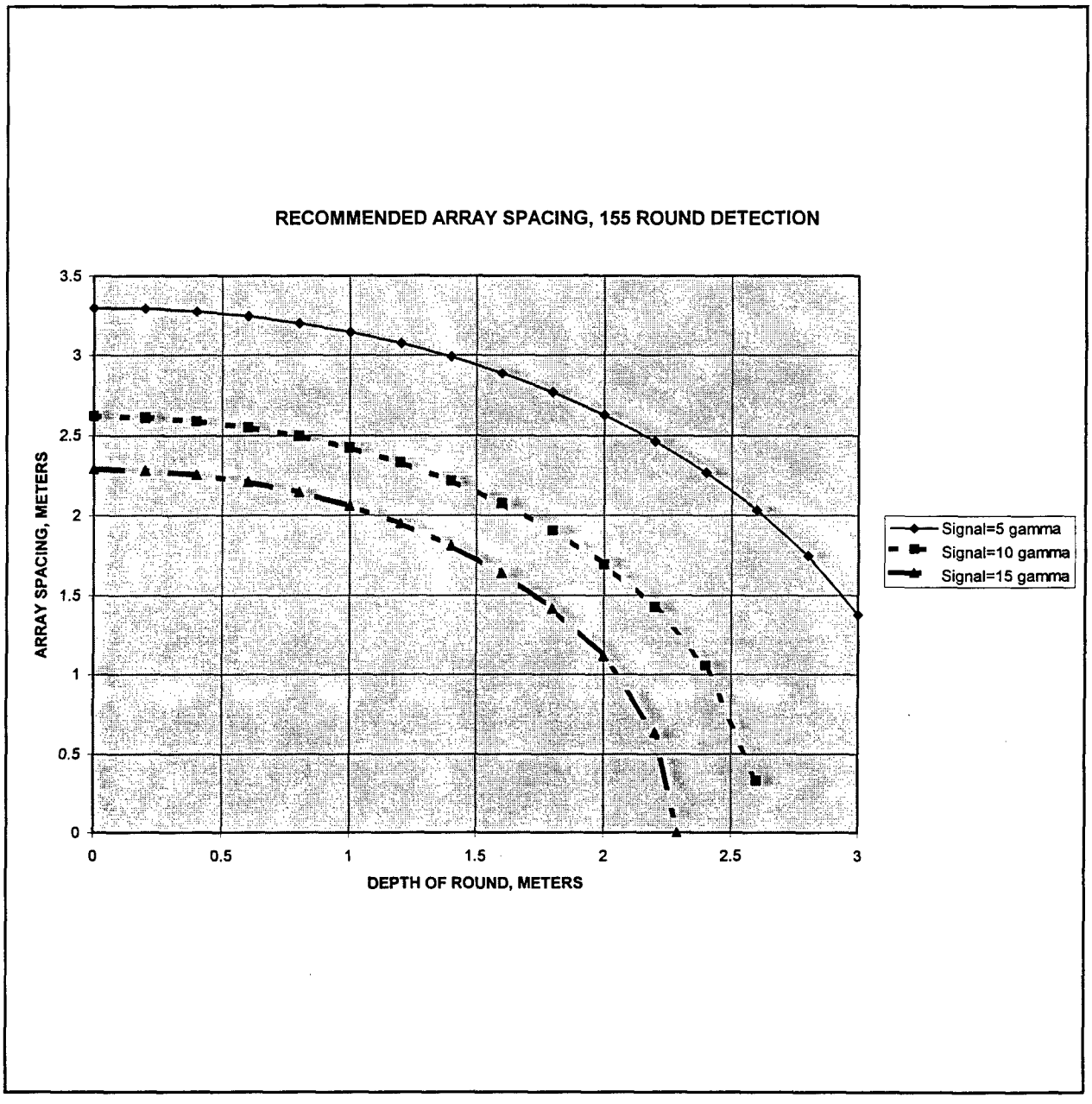

Figure 7-2. Recommended Array Spacing for 155 Round Detection

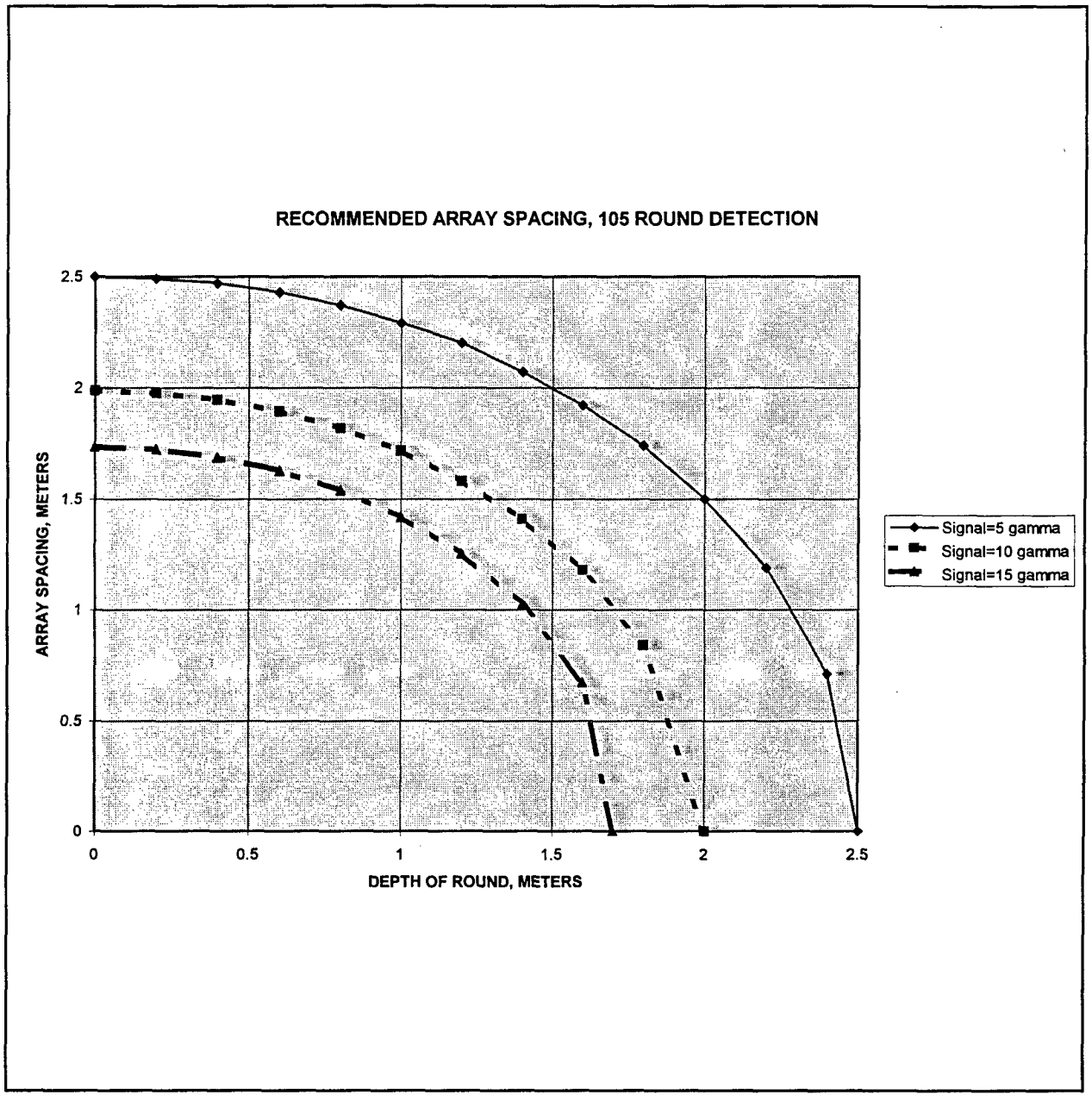

Figure 7-3. Recommended Array Spacing for 105 Round Detection

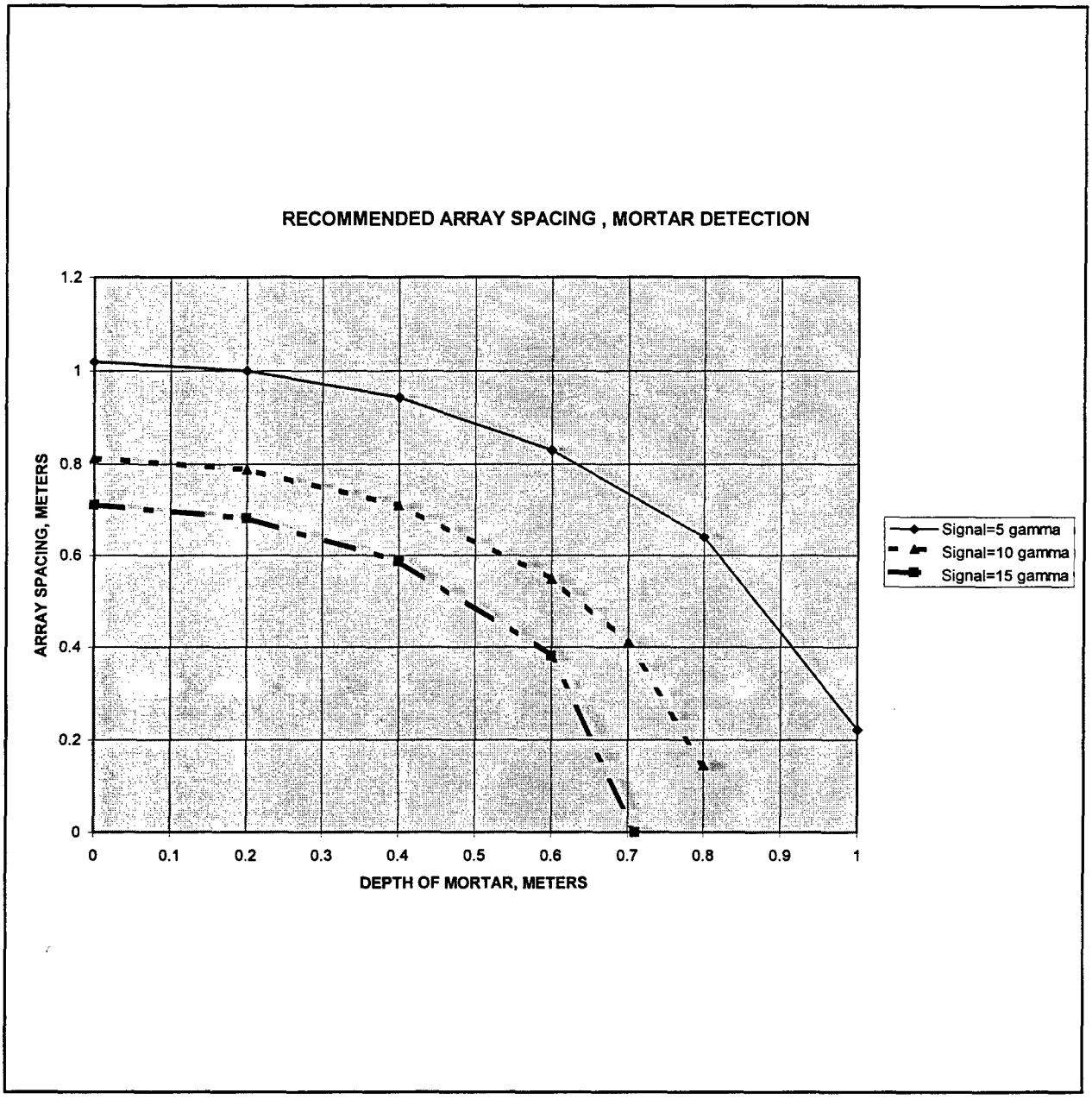

Figure 7-4. Recommended Array Spacing for Mortar Round Detection

true test will come when they are trained on much larger data sets than we have been able to assemble on this program. It appears that 20,000 training cycles through the data produce reasonable convergence on solutions for the predicted moments, depths, and distances. Predictions have correlated with measured values in the range of 70 to 99%. It also is recommended, after training of the neural networks, that they be exposed to new data sets that have not previously been seen. This process is recommended for larger data sets that include the wide variety of expected ordnance orientations and depths.

The Vallon iron detector has yielded H-field data that largely agree with the Geometrics 822, although it operates in a different, gradiometer, mode. We have experienced more difficulty in processing the data from this instrument, only because it was not provided with a computer aided data acquisition capability. Care must be taken to properly null the instrument and to maintain the mast in a vertical direction.

There were found to be distinctive features in the contour plots of the rounds. Both the mortar and 105 rounds have a permanent moment directed toward the base of the round. The 155 round, on the other hand, has a permanent moment directed toward the nose. The result is that a buried 105, in a horizontal plane, has a negative contour on the base side of the round and a positive contour on the nose side, regardless of it's cardinal pointing direction. The horizontal, buried 155 behaves differently-- the negative contour is on the nose side of the round when it is pointed east or west. It will have a negative contour on the north side when it is pointed north or south. (See Section 6.2). These results, although based upon testing of only two rounds of each type should have strong implications for the future training of neural networks.

We recommend that surveys be continued on controlled grids to collect a larger data base. The effects of multiple objects in close proximity should be examined, including assorted non-ordnance items and ferrous debris.

References

(1) U.S. Army Jefferson Proving Ground Evaluation, Madison, Indiana, Report to the Governor, April 20, 1989.

(2) ibid

(3) Broad Agency Announcement (BAA-94-01) For Fundamental Research and Applied Technologies in the Unexploded Ordnance Area, Commerce Business Daily, Issue No. PSA-0967, November 4, 1993.

(4) UXO Detection, Identification, and Remediation, BAA-94-1 Preproposal Program Bidder's Conference presentation, December 13, 1993.

(5) Final Study, Cleanup and Reuse Options, U.S. Army Jefferson Proving Ground, Madison IN, October 15, 1992.

(6) Sensor Technology Assessment for Ordnance and Explosive Waster Detection and Location, Jet Propulsion Laboratory , JPL D-11367, March 1, 1995.

(7) H. L Van Trees, Detection Estimation and Modulation Theory, Vol. 1, New York: Wiley, 1968.

(8) J.E.McFee and Y. Das, "Determination of the Parameters of a Dipole by Measurement of its Magnetic Field," IEEE Trans. Antenn. Propagat., Vol. AP-29, pp.282-287, 1980.

(9) E.R. Leach and J.F.X. Daum, "Analysis of Requirements for a Mobile Multiple Sensor Ordnance Detection System", A White Paper, Eugene R. Leach and Associates, July 16, 1993.

(10) G.T.Ruck, R.E. Beverly and E. R. Leach, "Electromagnetic Characterization and Susceptibility/Vulnerability Study of Mines" Task 4, Electromagnetic Field Calculations, Battelle Columbus Laboratories, December 17, 1976.

(11) T.W. Altshhuler, "Shape and Orientation Effects on Magnetic Signature Prediction for Unexploded Ordnance", Conference Proceedings, UXO Forum 1996, March 26-28, 1996.

(12) J. Hersey and J. Pennella, "Ordnance Locator Technologies--An Overview", NAVEODFAC Technical Report TR-188, Naval Explosive Ordnance Disposal Technology Center, Indian Head, MD, August 1978, 20 pp., ADB 028572L.

(13) R.H. Blount, "Operational Evaluation of MK 22 MOD 0 Ferrous Ordnance Locator", prepared by U.S. Navy Operational Test and Evaluation Force, Jan. 21, 1980, 50 pp., ADB043526L.

(14) S. Bennett, et. al., "Range Clearance Technology Assessment", prepared by Naval Explosive Ordnance Disposal Technology Center, Indian Head, MD, for the U.S. Army Corps of Engineers, Washington, D.C., March 1990, 49 pp.

(15) J. Hersey and J. Pennella, Ibid.

(16) E.R. Leach and D.W. Carpenter, "Magnetic Sensor Technology--Survey of the State of the Art", Final Report NEOD 9-3, prepared by Battelle Columbus Division, Columbus, OH, for Naval Explosive Ordnance Disposal Technology center, Indian Head, MD, March 1984, 17 pp., PA51551.

(17) E.R. Leach, "Survey of Magnetic Field Sensor Technology", Final Report R-6097, prepared by Battelle Columbus Division, Columbus, Oh, for Defense Advanced Research Projects Agency, Contract No. DAAH01-81-a277, May 1981.

(18) E.R. Leach and M.R. Seiler, "Magnetic Field Intensity Sensors for Low Frequency Applications", Final Report NEOD 7-2, prepared by Battelle Columbus Division, Columbus, OH, for Naval Explosive Ordnance Disposal Technology Center, Indian Head MD, March 1983, PA51220.

(19) Sensor Technology Assessment for Ordnance and Explosive Waster Detection and Location, Jet Profusion Laboratory , JPL D-11367, March 1, 1995.

(20) G-822L Cesium Magnetometer, Operation Manual, Release 1.18.

(21) G-822L Magnetometer, Ferrous Object & Ordnance Locator, Geometrics

(22) Iron Detector EL 1302A1, Operating Manual, Vallon GmbH.

(23) Fiber Optic Magnetometer, Technical Proposal Submitted to Armament Division, Eglin Air Force Base, Solicitation No. F08635-85-R-0069, April 19, 1985.

(24) "Prototype Fiber Optic Triaxial Magnetometer System(PTFOM)", Prepared by Optical Technologies, January 9, 1994.

(25) Fiber-Optic Magnetometer Engineering Support, final report, Contract No. N00600-88-D-3717, Delivery Order FG-IV. Optical Technologies, April 26, 1993

(26) H.H. Henegar, "Detection of Unexploded Ordnance", DDESB Technical Report 76-1, Ft. Belvoir, VA., April 1976.

(27) N. H. Farhat, "Microwave Diversity Imaging and Automated Target Identification Based on Models of Neural Networks", Pro. IEEE, Vol. 77, pp. 670-680, 1989.

(25) W. Pedrycz "Fuzzy Sets in Pattern Recognition", Pattern Recog., Vol. 23, pp121-146, 1990.

(26) P. K. Simpson, "Fuzzy Min-Max Neural Networks- Part 1:Classification," IEEE Trans. On Neural Networks, pp.776-786, 1992.

(30) I. Kadar and v. Libby, chairs/editors, "Signal Processing, Sensor Fusion and Target Recognition IV", SPIE Proceedings, Vol 2484, April 17-19, 1995.

(31) B. V. Dasarathy, "Adaptive Fusion Processor", SPIE vol 2484, Apr 95, pp 2-13.

(32) B. V. Dasarathy, "Adaptive Fusion Processor Paradigms for Fusion of Information Acquired at Different Levels of Detail", Optical Engr., Vol 35, no 3, Mar 1996, pp 634-649.

(33) H. S. Ranganath and S. R. F. Sims, "Self-partitioning Neural Networks", SPIE vol 2234, 1994.

(34) D. F. Specht, "Probabilistic Neural Networks", Neural Networks, Vol 3, no. 1, 1990, pp 109-118.